ABSTRACT

ROBERTS, LOREN P. Nonlinear Weighted Flux Methods for Solving Multidimensional Transport Problems. (Under the direction of Dmitriy Y. Anistratov.)

The goal of the research presented in this dissertation is to develop new parameterized flux methods for the accurate and efficient solution of multidimensional transport problems in Cartesian geometry. Development of such iterative methods are necessary for consideration of the interaction of radiation with matter using detailed descriptions of underlying physical phenomena. The primary application area considered is radiative transfer problems which contain diffusive subdomains. An accurate solution within diffusive material regions requires a transport method to possess the asymptotic diffusion limit in that the method must limit to an accurate form of the diffusion equation with boundary conditions that closely approximate that known from analysis of the transport equation.

We develop the NWF methods for the 1D slab geometry transport equation. The methods are derived by integrating the transport equation over $-1 \leq \mu \leq 0$ and $0 \leq \mu \leq 1$ with weight $1 + \beta|\mu|^\alpha$, where $\alpha \geq 0$. The asymptotic diffusion limit analysis enabled us to determine a particular method of this family the solution of which satisfies an accurate approximation of the diffusion limit. Note that none of the α-weighted nonlinear (α-WN) methods possess this combination of properties. The convergence properties are similar to that of the diffusion-synthetic acceleration (DSA), quasidiffusion (QD), and DSA-like α-WN methods.

The NWF methods are derived for 2D Cartesian geometry with linear and bilinear polynomial weights. Asymptotic diffusion limit analysis reveals conditions on the weights necessary for an accurate approximation of the diffusion equation. A degree of freedom remains for the bilinear weight and is utilized to improve the method's boundary condition in the diffu-

sion limit. Numerical results are presented to confirm the theoretical results and demonstrate performance of the NWF methods. The convergence properties are analyzed via Fourier analysis and numerical problems to show that the method is stable and that, for a wide range of problems, the NWF methods exhibit convergence properties very similar to DSA, QD, SQD, and ADR.

Nonlinear Weighted Flux Methods for Solving Multidimensional Transport Problems

by

Loren P. Roberts

A dissertation submitted to the Graduate Faculty of
North Carolina State University
in partial fulfillment of the
requirements for the Degree of
Doctor of Philosophy

Nuclear Engineering

Raleigh, North Carolina

2008

Approved By:

Dr. Robin P. Gardner	Dr. Zhilin Li
Dr. Dmitriy Y. Anistratov Chair of Advisory Committee	Dr. Paul J. Turinsky

DEDICATION

Dedicated to my wife, Kari.

"However beautiful the strategy, you should occasionally look at the results." - Winston Churchill

BIOGRAPHY

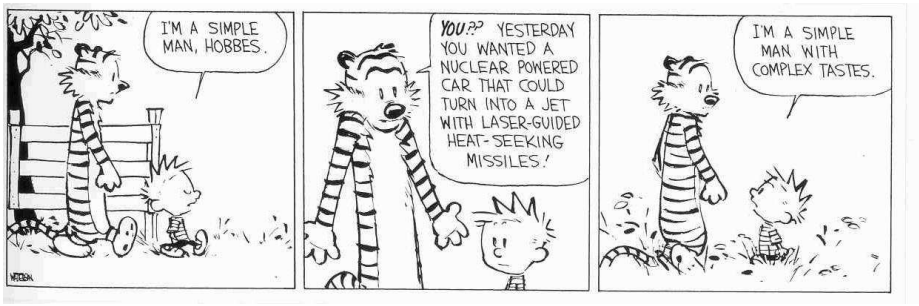

Loren Roberts was born on January 13th, 1980 to Kenneth and Barbara Roberts at Offut AFB in Nebraska, USA. He has two older brothers and one older sister. He grew up and attended school in Mulvane, Kansas, a semi-rural small town near Wichita.

After graduating from high school he attended Kansas State University in the Mechanical and Nuclear Engineering department. Influential nuclear engineering professors during his time at KSU were G.G. Simons, J.K. Shultis, N.D. Eckhoff, and H.J. Donnert. He met, dated, and then married Kari Bahner in the summer of 2002. He graduated Cum Laude in 2002 with a B.S. in the Nuclear Option of Mechanical Engineering.

Loren joined the Nuclear Engineering department of North Carolina State University in January 2003. He has continually gravitated to the options he feels are most challenging, and therefore chose radiation transport theory as a research area. He began working with advisor Dmitriy Y. Anistratov on the work contained in this dissertation later in 2003.

ACKNOWLEDGEMENTS

I would like to express my most sincere thanks and appreciation to my advisor, Dmitriy Y. Anistratov, for all of his guidance, frank discussions, and impromptu lectures. He provides a role model as an advisor, professor, and family man that I can only strive to come close to in life. I most appreciate his sincere attention and dedication in spending countless hours discussing and arguing anything and everything.

This work has been supported by the Nuclear Engineering and Health Physics Fellowship Program sponsored by the Office of Nuclear Energy, Science, and Technology of the U.S. Department of Energy, the Nuclear Engineering Education and Research (NEER) Program of the US Department of Energy under the grant No. DE-FG07-03ID14496, the Duke Energy Foundation Fellowship, and the NCSU College of Engineering Dean's Fellowship.

I would also like to thank everyone else that I have interacted with during my time at NCSU. Drs. Turinsky and Gardner have been influential with their discussions broadening my experiences and learning. I must thank the "Wiesel" for many spirited cross-cubicle discussions and white-board musings conducted in transport lingo code in defiance of the infinitely massive black holes and disruptional gravitational fields that surrounded us. May we all be so fortunate as to remember to "use our library voices."

Finally, my family is perhaps the only reason I ended up where I am today. My wife provides daily encouragement and support. My father and grandfather instilled an attitude of doing my best, working hard, getting the job done, and an appreciation of the subtleties of the world that surrounds us.

TABLE OF CONTENTS

LIST OF FIGURES

LIST OF TABLES

Chapter 1

INTRODUCTION

1.1 Overview

With present day computing power and having known the Boltzmann equation for more than a century, researchers still work on development of efficient methods for solving particle transport and radiative transfer problems. This is because of the complexity of the physical phenomena being modeled. In addition to innovative discretization methods and high-performance computers, iterative acceleration schemes are necessary for transport calculations. The required accuracy for today's exacting science and engineering calculations and applications has risen significantly. It is now necessary to consider the interaction of particles (radiation) with matter using detailed descriptions of underlying physical phenomena based on complicated multiphysics models. Coupling faster computers, parallel processing architectures, and innovative numerical methods to solve the transport equation (Linear Boltzmann) permits sophisticated physical models to be used rather than extremely simplified approximations. Most importantly, this yields results closer to the truth and allows for better decision-making in many

fields, without costly experimentation.

The work in this dissertation is applicable to science and engineering problems such as radiative transfer, reactor physics, radiation shielding, radiation effects, astrophysics, atmospheric sciences, etc. An example is the current effort being made in the United States to completely replace underground testing of nuclear weapons with the capability to fully simulate their performance and radiation effects on materials. This herculean task, and many others, can not be accomplished without improved numerical solution methods of the transport equation to model the inherent radiation physics. The research presented here is focused on the development of new nonlinear methods with necessary properties for the accurate and efficient solution of this class of problems.

The overall goal of the presented research is to develop a new family of flux methods which possess an accurate asymptotic diffusion limit for efficient solution of multidimensional transport problems that contain diffusive regions.

1.2 Background and Problem Descriptions

This work is particularly focused on developing numerical methods for the solution of the transport equation for radiative transfer problems. In this class of problems, material regions typically contain highly diffusive subdomains where particles (radiation) have short mean free paths and the physics are dominated by scattering (absorption and re-emission). The particle transport equation is an integro-differential equation. It can be written in abstract form as $L\psi = S\psi + Q$. Here, L is a particle streaming and removal operator. S is a scattering operator. Q is a general external source. In general, the transport equation depends upon seven

dimensions, namely space, time, angle, and energy (frequency). In this work, the steady-state monoenergetic transport equation with isotropic scattering,

$$\Omega_x \frac{\partial}{\partial x}\psi(\vec{r},\vec{\Omega}) + \Omega_y \frac{\partial}{\partial y}\psi(\vec{r},\vec{\Omega}) + \sigma_t(\vec{r})\psi(\vec{r},\vec{\Omega}) = \frac{1}{4\pi}\sigma_s(\vec{r})\int_{4\pi}\psi(\vec{r},\vec{\Omega}')d\vec{\Omega}' + \frac{1}{4\pi}q(\vec{r})\,, \tag{1.1}$$

$$\psi(\vec{r},\vec{\Omega})\Big|_{\vec{r}\in\partial\mathcal{D}} = \psi^{in}(\vec{r}_b,\vec{\Omega})\,, \quad \vec{\Omega}\cdot\vec{n} < 0\,, \tag{1.2}$$

$$\vec{r}\in\mathcal{D}\,, \quad \vec{r}_b\in\partial\mathcal{D}\,, \tag{1.3}$$

$$\vec{\Omega} = (\Omega_x,\Omega_y)\ , \tag{1.4}$$

is considered for Cartesian geometry, where $\mathcal{D} = \{0 \le x \le X,\ 0 \le y \le Y\}$. Here, Ω_x and Ω_y are directional cosines that define the direction of travel, ψ is the angular flux. Probabilities of interaction of particles (radiation) per unit path length are quantified by the total and scattering cross sections, σ_t and σ_s respectively. An external source is represented by q. It is reasonable to consider this form of the transport equation because the solution of deterministic energy dependent problems are generally discretized into coupled monoenergetic transport problems that are solved individually. Coupling between energy groups is through scattering and fission which is contained within the external source in (1.1). Thus, the performance properties of a method in solving (1.1) will be indicative of the performance for solving each monoenergetic equation of a coupled multi-group system.

Because of the structure of the transport equation, iterative methods must be used to solve it. The most basic iterative scheme is source iterations (SI)

$$\psi^{[k+1]} = L^{-1}[S\psi^{[k]} + Q]\,, \tag{1.5}$$

where k is the iteration index. The iterative procedure is outlined as:

$$\Omega_x \frac{\partial}{\partial x}\psi^{[k+1/2]}(\vec{r},\vec{\Omega}) + \Omega_y \frac{\partial}{\partial y}\psi^{[k+1/2]}(\vec{r},\vec{\Omega}) + \sigma_t(\vec{r})\psi^{[k+1/2]}(\vec{r},\vec{\Omega}) = \frac{1}{4\pi}\left(\sigma_s(\vec{r})\phi^{[k]}(\vec{r}) + q(\vec{r})\right), \tag{1.6}$$

$$\phi^{[k+1]} = \int_{4\pi} \psi^{[k+1/2]}(\vec{r},\vec{\Omega}')d\vec{\Omega}', \tag{1.7}$$

where ϕ is known in the nuclear-physics community as the scalar flux. This scheme has very poor convergence properties for the case of diffusive media. The spectral radius for an infinite medium is given by the scattering ratio $c = \sigma_s/\sigma_t$, which for diffusive media $c \approx 1$ and then $\rho \to 1$. To accelerate transport iterations, nonlinear projective-iteration (NPI) methods have been developed [1, 2]. Among these methods are the Quasidiffusion method [3], the First-Flux (FF) (averaged flux) method [4, 5], Second-Flux (SF) method [6], α-Weighted Nonlinear (α-WN) methods [7], nonlinear S_2-like methods [8], Angular Dependent Rebalance [9], and others [2].

The idea of NPI methods is to average the transport equation over the angular variable to produce a set of moment equations with lower dimensionality which can then be solved with less effort. The way in which the low-order problem is defined differentiates the resulting methods and their properties. The iteration scheme then consists of solving nonlinearly coupled high-order (transport equation) and low-order equations. The resulting nonlinear system of equations is equivalent to the original linear transport problem. They are coupled through nonlinear factors that are weakly dependent on the angular flux, particularly its shape and not its magnitude. This weak dependence results in fast convergence.

NPI methods have a distinct advantage in that they do not need to be discretized consistently with the transport equation. Note that the Diffusion-Synthetic Acceleration (DSA)

method must be consistently discretized with the transport discretization for stability. If a consistent discretization is used, then the solution of the high and low-order equations do not differ and a pure acceleration method results. If an independent discretization is used, then NPI methods give two solutions of the scalar flux, namely the high-order and low-order flux, which differ by a truncation error. These two solutions limit to each other for a fine mesh. NPI methods possess certain advantages for their use in multiphysics applications. NPI methods have some flexibility in coupling, for instance, radiative transfer and hydrodynamics equations.

In order for a method to accurately and efficiently solve radiative transfer problems with diffusive regions, it must possess certain properties. First, it is required to have an accurate asymptotic diffusion limit. In other words, the leading order solution of the method should limit to the solution of a correct diffusion equation inside of diffusive material regions. Also, the boundary condition fit by this diffusion equation should be accurate to the known analytic form from the transport equation. Second, a method must converge fast. Procedures to analyze the asymptotic diffusion limit and convergence properties have been developed and are summarized in this chapter. Next, a summary of previously developed transport acceleration methods is presented.

1.2.1 Synthetic Acceleration

Synthetic acceleration methods were developed beginning in the 1960's as a way to speed up the solution of the transport equation. The idea is to improve the current iterate's value of $\psi^{[k+1/2]}$ to be more accurate by the solving of another set of equations (preconditioner). The choice of equations (preconditioner) is what defines specific synthetic methods and their individual properties. In order to describe synthetic acceleration, first consider the transport

equation in operator form

$$L\psi^{[k+1/2]} = S\psi^{[k]} + q\,. \tag{1.8}$$

Now, subtract Eq. (1.8) from the exact transport equation $L\psi = S\psi + q$ to get an equation in terms of an additive correction, namely $(\psi - \psi^{[k+1/2]})$,

$$(L - S)(\psi - \psi^{[k+1/2]}) = S(\psi^{[k+1/2]} - \psi^{[k]})\,. \tag{1.9}$$

This equation can be solved for the exact solution, ψ, but then the operator $(L - S)$ must be inverted. Of course, this is not any easier than solving the original problem itself.

An approximation to $(L - S)$ must be made that is computationally cheaper to solve, yet is also close to the original operator in some physical sense. Approximating $M \approx (L - S)^{-1}$ yields

$$\psi^{[k+1]} = \psi^{[k+1/2]} + MS(\psi^{[k+1/2]} - \psi^{[k]})\,. \tag{1.10}$$

The synthetic solution algorithm is now comprised of equations (1.8) and (1.10) which represent the high-order and low-order problems, respectively. The solution of the low-order equations will satisfy the original transport equation no matter what the choice of M is, although method properties such as convergence rate will inherently vary based on the choice of M. It is possible to express the synthetic acceleration scheme as a preconditioned Richardson iteration scheme.

The development of synthetic acceleration schemes independently began with Kopp [10] and Lebedev [11]. Kopp introduced the idea of synthetic acceleration while Lebedev introduced KP acceleration schemes. The idea of both is to accelerate the convergence of the transport solution using at least one low-order equation solve. Other methods that have resulted from this line of work are the Diffusion Synthetic Acceleration (DSA), S2, and Transport Synthetic Acceleration (TSA).

The idea of using a diffusion operator as a preconditioner began in the West with Gelbard and Hageman to accelerate S_n iterations [12]. Note that Lebedev also studied a diffusion operator in the context of the KP methods. It was shown that the spectral radius of Gelbard and Hageman's method in continuous form was $< 0.2247c$, where c is the scattering ratio. For the discretized form, problems arise for meshes with optically thick cells [13]. A remedy for this is to derive the low-order discretization consistently with the transport equation discretization and was shown by Alcouffe in 1976 [14, 15]. The Four-Step method for defining consistent discretizations of the DSA method with respect to the transport discretization was later introduced [16, 17] which provides a recipe for deriving stable DSA discretizations. The development of an unconditionally stable acceleration scheme for the first-order form of the transport equation had and continues to have great impact on research and engineering applications.

Instead of a diffusion operator, the low-order S_2-like operator was studied in 1986 [18]. The S_2-like equations solve the discrete ordinates form of the transport equation in terms of an additive correction factor for two directions in 1D geometry. Continuous form, infinite medium Fourier analysis shows that the S_2-like methods have the same convergence properties as DSA in 1D. An advantage of the S_2-like methods is that the equations have a similar form to the transport equation and the same discretization methods can be utilized. On the other hand, the equations are harder to solve, do not have a small spectral radius in multidimensional geometry, and are only cheap to solve for the case of 1D geometry.

The TSA scheme was developed as a generalization of Morozov's method [19] to be used for multidimensional geometry [20]. The S_2-like method is contained within TSA as a specific case resulting from the choice of low-order quadrature. For example, an S_2 or S_4 angular

quadrature could be used with TSA. The equations of TSA are to be solved in multidimensional geometry for an additive correction factor to the scalar flux, but the solution is iterative and termed inner iterations. Iterative methods for the inner iterations include source iteration and other algebraic acceleration schemes. There also exists a free parameter, β, which partially determines the method's performance and whose optimal value is problem dependent. The iterative properties can degrade if one does not converge the low-order TSA equations in an inner iteration, for anisotropic scattering, multidimensional geometry, and some choices of the parameter β.

To describe each synthetic acceleration scheme, consider the monoenergetic 1D slab geometry transport equation with isotropic scattering,

$$\mu\frac{\partial}{\partial x}\psi^{[k+1/2]}(x,\mu)+\sigma_t(x)\psi^{[k+1/2]}(x,\mu)=\frac{\sigma_s}{2}\phi^{[k]}(x)+\frac{q(x)}{2}\,, \tag{1.11}$$

which can be written in terms of an additive correction factor

$$f^{[k+1/2]}(x,\mu)=\psi(x,\mu)-\psi^{[k+1/2]}(x,\mu)\,, \tag{1.12}$$

for the angular flux as

$$\mu\frac{\partial}{\partial x}f^{[k+1/2]}(x,\mu)+\sigma_t(x)f^{[k+1/2]}(x,\mu)-\frac{\sigma_s}{2}\int_{-1}^{1}f^{[k+1/2]}(x,\mu')d\mu'=\frac{\sigma_s}{2}(\phi^{[k+1/2]}(x)-\phi^{[k]}(x))\,. \tag{1.13}$$

The iterative procedure begins with an initial guess of $\phi^{[k]}$ which is used to solve the transport equation for $\psi^{[k+1/2]}$, i.e. a high-order transport sweep. Then, a low-order set of equations is solved in some manner for the additive correction factor. Next, the scalar flux in the scattering term of the transport equation is updated and another transport sweep is performed, and so on. There is an added cost in solving a low-order problem, but this is (ideally) justified by the improved iterative convergence properties of the new algorithm.

Then, the DSA method's low-order equations for Eq. (1.13) take the form:

$$-\frac{d}{dx}\frac{1}{3\sigma_t(x)}\frac{dF^{[k+1/2]}}{dx}(x)+\sigma_a(x)F^{[k+1/2]}(x)=\sigma_s(x)\left(\phi^{[k+1/2]}-\phi^{[k]}\right), \tag{1.14}$$

where

$$F^{[k+1/2]}(x)=\int_{-1}^{1}f^{[k+1/2]}(x,\mu)d\mu\,, \tag{1.15}$$

$$\phi^{[k+1]}(x)=\phi^{[k+1/2]}(x)+F^{[k+1/2]}(x)\,. \tag{1.16}$$

Obviously, this is the diffusion equation written in terms of the correction factor. The slowest converging components of the SI method are those with weak spatial and angular dependence. This method suppresses the flat error modes which are the source of trouble for SI by obtaining improved estimates of the scalar flux through the solution of the diffusion equation.

The low-order equations of the S_2-like method are formulated in terms of additive correction factors in the plus and minus directions. The system of equations are:

$$\pm\frac{1}{\sqrt{3}}\frac{df_{\pm}^{[k+1/2]}}{dx}+\sigma_t(x)f_{\pm}^{[k+1/2]}(x)-\frac{\sigma_s(x)}{2}\left(f_{+}^{[k+1/2]}(x)+f_{-}^{[k+1/2]}(x)\right)=\frac{\sigma_s(x)}{2}\left(\phi^{[k+1/2]}(x)-\phi^{[k]}(x)\right), \tag{1.17}$$

and the equation to update the scalar flux,

$$\phi^{[k+1]}(x)=\phi^{[k+1/2]}(x)+f_{+}^{[k+1/2]}(x)+f_{-}^{[k+1/2]}(x)\,. \tag{1.18}$$

Note the similarity of the form of Eq. (1.17) and Eq. (1.11). This is the advantage of these methods in that transport discretizations can be used with the low-order problem.

The TSA method also involves the solution of a low-order problem in terms of a correction factor. The TSA method can be written in discrete ordinates form as

$$\mu\frac{df_n^{[k+1/2]}}{dx}+\left[\sigma_t(x)-\beta\sigma_s(x)\right]f_n^{[k+1/2]}(x)-\frac{(1-\beta)\sigma_s(x)}{2}F^{[k+1/2]}(x)=$$

$$\frac{\sigma_s(x)}{2}\left(\phi^{[k+1/2]}(x)-\phi^{[k]}(x)\right), \tag{1.19}$$

where

$$f_n^{[k+1/2]}(x)=\psi(x,\mu_n)-\psi_n^{[k+1/2]}(x), \tag{1.20}$$

$$F^{[k+1/2]}(x)=\sum_{n=1}^{N}\zeta_n f_n^{[k+1/2]}(x), \tag{1.21}$$

$$n=1,\ldots,N,$$

which is termed the β-TSA form, and ζ_n are quadrature weights. Here, β is a free parameter that is optimally set based on the problem specifications and ranges from [0,1]. Note that for $\beta = 0$ this TSA scheme is equivalent to the S_N scheme. For $\beta = 1$, there is no scattering and the Larsen-Miller method results which converges in one sweep. The value of β affects the convergence properties of the method by adjusting the scattering cross section while keeping the absorption cross section constant. This equation for general β can be solved by inner source iterations or accelerated by some means. Thus, the computational burden may be a disadvantage without a generally efficient solution algorithm.

Finally, note that there exists many more "synthetic" type methods, of which these are a representative few.

1.2.2 Quasidiffusion Method

The Quasidiffusion (QD) method represents a historically and algorithmically very distinct approach to solving and accelerating the solution of the transport equation as compared to the synthetic methods. Its development began with Gol'din in the 1960's when the nonlinear QD method was introduced [3]. The QD method is again based on the solution of a low-order system of equations. These equations are formulated in terms of the scalar flux and current,

but also may be written in terms of a multiplicative correction factor. There is no requirement that the QD equations be discretized consistently with the transport equation for stability. This presents an opportunity to improve the quality of the low-order solution through discretizations of higher accuracy, without putting forth extra effort in the high-order problem.

The concept of the QD method is based upon projecting the transport equation's unknowns onto a subspace of lesser dimension. Namely, the angular dependence is removed. It is then computationally cheaper to operate within this subspace. This is accomplished through closing the low-order system of QD equations with nonlinear factors that are comprised of integrals of the angular flux over the angular domain. These factors have the property that they depend weakly on the angular flux. That is, they depend on the shape of the angular flux, not its magnitude. This results in fast convergence properties for the QD method. The equations of the low-order QD method in 1D are derived by integrating the transport equation (1.11) over the angular domain with weights of 1 and μ to give:

$$\frac{d}{dx}J^{[k+1]}(x) + \sigma_t(x)\phi^{[k+1]}(x) = \sigma_s(x)\phi^{[k+1]}(x) + q(x)\,, \tag{1.22}$$

$$\frac{d}{dx}\left(E^{[k+1/2]}(x)\phi^{[k+1]}(x)\right) + \sigma_t(x)J^{[k+1]}(x) = 0\,, \tag{1.23}$$

$$J^{[k+1]}(0) = C_L^{[k+1/2]}\phi^{[k+1]}(0)\,, \tag{1.24}$$

$$J^{[k+1]}(X) = C_R^{[k+1/2]}\phi^{[k+1]}(X)\,, \tag{1.25}$$

where

$$E^{[k+1/2]}(x) = \int_{-1}^{1}\mu^2\psi^{[k+1/2]}(x,\mu)d\mu \Big/ \int_{-1}^{1}\psi^{[k+1/2]}(x,\mu)d\mu\ , \tag{1.26}$$

$$C_L^{[k+1/2]} = \int_{-1}^{0}\mu\psi^{[k+1/2]}(0,\mu)d\mu \Big/ \int_{-1}^{0}\psi^{[k+1/2]}(0,\mu)d\mu\ , \tag{1.27}$$

$$C_R^{[k+1/2]} = \int_{0}^{1}\mu\psi^{[k+1/2]}(X,\mu)d\mu \Big/ \int_{0}^{1}\psi^{[k+1/2]}(X,\mu)d\mu\ , \tag{1.28}$$

and J is the particle (radiation) current. E is the linear fractional factor that is defined to close the system of equations. The QD boundary conditions are defined by relating the current and scalar flux on the boundary to each other through the linear fractional factors C_L and C_R. Note that the QD equations are easily manipulated into a diffusion-like equation.

1.2.3 Flux Methods

Flux methods came into being after QD, albeit initially under different names, through the work of Germogenova [4, 21] and Gol'din [5, 22]. Specific flux methods have been defined such as the First Flux (FF) method [1], Second Flux (SF) method [23], and a generalized flux method termed the α-Weighted methods (α-WN) [7]. These methods can be generally interpreted as the solving of the transport equation averaged over angular subdomains. The unknowns are partial scalar fluxes defined over these angular subdomains.

The FF method's equations are zeroth angular moments of the transport equation, the SF method's equations are first angular moments, and the α-WN method is a general parameterized flux method of which the former methods are a subset. An attractive feature of the flux methods is that discretization schemes similar to transport differencing schemes can be used to approximate their low-order equations. Note that for stability of these methods, there is no need to discretize the transport and low-order equations consistently. However, neither the FF method nor the SF method satisfies the diffusion limit unless the discretization of the low-order equations is consistent with the transport differencing scheme, which itself satisfies the diffusion limit [7, 1].

The low-order problem of the QD method, defined in terms of the scalar flux and current, is an elliptic one and the solution in any spatial point depends on the solution in all

other points. However, when particles stream without scattering in some direction, the nature of the relationship of the solution amongst various spatial points is different and based on the properties of the hyperbolic differential operator of the transport equation. The low-order equations of the flux and α-WN methods are formulated for the partial scalar fluxes and possess such a feature. The flux methods have been used successfully, for instance, to solve electron transport problems with highly anisotropic scattering and radiative transfer problems [22].

The family of the nonlinear α-weighted methods is the generalization of the flux methods [7]. In case of 1D slab geometry, these methods are derived by integrating the transport equation over $-1 \leq \mu \leq 0$ and $0 \leq \mu \leq 1$ with weight $|\mu|^\alpha$, $\alpha \geq 0$. The method with $\alpha = 0$ reduces to the FF method, and the method with $\alpha = 1$ is equivalent to the SF method. The study of the nonlinear α-weighted methods showed that the method with $\alpha \approx 0.366$ has convergence properties similar to the DSA method, and the equations of this method can be reduced to the diffusion equation in the diffusive regions. However, the solution of this method does not satisfy an accurate approximation of the asymptotic boundary condition in the diffusive problems. The work by Anistratov and Larsen [7] pointed out that a particular weight could be defined in order to obtain the desired property of optimal convergence.

The flux methods are defined here by the general α-WN method. First, the partial scalar fluxes are given as

$$\phi^{+[k+1/2]}(x) = \int_0^1 \psi^{[k+1/2]}(x,\mu)d\mu\,, \tag{1.29}$$

$$\phi^{-[k+1/2]}(x) = \int_{-1}^0 \psi^{[k+1/2]}(x,\mu)d\mu\,. \tag{1.30}$$

Nonlinear factors, in the same spirit as the QD factors developed earlier, are defined in order

to close the system of equations

$$A^{\pm[k+1/2]}(x) = (\alpha+1)\frac{\int_0^{\pm1}|\mu|^{\alpha+1}\psi^{[k+1/2]}(x,\mu)d\mu}{\int_0^{\pm1}\psi^{[k+1/2]}(x,\mu)d\mu}\,, \tag{1.31}$$

$$B^{\pm[k+1/2]}(x) = (\alpha+1)\frac{\int_0^{\pm1}|\mu|^{\alpha}\psi^{[k+1/2]}(x,\mu)d\mu}{\int_0^{\pm1}\psi^{[k+1/2]}(x,\mu)d\mu}\,. \tag{1.32}$$

Then, the two low-order equations are given by

$$\pm\frac{d}{dx}A^{\pm[k+1/2]}(x)\phi^{\pm[k+1]}(x)+\sigma_t(x)B^{\pm[k+1/2]}(x)\phi^{\pm[k+1]}(x) = \frac{\sigma_s(x)}{2}\left(\phi^{+[k+1]}(x)+\phi^{-[k+1]}(x)\right)+\frac{q(x)}{2}\,. \tag{1.33}$$

The form of the low-order equations are similar to that of the S_2 form of the transport equation. Thus, the 1D flux methods are like solving the transport equation averaged over two directions. Finally, note that a linear version of these methods can be formed [7].

1.2.4 Angular Dependent Rebalance Methods

Rebalance methods were conceived early on as a simple way to accelerate the solution of transport problems [24, 25]. The idea is to solve a low-order system of equations that enforces a particle balance over individual coarse mesh cells. The terms "coarse" and "fine" are used to refer to the low-order and high-order meshes, respectively. The coarse mesh can be the same as the fine mesh, which is termed Fine Mesh Rebalance (FMR) [26]. Coarse Mesh Rebalance (CMR) uses a mesh that is comprised of groups of fine-mesh cells. The coarse-mesh balance equation is formulated in terms of rebalance factors. These factors are then used to update the solution in each fine-mesh cell. Rebalance methods are easy to conceptualize and implement in codes. This simplicity is offset by the user determining the coarse mesh in order to optimize performance. In general, rebalance diverges for problems of small optical thickness or scattering ratios near one.

In 1986, Adams and Martin presented a new approach to synthetic acceleration termed Boundary Projection Acceleration (BPA) [27]. Low-order equations are defined by projecting corrections to the solution of the high-order equations onto a coarse angular mesh and only on cell boundaries. The BPA method is derived for general projection operators and can be applied regardless of geometry, discretization, and mesh shape. The choice of projection operator then defines the form of the low-order equations (preconditioner). Results of a Fourier Analysis of the BPA method in slab geometry for the diamond differencing (DD), step differencing (SD), linear discontinuous (LD), and linear moments (LM) spatial discretization schemes with coarse-mesh angular subspaces of DP_0 and DP_1 were presented in [28]. The Fourier analysis showed that the BPA methods are unconditionally stable with the slowest method having a spectral radius $\rho \leq \frac{c}{3}$ and that the selection of projection operator significantly affects convergence properties. At the same time, Lawrence independently developed another BPA method called Interface-Current Synthetic Acceleration [29].

Adams introduced a nonlinear form of BPA termed NLBPA in 1993 [8]. This method has similarities to the nonlinear α-WN and QD methods in that the low-order equations use angular shape functions that depend only on the shape of the angular flux, not the magnitude. In this work, Adams formulates the low-order equations as generally-weighted angular integrals of spatially-discretized S_N equations resulting in an S_2-like form. As with BPA, the low-order equations are derived only for cell boundaries. The linearized form of the NLBPA method is equivalent to an S_2-like BPA method. Adams analyzed this method with a Fourier analysis and found that it is always stable for a choice of weight function proportional to $|\mu|$. He also showed that the NLBPA methods can be independently discretized from the high-order problem. The

Angular Dependent Rebalance (ADR) family of methods were presented by Cho and others in 1997 and 2001 [9, 30] to address the convergence deficiencies of rebalance. The ADR methods are identical to Adam's NLBPA method, except that Cho considers a DP_N form of the low-order equations. Thus the S_2-like NLBPA equations are a member of the ADR family of methods, specifically the DP_0 case. Note that linearized ADR is also equivalent to the BPA method.

The development of the Additive Angular Dependent Rebalance (AADR) [30, 31] scheme builds upon the earlier work of ADR, BPA, and NLBPA. AADR is formulated linearly such that the rebalance factor is an additive correction rather than multiplicative. In deriving the low-order rebalance equations a general angular dependent weighting function is used, which is similar to the projection operator of Adam's BPA method. The form of the weighting function is chosen to optimize the convergence rate via Fourier analysis. Park and Cho consider weights of $\Upsilon_n = 1$, $|\mu_n|$, and $\frac{1+|\mu_n|}{2}$ for use with the Linear Multiple Balance (LMB) discretization in slab geometry [30]. It is found that the AADR method with LMB discretization and weight $\Upsilon_n = \frac{1+|\mu_n|}{2}$ has a spectral radius $\rho < 0.2069c$. Note that DSA has a spectral radius $\rho < 0.2247c$. AADR also has generality with respect to the choice of discretization, geometry, and mesh shape. As an example, the AADR scheme in S_2-like form is given for the transport equation (1.11) and general weight function $\Upsilon(\mu)$ as

$$l_1 \frac{d}{dx} f^{+[k+1]} + l_0 \sigma_t f^{+[k+1]} = l_0 \frac{\sigma_s}{2} \left(\phi^{[k+1]} - \phi^{[k]} \right) , \tag{1.34}$$

$$-l_1 \frac{d}{dx} f^{-[k+1]} + l_0 \sigma_t f^{-[k+1]} = l_0 \frac{\sigma_s}{2} \left(\phi^{[k+1]} - \phi^{[k]} \right) , \tag{1.35}$$

where

$$f^{+[k+1]} = \psi^{[k+1]}(\mu) - \psi^{[k+1/2]}(\mu) \, , \, \mu > 0 \, , \tag{1.36}$$

$$f^{-[k+1]} = \psi^{[k+1]}(\mu) - \psi^{[k+1/2]}(\mu) \, , \, \mu < 0 \, , \tag{1.37}$$

$$l_0 = \int_0^1 \Upsilon(\mu) d\mu \,, \tag{1.38}$$

$$l_1 = \int_0^1 \mu \Upsilon(\mu) d\mu \,. \tag{1.39}$$

The scalar flux is updated by

$$\phi^{[k+1]} = \phi^{[k+1/2]} + f^{+[k+1]} + f^{-[k+1]} \tag{1.40}$$

with

$$\phi^{[k+1/2]} = \int_{-1}^1 \psi^{[k+1/2]}(\mu) d\mu \,. \tag{1.41}$$

The rebalance factors in S_2-like form are f^+ and f^-. Note that the AADR method can be derived as S_N-like and DP_N-like schemes. The AADR method has been extended to 2D Cartesian geometry in [31] using angularly dependent weights. The rebalance factors are defined over a varying number of angular domain ranges which in turn varies the number of unknowns in the low-order equations. This generally results in faster convergence as more rebalance factors are solved for, but creates an increased computational burden requiring efficient solution of the resulting low-order equations.

1.2.5 Asymptotic Diffusion Limit Analysis

We consider radiative transfer problems which typically have regions that are very optically thick. The total cross section can be greater than $10^6\,\mathrm{cm}^{-1}$ for such problems. We are particularly interested in regions that are highly optically thick, highly scattering, and have small external sources of radiation. Such regions will be referred to as "diffusive".

An example of such a radiative transfer problem where a diffusive region is contained within non-diffusive material is shown in Figure 1.1 as an approximation of a piece of the larger

more complex radiative transfer problem of the Wolf-Rayet star WR124 and nebula in the constellation Sagittarius. It is characterized by a diffusive region surrounded by non-diffusive

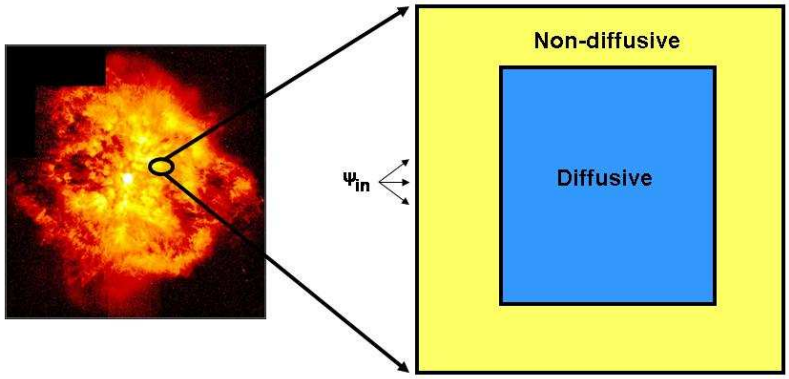

Figure 1.1: An example radiative transfer problem with diffusive region.

material which has properties unlike that of the diffusive material. This is typical of a radiative transfer problem where photons encounter both materials that are highly optically thick to their frequency and materials that are not. The physics are that an angular flux in the non-diffusive region enters the diffusive region with some angular distribution. Within a few mean free paths (mfp) beyond the interface the angular flux fully transitions to isotropic. The term "corner" is defined for later use as a location along the diffusive region material interface where an angular flux from the non-diffusive region enters a local volume of the diffusive region from more than one side. This results in an angular flux with multidimensional spatial dependence at the corner. This type of diffusive problem will be used throughout this work for analysis of

and obtaining numerical results for transport algorithms in one and two dimensions.

It is known that the diffusion equation is an asymptotic limit of the transport equation in diffusive regions [32]. Consider the 1D monoenergetic slab geometry transport equation with isotropic scattering

$$\mu\frac{\partial}{\partial x}\psi(x,\mu)+\sigma_t(x)\psi(x,\mu)=\frac{\sigma_s}{2}\int_{-1}^{1}\psi(x,\mu)d\mu+\frac{q(x)}{2}\,, \tag{1.42}$$

$$-1\le\mu\le 1\,,\,0\le x\le X\,,$$

where,

$$\psi(0,\mu)=f(\mu)\,,\,0<\mu\le 1\,, \tag{1.43}$$

$$\psi(X,\mu)=g(\mu)\,,\,-1\le\mu<0\,. \tag{1.44}$$

To examine the asymptotic limit of the transport equation (1.42), a scaling of the cross sections and source is made as

$$\sigma_t(x)=\frac{\bar{\sigma}_t(x)}{\varepsilon}\,,\quad \sigma_a(x)=\varepsilon\bar{\sigma}_a(x)\,,\quad q(x)=\varepsilon\bar{q}(x)\,, \tag{1.45}$$

where $\varepsilon\to 0$, $\sigma_s=\sigma_t-\sigma_a$, and each cross section and source are O(1). The physical interpretation of this small parameter is

$$\varepsilon=\frac{\text{typical mean free path of the problem}}{\text{typical dimension in mfp of the problem}}\,. \tag{1.46}$$

This is not the only possible scaling, but it does have the desirable properties that it does not depend on the physical size of the problem, gives an infinite-medium solution and diffusion length ($L=(3\sigma_a\sigma_t)^{-1/2}$) that are O(1), and the diffusion equation is invariant with respect to this scaling. An asymptotic diffusion limit analysis of the transport equation (1.42) proceeds as:

1. The scaled cross sections and external source (1.45) are introduced into (1.42).

2. The angular flux is assumed to be able to be expanded in a power series of ε as

$$\psi(x,\mu) = \sum_{l=0}^{\infty} \varepsilon^l \psi^{[l]}(x,\mu)\,. \tag{1.47}$$

3. The previous ansatz is substituted into the scaled transport equation.

4. The coefficients of each power of epsilon are equated to obtain a system of equations for the expansion coefficients $\psi^{[l]}$.

5. The system of equations are recursively solved to obtain an equation comprised solely of leading order terms. These equations are then unscaled by performing the reverse of step 1.

The leading order solution of the transport equation in the asymptotic diffusion limit then fits the diffusion equation

$$-\frac{d}{dx}\frac{1}{3\sigma_t}\frac{d}{dx}\phi^{[0]}(x) + \sigma_a(x)\phi^{[0]}(x) = q(x)\,. \tag{1.48}$$

Further analysis at the boundary of the diffusive region (material interface) yields that the leading-order solution of equation (1.42) in a diffusive region satisfies the Dirichlet boundary conditions [32, 33, 34]

$$\phi^{[0]}(0) = 2\int_0^1 W(\mu) f(\mu) d\mu\,, \tag{1.49}$$

$$\phi^{[0]}(X) = 2\int_{-1}^0 W(-\mu) g(\mu) d\mu\,, \tag{1.50}$$

where

$$W(\mu) = \frac{\mu}{X(-\mu)}\left(\int_0^1 \frac{s}{X(-s)} ds\right)^{-1}\,, \tag{1.51}$$

$$W(\mu) \approx \widehat{W}(\mu) = 0.956\mu + 1.565\mu^2\,, \tag{1.52}$$

$$\sup_{0\leq\mu\leq1} |W(\mu) - \widehat{W}(\mu)| = 0.0035\,. \tag{1.53}$$

The function $X(-\mu)$ is tabulated in [34] and $W(\mu)$ is termed the asymptotic boundary condition weight function.

This analysis has been used in 1D for the interior of diffusive regions which allowed for the evaluation and downselection of many commonly used discretization schemes [35]. Consider that even with modern computers it is not feasible to treat most practical problems with a fine enough mesh (on the scale of ε) to fully resolve the solution's true behavior at the interior of diffusive region material interfaces. This analysis was extended in order to determine the leading order asymptotic boundary condition for the diffusion equation in diffusive regions with unresolved boundary layers [36, 37]. This is important because any errors in the asymptotic boundary condition cause inaccuracies inside the diffusion region. It is not uncommon for the solution to be in error by a factor of two. The asymptotic diffusion limit analysis is a powerful tool and continues to be applied to all forms and discretization schemes of the transport equation that are used to solve problems containing diffusive regions [37, 38, 39, 40].

In order for a method to produce an accurate solution in diffusive regions on a coarse mesh (relative to a mfp) it must have two properties:

1. The leading order solution of the method must limit to a stable and consistent discretization of the diffusion equation.

2. The method must suitably resolve boundary layers at interfaces of diffusive regions.

Asymptotic analysis of methods in continuous and discrete form provide a pathway for developing methods that possess the asymptotic diffusion limit. In the following chapters, asymptotic diffusion limit analysis will be performed for transport methodologies in continuous form, dis-

cretized form, inside diffusive regions, and at diffusive region interfaces far from corners in terms of mfp to determine their properties. The same basic steps will be used as shown above. The analysis predicts precisely how methods behave in such problems.

1.2.6 Fourier Analysis

Characterization of any iterative method would not be complete without an analysis of the method's stability properties. Most simply, the performance of the NWF methods may be tested on numerical problems with varying parameters such as optical thickness and scattering ratio by numerically estimating the spectral radius. Iterative matrix analysis can be used to determine the spectral radius of an iterative process by formulating the system $\mathbf{x}^{(k+1)} = A\mathbf{x}^{(k)}$. This is for finite domain problems. A powerful tool for determining the convergence properties of an iterative method for infinite domain problems is Fourier analysis.

A Fourier analysis has been used to analytically determine the spectral radius of linear transport methods in continuous and discretized form [16, 13]. Fourier analysis is a classic and well-known tool, but the methods must be linear in order to use it. Since the NWF methods are nonlinear, they must first be linearized. This is accomplished by linearizing the method around the solution of a special class of infinite medium problems before performing the analysis [41]. The iterative solution is assumed to begin "near" that of an infinite medium homogenous problem's flat solution with an initial error. Then, the iterative behavior of this error is analyzed with a standard Fourier analysis. The rate at which this error changes gives the spectral radius of the iterative scheme. The spectral radius depends upon the scattering ratio, cell optical thickness, and of course the formulation of the method itself.

1.3 Main Results Presented for the Defense

The goal of this research is the development of a new parameterized family of Nonlinear Weighted Flux (NWF) methods with advanced properties for the accurate solution of the transport equation in multidimensional Cartesian geometry. In this dissertation we present the following results:

1. A new 1D family of flux methods is developed that satisfies an accurate approximation of the diffusion equation and asymptotic boundary condition in diffusive regions which converges fast.

2. The new family of flux methods is developed for 2D Cartesian geometry.

3. The 2D methods are analyzed by asymptotic diffusion limit analysis and a specific method formulated that limits to the diffusion equation with accurate boundary conditions in the asymptotic diffusion limit.

4. The convergence properties of the 2D methods are analyzed by Fourier analysis and numerical problems.

The results of item 1 have been published and presented at the American Nuclear Society (ANS) Mathematics and Computation (M&C) division's topical meeting in September, 2005 [42]. A full version of this paper has been published in the journal Transport Theory and Statistical Physics [43]. The initial 2D results have been published and presented at the ANS M&C topical meeting in April, 2007 [44]. An extended version of the 2D work will be submitted to the journal Nuclear Science and Engineering.

1.4 Dissertation Organization

The dissertation is organized as follows:

Chapter 2: The NWF family of methods is developed in 1D Cartesian geometry, discretized, and analyzed by both asymptotic diffusion limit analysis and Fourier analysis. Numerical results are presented.

Chapter 3: The NWF family of methods is developed in 2D Cartesian geometry in general form and discretized. An asymptotic diffusion limit analysis is applied to the 2D NWF methods in differential and discretized form in order to define specific methods within the family with the desired property of an accurate diffusion limit. Numerical results are presented.

Chapter 4: A Fourier analysis of the 2D NWF family of methods is presented in differential form. Numerical convergence results are presented.

Chapter 5: Conclusions and recommendations for future work are presented.

Chapter 2

DEVELOPMENT AND ANALYSIS OF THE 1D NWF METHOD

In this chapter, the development of the 1D Nonlinear Weighted Flux methods is shown. It is the objective of the 1D work to develop a new nonlinear flux-type method with an accurate asymptotic diffusion limit. This is necessary to guide the development of the NWF methods in 2D.

A new parameterized family of iterative methods for the 1D slab geometry transport equation is presented. The new methods are derived by integrating the transport equation over angular subdomains with general weights of the directional cosine, μ. The asymptotic diffusion analysis enables the determination of a particular method of this family the solution of which satisfies an accurate approximation of both the diffusion equation and asymptotic boundary condition in the diffusive regions. The iterative convergence properties of the new family of methods are analyzed by Fourier analysis. Finally, numerical results are presented

to demonstrate the performance of the derived method. The results presented in this chapter were published in [42, 43].

2.1 Formulation of the Family of Methods

Consider the one-group transport equation for 1D slab geometry with isotropic scattering:

$$\mu\frac{\partial}{\partial x}\psi(x,\mu)+\sigma_t(x)\psi(x,\mu)=\frac{1}{2}\sigma_s(x)\int_{-1}^{1}\psi(x,\mu')d\mu'+\frac{1}{2}q(x)\,, \tag{2.1}$$
$$-1\le\mu\le 1\,,\quad 0\le x\le L\,,$$

with the reflective boundary condition at $x=0$

$$\psi(0,\mu)=\psi(0,-\mu)\,,\quad \text{for}\quad \mu>0\,, \tag{2.2}$$

and an incident flux at $x=L$

$$\psi(L,\mu)=\Psi_{in}(\mu)\,,\quad \text{for}\quad \mu<0\,. \tag{2.3}$$

Here $\psi(x,\mu)$ is the angular flux, σ_t and σ_s are total and scattering cross sections, correspondingly, q is an external source of particles.

The approach of developing transport methods using various weight functions was proposed and applied in [4, 5, 7]. The α-WN methods are derived with a general weight $|\mu|^\alpha$ (See 1.2.3) where it is possible to optimize the value of α to achieve an optimal convergence rate, or to get low-order equations that can be reduced to the diffusion equation. It is this idea that a general weight can be fixed in order to obtain necessary properties of a method for a specific class of problems that is expanded upon in this work.

To derive the new family of flux methods, we formulate the low-order equations in terms of the partial scalar fluxes

$$\phi^{-}(x) = \int_{-1}^{0} \psi(x,\mu)d\mu\,, \tag{2.4}$$

$$\phi^{+}(x) = \int_{0}^{1} \psi(x,\mu)d\mu\,, \tag{2.5}$$

by operating on the transport equation (Eq. (2.1)) with the following weights:

$$\gamma \int_{-1}^{0} (1+\beta|\mu|^{\alpha}))(\cdot)d\mu\,, \tag{2.6}$$

$$\gamma \int_{0}^{1} (1+\beta\mu^{\alpha})(\cdot)d\mu\,. \tag{2.7}$$

Here, $\alpha \geq 0$ and β are parameters, and

$$\gamma = \left(1 + \frac{\beta}{\alpha+1}\right)^{-1}\,. \tag{2.8}$$

This general linear weight is selected for study for two reasons known apriori. First, the absolute value of μ is considered so that the resulting weight is a well-defined real function over the angular domain for arbitrary $\alpha \geq 0$. Second, this weight has one more degree of freedom than the α-WN methods.

Operating on the transport equation (Eq. 2.1) with the weights (Eqs. 2.6 and 2.7) results in the following equations

$$-\frac{d}{dx}\left(\gamma \int_{0}^{-1} (1+\beta|\mu|^{\alpha})|\mu|\psi(x,\mu)d\mu\right) + \sigma_t(x)\gamma \int_{0}^{-1} (1+\beta|\mu|^{\alpha})\psi(x,\mu)d\mu = \frac{1}{2}\left(\sigma_s(x)\phi(x) + q(x)\right)\,, \tag{2.9}$$

$$\frac{d}{dx}\left(\gamma \int_{0}^{1} (1+\beta|\mu|^{\alpha})|\mu|\psi(x,\mu)d\mu\right) + \sigma_t(x)\gamma \int_{0}^{1} (1+\beta|\mu|^{\alpha})\psi(x,\mu)d\mu = \frac{1}{2}\left(\sigma_s(x)\phi(x) + q(x)\right)\,. \tag{2.10}$$

These equations must be closed, and this is done by defining the linear fractional factors

$$G^{\pm}(x) = \frac{\gamma \int_0^{\pm 1} (1+\beta|\mu|^{\alpha})\psi(x,\mu)d\mu}{\int_0^{\pm 1} \psi(x,\mu)d\mu}, \tag{2.11}$$

$$F^{\pm}(x) = \frac{\gamma \int_0^{\pm 1} |\mu|(1+\beta|\mu|^{\alpha})\psi(x,\mu)d\mu}{\int_0^{\pm 1} \psi(x,\mu)d\mu}, \tag{2.12}$$

which nonlinearly depend on the transport solution. The physical interpretation of the factors are an average value of the polynomial weight of directional cosines with the angular flux as the averaging function. Using the factors (2.11)-(2.12) in (2.9)-(2.10) and formulating in terms of the partial scalar fluxes gives the low-order NWF equations as

$$-\frac{d}{dx}\left(F^{-}(x)\phi^{-}(x)\right) + \left(\sigma_t(x)G^{-}(x) - \frac{1}{2}\sigma_s(x)\right)\phi^{-}(x) = \frac{1}{2}\left(\sigma_s(x)\phi^{+}(x) + q(x)\right), \tag{2.13}$$

$$\frac{d}{dx}\left(F^{+}(x)\phi^{+}(x)\right) + \left(\sigma_t(x)G^{+}(x) - \frac{1}{2}\sigma_s(x)\right)\phi^{+}(x) = \frac{1}{2}\left(\sigma_s(x)\phi^{-}(x) + q(x)\right), \tag{2.14}$$

The nonlinear weighted flux (NWF) methods are defined by the following set of equations:

$$\mu\frac{\partial}{\partial x}\psi^{(k+1/2)} + \sigma_t\psi^{(k+1/2)} = \frac{1}{2}\left(\sigma_s\phi^{(k)} + q\right), \tag{2.15}$$

$$\psi^{(k+1/2)}(0,\mu) = \psi^{(k+1/2)}(0,-\mu), \quad \text{for } \mu > 0, \tag{2.16}$$

$$\psi^{(k+1/2)}(L,\mu) = \Psi_{in}(\mu), \quad \text{for } \mu < 0, \tag{2.17}$$

$$G^{\pm(k+1/2)} = \frac{\gamma \int_0^{\pm 1} (1+\beta|\mu|^{\alpha})\psi^{(k+1/2)}d\mu}{\int_0^{\pm 1} \psi^{(k+1/2)}d\mu}, \tag{2.18}$$

$$F^{\pm(k+1/2)} = \frac{\gamma \int_0^{\pm 1} |\mu|(1+\beta|\mu|^{\alpha})\psi^{(k+1/2)}d\mu}{\int_0^{\pm 1} \psi^{(k+1/2)}d\mu}, \tag{2.19}$$

$$-\frac{d}{dx}\left(F^{-(k+1/2)}\phi^{-(k+1)}\right)+\left(\sigma_t G^{-(k+1/2)}-\frac{1}{2}\sigma_s\right)\phi^{-(k+1)}=\frac{1}{2}\left(\sigma_s\phi^{+(k+1)}+q\right), \tag{2.20}$$

$$\frac{d}{dx}\left(F^{+(k+1/2)}\phi^{+(k+1)}\right)+\left(\sigma_t G^{+(k+1/2)}-\frac{1}{2}\sigma_s\right)\phi^{+(k+1)}=\frac{1}{2}\left(\sigma_s\phi^{-(k+1)}+q\right), \tag{2.21}$$

$$\phi^{+(k+1)}(0)=\phi^{-(k+1)}(0), \tag{2.22}$$

$$\phi^{-(k+1)}(L)=\Phi^{-}_{in}, \quad \text{where} \quad \Phi^{-}_{in}=\int_{-1}^{0}\Psi_{in}(\mu)d\mu, \tag{2.23}$$

$$\phi^{(k+1)}=\phi^{+(k+1)}+\phi^{-(k+1)}. \tag{2.24}$$

Here k is the iteration index. The structure of Eqs. (2.20)-(2.21) is similar in form to that of the transport equation. Note that no approximation has been made in deriving this system of equations. As a result, the system of equations (2.1)-(2.3) and (2.11)-(2.14) is equivalent to the original linear transport problem. Boundary conditions are easy to define in the context of partial scalar fluxes as shown by Eqs. (2.23) and (2.22).

The nonlinear iteration scheme consists of three stages:

1. A transport sweep to calculate the angular flux $\psi^{(k+1/2)}$ (Eqs. (2.15)-(2.17)).
2. The calculation of the factors $G^{\pm(k+1/2)}$ and $F^{\pm(k+1/2)}$ from $\psi^{(k+1/2)}$ (Eqs. (2.18)-(2.19)).
3. Solving the low-order problem (Eqs. (2.20)-(2.23)) for $\phi^{\pm(k+1)}$ using $G^{\pm(k+1/2)}$ and $F^{\pm(k+1/2)}$.

The initial guess is generated by solving the low-order equations with factors evaluated with an isotropic angular flux.

2.2 Discretization

We now spatially discretize the equations of the NWF methods using independent differencing schemes for the transport and low-order equations. A discretization method that

is known to work well for the transport equation can be utilized because of the similar form of the low-order equations. This will produce a method which is not purely an acceleration method, but a fast convergent transport iterative method.

The approximation of the low-order equations is based on the linear discontinuous (LD) finite element method that was formulated for the transport equation [45, 46]. It has been shown to be very accurate in the asymptotic diffusion limit of 1D problems [36]. The spatial mesh $\{x_{j-1/2},\ j=1,...,N,\ x_{1/2}=0,\ x_{N+1/2}=L\}$ is introduced. Cell average unknowns are denoted by X_j and cell edge unknowns as $X_{j\pm1/2}$. The equations (2.20) and (2.21) are integrated over the jth cell with weights 1 and $x-x_j$, where $x_j=0.5(x_{j+1/2}+x_{j-1/2})$. Then, the auxiliary conditions are formulated using the assumption that $\phi^{\pm}$ in the cell are linear functions defined by their zeroth and first spatial moments. The resulting discretized low-order equations of the NWF methods have the following form:

$$-(F^-_{j+1/2}\phi^-_{j+1/2}-F^-_{j-1/2}\phi^-_{j-1/2})+(\sigma_{t,j}G^-_j-0.5\sigma_{s,j})\phi^-_j\Delta x_j=0.5(\sigma_{s,j}\phi^+_j+q_j)\Delta x_j\ , \quad (2.25)$$

$$F^+_{j+1/2}\phi^+_{j+1/2}-F^+_{j-1/2}\phi^+_{j-1/2}+(\sigma_{t,j}G^+_j-0.5\sigma_{s,j})\phi^+_j\Delta x_j=0.5(\sigma_{s,j}\phi^-_j+q_j)\Delta x_j\ , \quad (2.26)$$

$$\begin{aligned}-\theta_j(F^-_{j+1/2}\phi^-_{j+1/2}+F^-_{j-1/2}\phi^-_{j-1/2}-2F^-_j\phi^-_j)+(\sigma_{t,j}G^-_j-0.5\sigma_{s,j})\hat{\phi}^-_j\Delta x_j\\ =0.5(\sigma_{s,j}\hat{\phi}^+_j+\hat{q}_j)\Delta x_j\ ,\end{aligned} \quad (2.27)$$

$$\begin{aligned}\theta_j(F^+_{j+1/2}\phi^+_{j+1/2}+F^+_{j-1/2}\phi^+_{j-1/2}-2F^+_j\phi^+_j)+(\sigma_{t,j}G^+_j-0.5\sigma_{s,j})\hat{\phi}^+_j\Delta x_j\\ =0.5(\sigma_{s,j}\hat{\phi}^-_j+\hat{q}_j)\Delta x_j\ ,\end{aligned} \quad (2.28)$$

$$\hat{\phi}^-_j=\phi^-_j-\phi^-_{j-1/2}\ , \quad (2.29)$$

$$\hat{\phi}^+_j=\phi^+_{j+1/2}-\phi^+_j\ , \quad (2.30)$$

$$\phi^+_{1/2} = \phi^-_{1/2} \,, \tag{2.31}$$

$$\phi^-_{N+1/2} = \Phi^-_{in} \,, \tag{2.32}$$

$$F^\pm_j = 0.5(F^\pm_{j+1/2} + F^\pm_{j-1/2}) \,, \tag{2.33}$$

$$G^\pm_j = 0.5(G^\pm_{j+1/2} + G^\pm_{j-1/2}) \,, \tag{2.34}$$

where

$$\hat{\phi}^\pm_j = \frac{6}{\Delta x_j^2} \int_{x_{j-1/2}}^{x_{j+1/2}} (x - x_j)\phi^\pm(x)dx \,, \tag{2.35}$$

$$\hat{q}_j = \frac{6}{\Delta x_j^2} \int_{x_{j-1/2}}^{x_{j+1/2}} (x - x_j)q(x)dx \,, \tag{2.36}$$

$$\Delta x_j = x_{j+1/2} - x_{j-1/2} \,. \tag{2.37}$$

Again, integer $\pm\frac{1}{2}$ subscripts refer to cell-edge quantities, and integer subscripts refer to cell-average quantities. Here θ_j is a "lumping" parameter; $\theta_j = 3$ corresponds to the standard LD method; $\theta_j = 1$ corresponds to a lumped LD method [36] that is used for optically thick cells. Lumping adds robustness to a method, although usually at the cost of accuracy. In this case, it turns out that lumping is necessary in order to obtain the correct form of the discretized diffusion equation in the asymptotic diffusion limit. In case the jth interval is optically thick, the values of the cell-average factors are defined in terms of downstream located factors

$$F^-_j = F^-_{j-1/2}, \quad G^-_j = G^-_{j-1/2} \,, \tag{2.38}$$

$$F^+_j = F^+_{j+1/2}, \quad G^+_j = G^+_{j+1/2} \,. \tag{2.39}$$

To solve the transport equation, the Step Characteristic (SC) method is used

$$\mu_m(\psi_{m,j+1/2} - \psi_{m,j-1/2}) + \sigma_{t,j}\Delta x_j(T_{m,j}\psi_{m,j-1/2} + (1 - T_{m,j})\psi_{m,j+1/2}) = 0.5(\sigma_{s,j}\phi_j + q_j)\Delta x_j \,, \tag{2.40}$$

$$T_{m,j} = \frac{1}{\tau_{m,j}} - \frac{1}{e^{\tau_{m,j}} - 1} \quad , \quad \text{where} \quad \tau_{m,j} = \frac{\sigma_{t,j}\Delta x_j}{\mu_m} \quad . \tag{2.41}$$

$$m = 1, ..., M \, . \tag{2.42}$$

The subscript m denotes the discrete ordinates number. This provides a monotonic and non-negative angular flux solution for the calculation of the low-order factors (2.18) and (2.19). The SC method is solved by sweeping cells in the mesh for each angle.

2.3 Continuous Form Asymptotic Diffusion Analysis

The focus of this work is in the development of methods the low-order equations of which can be reduced to the diffusion equation in an optically thick medium. Preliminary to putting forth the effort of a full discretized asymptotic diffusion limit analysis of the NWF methods, an asymptotic analysis is performed for the continuous form of the method. Following the procedure outlined in the introduction (see Section 1.2.5), scaled cross sections (1.45) and the ansatz (1.47) are substituted into Eqs. (2.15), and (2.18)-(2.21). Then coefficients of equal order of ε are equated to form a set of linear equations.

As a result of analyzing the scaled and expanded Eq. (2.15), the leading order angular flux, $\psi^{[0]}(x, \mu)$, is isotropic. Then,

$$G^{\pm} = 1 \, , \tag{2.43}$$

$$F^{\pm} = \zeta \, , \tag{2.44}$$

where

$$\zeta = \left(\frac{1}{2} + \frac{\beta}{\alpha + 2} \right) \left(1 + \frac{\beta}{\alpha + 1} \right)^{-1} \, . \tag{2.45}$$

After some straightforward manipulations, the resulting equations from the low-order equations (2.20) and (2.21) are:

$\underline{O(\varepsilon^{-1})}$:

$$\phi^{\pm[0]} = \frac{1}{2}\phi^{[0]}\,, \tag{2.46}$$

$\underline{O(1)}$:

$$\zeta\frac{d}{dx}\left(\phi^{+[0]} + \phi^{-[0]}\right) = \bar{\sigma}_t\left(\phi^{-[1]} - \phi^{+[1]}\right)\,, \tag{2.47}$$

$\underline{O(\varepsilon^{1})}$:

$$\zeta\frac{d}{dx}\left(\phi^{-[1]} - \phi^{+[1]}\right) - \bar{\sigma}_a\phi^{[0]} = -\bar{q}\,. \tag{2.48}$$

Next, equations (2.43)-(2.48) are easily reduced and unscaled to the following second-order equation for the partial scalar fluxes:

$$-\zeta^2\frac{d}{dx}\frac{1}{\sigma_t}\frac{d}{dx}\phi^{[0]} + \sigma_a\phi^{[0]} = q\,, \tag{2.49}$$

where

$$\phi^{[0]} = \phi^{+[0]} + \phi^{-[0]}\,, \tag{2.50}$$

$$\sigma_a = \sigma_t - \sigma_s\,, \tag{2.51}$$

are the leading-order scalar flux and the absorption cross section, respectively. The diffusion coefficient of this equation is given by $\frac{\zeta^2}{\sigma_t}$. Clearly, if

$$\zeta = \frac{1}{\sqrt{3}}\,, \tag{2.52}$$

then Eq. (2.49) is equivalent to the diffusion equation with the correct diffusion coefficient, $\frac{1}{3\sigma_t}$. Equation (2.52) is the first condition on the α and β parameters of the methods. Another

important issue of the asymptotic diffusion limit is related to boundary conditions. The detailed asymptotic analysis presented below (see Section 2.4) provides the second condition on these parameters.

2.4 Discretized Form Asymptotic Diffusion Analysis

An asymptotic diffusion analysis [37] of the discretized equations of the NWF methods is performed in order to determine if they limit to a stable and consistent diffusion equation. We analyze the form of the asymptotic boundary condition and determine the remaining constraint on α and β . The analysis proceeds as outlined in Section 1.2.5, except the discretized equations are used. A brief summary of the steps is reproduced here.

First, define a small parameter ε, scaled cross sections and sources

$$\sigma_{t,j} = \frac{\bar{\sigma}_{t,j}}{\varepsilon}\,, \quad \sigma_{a,j} = \varepsilon\bar{\sigma}_{a,j}\,, \quad q_j = \varepsilon\bar{q}_j\,, \quad \hat{q}_j = \varepsilon\breve{q}_j\,, \tag{2.53}$$

and consider the transport problem as $\varepsilon \to 0$. It is assumed that the solution can be expanded in an asymptotic power series in ε:

$$\psi_{m,j+1/2} = \sum_{l=0}^{\infty} \varepsilon^l \psi^{[l]}_{m,j+1/2}\,, \quad \phi^{\pm}_{j} = \sum_{l=0}^{\infty} \varepsilon^l \phi^{\pm[l]}_{j}\,, \quad \phi^{\pm}_{j+1/2} = \sum_{l=0}^{\infty} \varepsilon^l \phi^{\pm[l]}_{j+1/2}\,, \quad \hat{\phi}^{\pm}_{j} = \sum_{l=0}^{\infty} \varepsilon^l \hat{\phi}^{\pm[l]}_{j} \tag{2.54}$$

and introduce (2.54) into Eqs. (2.25)-(2.32) and (2.38)-(2.41). The angular flux is again isotropic in the leading order term and the factors $G^{\pm}_{j-1/2}$ and $F^{\pm}_{j-1/2}$ have values of 1 and ζ at each interior cell edge where they are calculated, respectively.

Next, the coefficients of different powers of ε are equated. After simple manipulations, the resulting equations are:

$\underline{O(\varepsilon^{-1})}$:

$$\phi_j^{\pm[0]} = \frac{1}{2}\phi_j^{[0]}\,, \tag{2.55}$$

$$\widehat{\phi}_j^{\pm[0]} = \frac{1}{2}\widehat{\phi}_j^{[0]}\,, \tag{2.56}$$

$\underline{O(1)}$:

$$\phi_{j+1/2}^{\pm[0]} = \frac{1}{2}\phi_{j+1/2}^{[0]}\,, \tag{2.57}$$

$$\widehat{\phi}_j^{[0]} = \frac{1}{2}\left(\phi_{j+1/2}^{[0]} - \phi_{j-1/2}^{[0]}\right)\,, \tag{2.58}$$

$$\phi_j^{[0]} = \frac{1}{2}\left(\phi_{j-1/2}^{[0]} + \phi_{j+1/2}^{[0]}\right)\,, \tag{2.59}$$

$$\phi_j^{-[1]} - \phi_j^{+[1]} = \frac{\zeta}{\bar{\sigma}_{t,j}\Delta x_j}\left(\phi_{j+1/2}^{[0]} - \phi_{j-1/2}^{[0]}\right)\,, \tag{2.60}$$

$\underline{O(\varepsilon^{1})}$:

$$\phi_{j+1/2}^{-[1]} - \phi_{j+1/2}^{+[1]} + \phi_{j-1/2}^{+[1]} - \phi_{j-1/2}^{-[1]} = \frac{\Delta x_j}{\gamma}\left(\bar{\sigma}_{a,j}\phi_j^{[0]} - \bar{q}\right)\,, \tag{2.61}$$

$$\phi_{j+1/2}^{-[1]} - \phi_{j+1/2}^{+[1]} + \phi_{j-1/2}^{-[1]} - \phi_{j-1/2}^{+[1]} = \frac{4\zeta}{\bar{\sigma}_{t,j}\Delta x_j}\widehat{\phi}_j^{[0]} + \frac{\Delta x_j}{\theta_j\zeta}\left(\bar{\sigma}_{a,j}\widehat{\phi}_j^{[0]} - \breve{q}_j\right)\,, \tag{2.62}$$

where $\Delta x_j = x_{j+1/2} - x_{j-1/2}$.

The analysis of the obtained scaled and expanded equations shows that the leading-order solution satisfies the following equation in the interior of the diffusion region:

$$-\zeta^2\Big(\frac{1}{\sigma_{t,j+1}\Delta x_{j+1}}(\phi_{j+3/2}^{[0]} - \phi_{j+1/2}^{[0]}) - \frac{1}{\sigma_{t,j}\Delta x_j}(\phi_{j+1/2}^{[0]} - \phi_{j-1/2}^{[0]})\Big) \tag{2.63}$$

$$+0.5(\sigma_{a,j}\Delta x_j + \sigma_{a,j+1}\Delta x_{j+1})\phi_{j+1/2}^{[0]} = 0.5\Big((q_j + \hat{q}_j)\Delta x_j + (q_{j+1} - \hat{q}_{j+1})\Delta x_{j+1}\Big)\,,$$

$$\phi_{j+1/2}^{\pm[0]} = 0.5\phi_{j+1/2}^{[0]}\,, \tag{2.64}$$

which is easily recognized as a discretized form of the diffusion equation over two cells. The diffusion coefficient is generally given by $\zeta^2/\sigma_{t,j}$ in each cell. This is the same as the continuous

form analysis result. These results demonstrate that if $\zeta = \frac{1}{\sqrt{3}}$, the leading-order solution meets a reasonable spatial approximation of the correct diffusion equation that represents a stable and consistent discretization of this partial differential equation. At this point, the one remaining degree of freedom still remains unfixed.

Next, the asymptotic analysis is applied to the method in the boundary cell (2.32) to determine the asymptotic boundary condition. Eqs. (2.55)-(2.62) are considered for $j = N$, the right hand side boundary cell. Note that only the linear-fractional factors for outgoing directions on the boundary edge will be calculated from isotropic angular fluxes. Incoming direction factors are evaluated with the incoming angular flux. An equation for the leading-order cell-edge scalar flux at the boundary is algebraically solved for. As a result, the boundary condition for the leading order solution (2.63) is defined as

$$\phi^{[0]}_{N+1/2} = 2\frac{F^{-}_{N+1/2}}{\zeta}\phi^{-[0]}_{N+1/2}\,, \tag{2.65}$$

where

$$F^{-}_{N+1/2} = \sum_{\mu_m \leq 0} |\mu_m|(1+\beta|\mu_m|^{\alpha})\Psi_{in}(\mu_m)w_m\,, \tag{2.66}$$

$$\phi^{-[0]}_{N+1/2} = \sum_{\mu_m \leq 0} \Psi_{in}(\mu_m)w_m\,, \tag{2.67}$$

and w_m are quadrature weights. Rewriting gives

$$\phi^{[0]}_{N+1/2} = \frac{2}{\frac{1}{2}+\frac{\beta}{\alpha+2}} \sum_{\mu_m \leq 0} \left(|\mu_m| + \beta|\mu_m|^{\alpha+1}\right)\Psi_{in}(\mu_m)w_m\,. \tag{2.68}$$

Remember from Section 1.2.5 that the asymptotic diffusion analysis of the transport equation in continuous form yields that the leading-order solution meets the boundary condition

$$\phi(L) = 2\int_{-1}^{0} W(-\mu)\Psi_{in}(\mu)d\mu\,, \tag{2.69}$$

where

$$W(\mu) = \frac{\mu}{X(-\mu)} \left(\int_0^1 \frac{s}{X(-s)} ds \right)^{-1} \approx 0.956\mu + 1.565\mu^2 \,. \tag{2.70}$$

The NWF method's boundary condition satisfied by the leading-order solution (Eq. 2.68) can be interpreted as an approximation of the following boundary condition in continuous form:

$$\phi^{[0]}(L) = 2 \int_{-1}^{0} \widetilde{W}(-\mu) \Psi_{in}(\mu) d\mu \,, \tag{2.71}$$

where

$$\widetilde{W}(\mu) = \frac{1}{\frac{1}{2} + \frac{\beta}{\alpha+2}} (\mu + \beta \mu^{\alpha+1}) \,. \tag{2.72}$$

Notice that the polynomial of μ is quadratic in Eq. (2.70) and of order $\alpha + 1$ in Eq. (2.72). It is then natural to take $\alpha = 1$ as the second requirement on the linear weight which then fixes $\beta = \sqrt{3}$ by using the earlier requirement on the diffusion coefficient. This defines a particular member of the NWF family of methods with desired properties. The NWF method with $\alpha = 1$ and $\beta = \sqrt{3}$ gives rise to

$$\zeta = \frac{1}{\sqrt{3}} \,, \tag{2.73}$$

$$\widetilde{W}(\mu) = \frac{2\sqrt{3}}{2 + \sqrt{3}} (\mu + \sqrt{3}\mu^2) \approx 0.9282\mu + 1.608\mu^2 \,. \tag{2.74}$$

The comparison between the quadratic polynomial approximation of $W(\mu)$ and the function $\widetilde{W}(\mu)$ over interval $0 \leq \mu \leq 1$ shows that

$$\max_{0 \leq \mu \leq 1} |W(\mu) - \widetilde{W}(\mu)| = 0.0177 \,, \tag{2.75}$$

$$\|W(\mu) - \widetilde{W}(\mu)\|_{L_1} = 0.0043 \,, \tag{2.76}$$

and in discrete form with the double S_8 Gauss-Legendre quadrature set

$$\max_m |W(\mu_m) - \widetilde{W}(\mu_m)| = 0.0138 \,, \tag{2.77}$$

which are all small quantities.

The NWF method with such set of parameters α and β generates the solution in the diffusive regions that satisfies a reasonable approximation of the diffusion equation and asymptotic boundary condition. This is a combination of properties that no other flux method in 1D is known to possess.

2.5 Fourier Analysis

In order to determine how effective an iterative method is, the convergence properties must be studied. The convergence rate will be a function of the method, the optical thickness of the mesh, and the scattering ratio. The convergence rate is determined by performing a Fourier analysis of the discretized equations, but it is first necessary to linearize the NWF method.

The NWF methods in discretized form are linearized around an exact solution of an infinite-medium problem with constant cross sections and source of the following form:

$$\psi_{m,j+1/2} = \frac{q}{2\sigma_a} \,. \tag{2.78}$$

Then consider such iterations that the estimation of the solution begins close to the exact solution and assume that

$$\psi_{m,j+1/2}^{(k+1/2)} = \frac{q}{\sigma_a}\left(\frac{1}{2} + \epsilon\eta_{m,j+1/2}^{(k+1/2)}\right), \tag{2.79}$$

$$\phi_{j+1/2}^{\pm(k)} = \frac{q}{\sigma_a}\left(\frac{1}{2} + \epsilon\xi_{j+1/2}^{\pm(k)}\right), \tag{2.80}$$

$$\phi_{j}^{\pm(k)} = \frac{q}{\sigma_a}\left(\frac{1}{2} + \epsilon\xi_{j}^{\pm(k)}\right), \tag{2.81}$$

$$\phi_{j}^{(k)} = \frac{q}{\sigma_a}\left(1 + \epsilon\xi_{j}^{(k)}\right), \tag{2.82}$$

where $\epsilon \ll 1$. The rate at which the error terms in the equations go to zero will give the convergence rate of the method for this class of problems.

The next step in linearization is to introduce this ansatz (Eqs. (2.79)-(2.82)) into Eqs. (2.25)-(2.30), and (2.40), taking into account the iteration process (2.15)-(2.24). All terms in the equations are expanded and grouped by powers of ϵ. The O(1) terms cancel out because they directly satisfy the original equations of the method. Neglect the quadratic and higher ϵ terms. Finally, the following set of linearized equations are obtained,

$$\mu_m(\eta_{m,j+1/2}^{(k+1/2)} - \eta_{m,j-1/2}^{(k+1/2)}) + \sigma_t \Delta x_j (T_m \eta_{m,j-1/2}^{(k+1/2)} + (1 - T_m)\eta_{m,j+1/2}^{(k+1/2)}) = 0.5\sigma_s \Delta x_j \xi_j^{(k)} \ , \quad (2.83)$$

$$\begin{aligned} -\zeta(\xi_{j+1/2}^{-(k+1)} - \xi_{j-1/2}^{-(k+1)}) + (\sigma_t - 0.5\sigma_s)\Delta x_j \xi_j^{-(k+1)} - 0.5\sigma_s \Delta x_j \xi_j^{+(k+1)} \\ = f_{j+1/2}^{-(k+1/2)} - f_{j-1/2}^{-(k+1/2)} - 0.5\sigma_t \Delta x_j (g_{j-1/2}^{-(k+1/2)} + g_{j+1/2}^{-(k+1/2)}) \ , \end{aligned} \quad (2.84)$$

$$\begin{aligned} \zeta(\xi_{j+1/2}^{+(k+1)} - \xi_{j-1/2}^{+(k+1)}) + (\sigma_t - 0.5\sigma_s)\Delta x_j \xi_j^{+(k+1)} - 0.5\sigma_s \Delta x_j \xi_j^{-(k+1)} \\ = f_{j-1/2}^{+(k+1/2)} - f_{j+1/2}^{+(k+1/2)} - 0.5\sigma_t \Delta x_j (g_{j-1/2}^{+(k+1/2)} + g_{j+1/2}^{+(k+1/2)}) \ , \end{aligned} \quad (2.85)$$

$$\begin{aligned} -\theta\zeta(\xi_{j+1/2}^{-(k+1)} + \xi_{j-1/2}^{-(k+1)} - 2\xi_j^{-(k+1)}) + (\sigma_t - 0.5\sigma_s)\Delta x_j (\xi_j^{-(k+1)} - \xi_{j-1/2}^{-(k+1)}) \\ -0.5\sigma_s \Delta x_j (\xi_{j+1/2}^{+(k+1)} - \xi_j^{+(k+1)}) = 0 \ , \end{aligned} \quad (2.86)$$

$$\begin{aligned} \theta\zeta(\xi_{j+1/2}^{+(k+1)} + \xi_{j-1/2}^{+(k+1)} - 2\xi_j^{+(k+1)}) + (\sigma_t - 0.5\sigma_s)\Delta x_j (\xi_{j+1/2}^{+(k+1)} - \xi_j^{+(k+1)}) \\ -0.5\sigma_s \Delta x_j (\xi_j^{-(k+1)} - \xi_{j-1/2}^{-(k+1)}) = 0 \ , \end{aligned} \quad (2.87)$$

$$\xi_j^{(k+1)} = \xi_j^{-(k+1)} + \xi_j^{+(k+1)}, \quad (2.88)$$

where

$$g_{j+1/2}^{\pm(k+1/2)} = \sum_{\mu_m \gtrless 0} (\gamma(1 + \beta|\mu_m|^\alpha) - 1)\eta_{m,j+1/2}^{(k+1/2)} w_m \ , \quad (2.89)$$

$$f_{j+1/2}^{\pm(k+1/2)} = \sum_{\mu_m \gtrless 0} (\gamma|\mu_m|(1+\beta|\mu_m|^{\alpha}) - \zeta)\eta_{m,j+1/2}^{(k+1/2)} w_m \ . \tag{2.90}$$

The set of equations (2.83)-(2.90) represent the linearized form of the 1D NWF methods for the special class of infinite-medium problems considered.

A Fourier analysis is applied to the linearized discretized equations for the case of a uniform spatial mesh. Introduce the following Fourier ansatz:

$$\eta_{m,j+1/2}^{(k+1/2)} = a_m \omega^k e^{i\lambda\sigma_t x_{j+1/2}} \ , \tag{2.91}$$

$$\xi_{j+1/2}^{\pm(k)} = A^{\pm} \omega^k e^{i\lambda\sigma_t x_{j+1/2}} \ , \tag{2.92}$$

$$\xi_{j}^{\pm(k)} = B^{\pm} \omega^k e^{i\lambda\sigma_t x_{j}} \ , \tag{2.93}$$

$$\xi_{j}^{(k)} = \omega^k e^{i\lambda\sigma_t x_{j}} \ , \tag{2.94}$$

into Eqs. (2.83)-(2.90). Upon this substitution, a system of equations in terms of the eigenvalue spectrum and the magnitudes of the error modes, namely $\omega(\lambda)$, $A^{\pm}$ and $B^{\pm}$ is obtained. It is then found that

$$\omega(\chi) = \frac{\sigma_s}{\sigma_t} \frac{P\left(\zeta\nu_t\nu_a(0.5\sigma_t\Delta x g_1 - f_0)\tan^2\chi - \sigma_t\Delta x(0.5\sigma_t\Delta x g_0 + f_1\tan^2\chi)(P + 2\zeta\nu_a\tan^2\chi)\right)}{\sigma_t\sigma_a\Delta x^2(P+2\zeta\nu_t\tan^2\chi)(P+2\zeta\nu_a\tan^2\chi) + 4\zeta^2\nu_t^2\nu_a^2\tan^2\chi} \ , \tag{2.95}$$

$$\chi = 0.5\lambda\sigma_t\Delta x \ , \tag{2.96}$$

$$\nu_t = 2\zeta\theta + \sigma_t\Delta x \ , \tag{2.97}$$

$$\nu_a = 2\zeta\theta + \sigma_a\Delta x \ , \tag{2.98}$$

$$P = \nu_t\nu_a + \sigma_t\sigma_a\Delta x^2\tan^2\chi \, , \tag{2.99}$$

$$g_n = \sum_{\mu_m \geq 0} \left(\gamma(1+\beta\mu_m^{\alpha}) - 1\right) b_{n,m} w_m \ , \quad n = 0, 1 \, , \tag{2.100}$$

$$f_n = \sum_{\mu_m \geq 0} \left(\gamma\mu_m(1+\beta\mu_m^{\alpha}) - \zeta\right) b_{n,m} w_m \ , \quad n = 0, 1 \, , \tag{2.101}$$

$$b_{0,m} = \left(1 + \left(\frac{1+e^{-\tau_m}}{1-e^{-\tau_m}}\right)^2 \tan^2\chi\right)^{-1}, \tag{2.102}$$

$$b_{1,m} = \frac{1+e^{-\tau_m}}{1-e^{-\tau_m}} b_{0,m}\,, \tag{2.103}$$

$$\tau_m = \frac{\sigma_t \Delta x}{\mu_m}\,. \tag{2.104}$$

where the λ dependence of ω is now contained in the parameter χ. The spectral radius is defined by

$$\rho = \sup_{0\le\chi\le\frac{\pi}{2}} |\omega(\chi)| \ . \tag{2.105}$$

A similar Fourier analysis of the convergence properties of the NWF methods in the differential form was also performed. This analysis shows that in the vicinity of the solution of the considered special class of infinite medium problems one gets

$$\omega(\lambda) = c\left(\frac{1}{1+\lambda^2\zeta^2 - c}\right)\left[(1+\lambda^2\zeta^2)\frac{\tan^{-1}\lambda}{\lambda} - 1\right], \quad c = \frac{\sigma_s}{\sigma_t}\,. \tag{2.106}$$

If the condition (2.52) is met, then Eq. (2.106) leads to the formula for the DSA method and linearized QD method [41]. In such case the value of the spectral radius as $c \to 1$ equals 0.2247.

Table 2.1 contains the theoretically estimated spectral radii of the NWF method with $\alpha = 1$ and $\beta = \sqrt{3}$ using the formula (2.95). The double S_5 Gauss-Legendre quadrature set was utilized to calculate Eqs. (2.100) and (2.101).

Table 2.1: Theoretically Estimated Spectral Radii ρ for the Discretized NWF Method with $\alpha = 1$ and $\beta = \sqrt{3}$ versus $\sigma_t h$ and c.

	$\sigma_t h$						
c	0.01	0.1	1.	2.	3.	5.	10
0.9999	2.2E-1	2.2E-1	1.5E-1	8.5E-2	5.9E-2	1.8E-2	3.2E-4
0.99	2.2E-1	2.2E-1	1.4E-1	7.6E-2	4.0E-2	7.9E-3	6.3E-5
0.9	1.9E-1	1.9E-1	1.1E-1	4.5E-2	1.7E-2	1.9E-3	9.8E-6
0.7	1.4E-1	1.4E-1	7.0E-2	2.3E-2	7.1E-3	6.9E-4	3.1E-6

The data in Table 2.1 exhibit trends of the iterative convergence properties. First, as the optical thickness of the mesh is decreased, there is an increase of the spectral radius. This is evidenced by each value of c considered. This is caused by the discretized equations approaching the continuous form of the method. Note, that as $c \to 1$ for optically thin mesh the spectral radius approaches that of the preceding differential form Fourier analysis for $c = 1$. Second, the spectral radius increases as the scattering ratio increases. This demonstrates theoretically that the convergence is fast and stable for a wide range of scattering ratios and optical thicknesses of mesh intervals for the specific method with $\alpha = 1$ and $\beta = \sqrt{3}$.

In summary, this chapter shows that a new family of flux methods have been developed for 1D slab geometry which are accurate in the diffusion limit and converge fast. The most important acceleration needs of the transport equation are for optically thick mesh and high scattering ratios, which the NWF method with $\alpha = 1$ and $\beta = \sqrt{3}$ has been shown to perform very well for.

2.6 Numerical Results

To demonstrate the performance of the proposed NWF method with the particular linear weight function ($\alpha = 1$ and $\beta = \sqrt{3}$), numerical results are presented for problems that test the convergence properties of the proposed method and its behavior in the diffusive domains. Note that in the calculations below the lumping parameter $\theta_j = 1$ if $\sigma_{t,j}\Delta x_j \geq 5$. It should be noted that all derived quantities presented are derived from the low-order equations' solution, not that of the transport equation (high-order).

2.6.1 Problem 1

This problem tests the convergence properties of the method as optical thickness is varied. Consider a slab geometry problem with constant cross sections and source to be $\sigma_t = 1$, $\sigma_s = 0.99$, $q = 1$, a reflecting boundary at $x = 0$, and a vacuum boundary at $x = L$ [41]. $L = 10^3 h$ is used, where h is the width of the spatial cell. For a large h, the problem approaches that of an infinite medium. The angular quadrature is double S_5 Gauss-Legendre. The relative pointwise convergence criterion

$$\max_j \left| 1 - \frac{\phi_j^{(k)}}{\phi_j^{(k-1)}} \right| < \tilde{\epsilon} \tag{2.107}$$

with $\tilde{\epsilon} = 10^{-12}$ is used.

Table 2.2 contains the numerically estimated spectral radii that were determined by means of the formula

$$\rho = \frac{\|\phi^{(k)} - \phi^{(k-1)}\|_{L_2}}{\|\phi^{(k-1)} - \phi^{(k-2)}\|_{L_2}} \tag{2.108}$$

for the last iteration in each problem. The value at the last iteration is used because the method is "near" to the converged solution at this point as was assumed in the linearization process. Generally, the numerical spectral radius calculated at each iteration will approach a limiting value after a few iterations and this can be best sampled by the last iteration's spectral radius.

Table 2.2: Numerically Estimated Spectral Radii ρ for the Discretized NWF Method with $\alpha = 1$ and $\beta = \sqrt{3}$ versus $\sigma_t h$ for Problem No. 1 (c=0.99).

$\sigma_t h$	0.01	0.1	1.	2.	3.	5.	10
ρ	1.9E-1	1.9E-1	1.4E-1	8.0E-2	4.2E-2	4.2E-3	4.9E-4

These results enable us to compare theoretically and numerically estimated values. Looking back at the $c = 0.99$ row of Table 2.1 shows that the numerical spectral radii closely correspond to the analytic values and behave according to the same trend across varying optical

thicknesses. The reason that the numerical values are lower is that this problem is not infinite in dimension, although it is optically thick. Particles (radiation) are able to leak from the right side boundary, effectively killing them before their lifetime would have ended in a truly infinite-medium problem with such a high scattering ratio. Note that the Fourier analysis then approximately predicts the values of the spectral radii for the proposed NWF method.

2.6.2 Problem 2

This is a practical, yet simple problem, for which convergence results have been published for other iterative methods [47, 7]. Consider a slab $0 \leq x \leq 20$ having $\sigma_t = 1$, $\sigma_s = 0.97$, and $q = 0$. The left boundary has an isotropic incident flux with magnitude unity, and the right boundary is reflecting [47]. A spatial mesh consisting of J equal cells with cell width $h = 20/J$ is used. The double S_4 Gauss-Legendre quadrature set is utilized. The relative pointwise convergence criterion with $\tilde{\epsilon} = 10^{-12}$ is imposed.

Table 2.3 shows the numbers of iterations for the NWF method with $\alpha = 1$ and $\beta = \sqrt{3}$, as well as for the α-WN method with α=0.366, the QD and DSA methods that were taken from [7, 47]. The iteration counts of each method obey the expected trend of faster

Table 2.3: Number of Iterations for Problem No. 2.

$\sigma_t h$	5.	2.	1.	0.5	0.25	0.125
NWF Method ($\alpha = 1$, $\beta = \sqrt{3}$)	7	12	15	17	17	17
α-WN method (α=0.366)	7	11	13	15	16	16
QD method	10	14	14	15	15	15
DSA Method	14	16	16	16	16	16

convergence on optically thick coarse cells. Note that the NWF, α-WN, and QD methods each use the step characteristics method to solve the high-order problem.

The results of problems 1 and 2 show that the developed method converges fast, and its convergence properties are close to those of the α-WN method with α=0.366, the QD and DSA methods.

2.6.3 Problem 3

The purpose of this problem is to test the ability of a method to reproduce an accurate solution in the interior of a diffusive region which has an unresolved boundary layer. It is generally not practical to refine a spatial mesh to resolve boundary layers when cross sections can be on the order of 10^6 in radiative transfer problems. This situation corresponds directly to the asymptotic diffusion limit analysis performed in Section 2.4.

Consider a slab $0 \leq x \leq 11$ with pure absorbing ($0 \leq x \leq 1$) and diffusive ($1 \leq x \leq 11$) regions [36]. The parameters of the problem are listed in Table 2.4. The right boundary is vacuum. There is an isotropic incident angular flux $\psi(x, \mu)$=1 on the left boundary. A spatial mesh has 10 uniform cells in each region. The double S_8 Gauss-Legendre quadrature set is utilized.

Table 2.4: Parameters of Problem No. 3.

Region	Domain	σ_t	σ_s	q	h
1	$0 \leq x \leq 1$	2	0	0	0.1
2	$1 \leq x \leq 11$	100	100	0	1

The numerical solution obtained with the proposed NWF method is demonstrated in Figure 2.1. Both the cell-edge and cell-average scalar fluxes calculated from the low-order equations are plotted. The markers that indicate the cell-average values have smaller size compared to those for the cell-edge values. The results calculated by means of other flux

methods, namely, the FF, SF, and α-WN (α=0.366) methods are also shown. The low-order equations of these methods were discretized by the lumped LD method, and the SC method was used for the transport equation [7]. The relative pointwise convergence criterion with $\tilde{\epsilon} = 10^{-7}$ is used. All methods converged in 3 iterations.

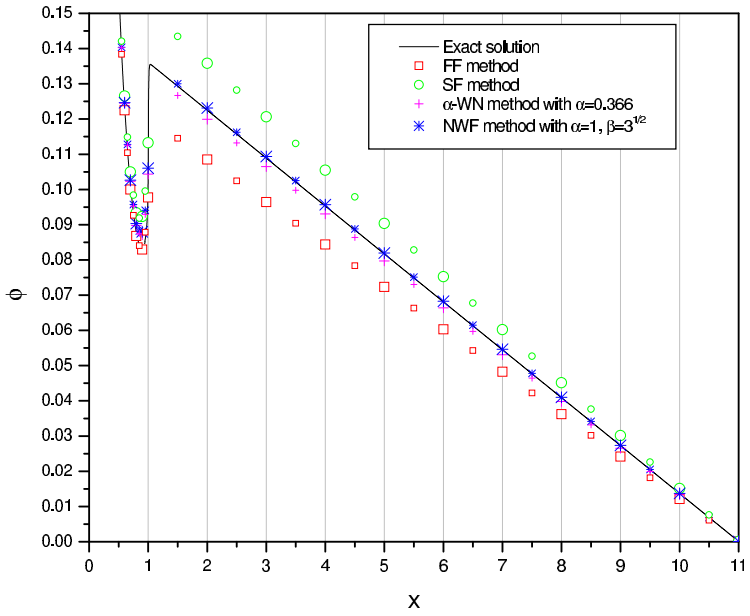

Figure 2.1: Problem 3. The scalar flux ϕ obtained by the NWF, FF, SF, and α-WN methods discretized with the lumped LD method.

The physics of this problem is straightforward, but it is hard to reproduce with a numerical method. The incoming angular flux will pass through two mean free paths (mfp) of pure absorbing material and become partially attenuated and anisotropic. The mesh is 0.2 mfp thick in this region. This anisotropic flux will enter the diffusive region where each cell is 100 mfp thick and the solution varies significantly across the first cell's width. The true solution is that the angular flux will become isotropic within a distance of a few ε (ε =1E-2) upon passing the material interface and the scalar flux will rise in magnitude as particles are trapped in the pure scatterer. Then, the scalar flux will decrease linearly to zero at the right side boundary.

Because the scattering region is not resolved, it is generally expected that the numerical solution will take at least one full cell's width to obtain a correct magnitude. The NWF methods have the property that they limit to the solution of a diffusion equation in diffusive regions which is fit to a boundary condition that is inherent to the method. Thus, it is a goal of this work for the NWF method to reproduce the correct solution throughout the whole of the diffusive region. An accurate solution calculated by the QD method on a suitably fine mesh is shown and can be taken as representative of the true physical behavior of the scalar flux. Note that the QD method possesses the diffusion limit and the boundary layer is well resolved for this case.

A physical understanding of the asymptotic diffusion limit boundary condition can be grasped by examining Figure 2.1. The solution in the interior of the diffusive region is linear and can be extrapolated back to the material interface at $x = 1$. This intercept value is the numerical value of the asymptotic boundary condition satisfied by the two methods that limit to the diffusion equation, namely the latter two in the figure. Note that the value of the exact QD solution is much lower than this at $x = 1$ and does not correspond. This is because the asymptotic boundary condition is the value necessary to reproduce the correct solution inside, not the true value of the solution at the boundary!

These results show that the proposed NWF method with $\alpha = 1$ and $\beta = \sqrt{3}$ performs very well in the thick diffusive region. The solution is close to the exact solution and quickly rises to the correct magnitude after the material interface. Note that the solutions of FF and SF methods have large errors in the diffusive region. The reason is that the low-order equations of these methods do not reduce to the diffusion equation in this case. The solution of the

α-WN method (α=0.366) is considerably better, because it satisfies a good discretization of the diffusion equation. However, it is not well enough due to an inaccurate asymptotic boundary condition that this method generates at the interface with the diffusive region. The relative errors in the scalar flux in the diffusive region versus position for the NWF and α-WN methods are presented in Table 2.5. These data show that in the thick diffusive region (after the boundary

Table 2.5: Problem 3. Relative Errors in the Scalar Flux in the Diffusive Region.

x	α-WN (α=0.366)	NWF (α=1, β=$\sqrt{3}$)
1.	-4.1E-2	-7.1E-2
2.	2.6E-2	8.2E-5
3.	2.5E-2	9.2E-5
4.	2.5E-2	-1.1E-4
5.	2.5E-2	-3.1E-4
6.	2.4E-2	-5.0E-4
7.	2.4E-2	-5.5E-4
8.	2.4E-2	-4.9E-4
9.	2.3E-2	-3.7E-4
10.	2.4E-2	-3.7E-4

layer) the new method generates the solution with significantly higher accuracy than the α-WN method with α=0.366. This exemplifies the effect of having an accurate asymptotic boundary condition for problems containing unresolved boundary layers.

Chapter 3

DEVELOPMENT AND ASYMPTOTIC ANALYSIS OF THE 2D NWF METHOD

In this chapter, the development of the 2D Nonlinear Weighted Flux methods is shown. It is the objective of this chapter to extend the methods developed for 1D into 2D and maintain the desirable properties that were obtained in 1D. This chapter presents the definition and discretization of the 2D NWF methods in general form. An asymptotic diffusion limit analysis of the 2D NWF methods is presented for Cartesian geometry with uniform grids. The asymptotic analysis enables the determination of a particular method of this family the solution of which satisfies a good approximation of both the diffusion equation and asymptotic boundary condition in optically thick diffusive regions. It is performed for the continuous form equations, discretized equations, and the discretized equations at an unresolved boundary layer. The 2D

work has been published in [44].

3.1 Formulation Of The Family Of 2D NWF Methods

We consider the one-group steady-state transport equation in 2D Cartesian geometry with isotropic scattering and source:

$$\Omega_x \frac{\partial}{\partial x}\psi(\vec{r},\vec{\Omega})+\Omega_y \frac{\partial}{\partial y}\psi(\vec{r},\vec{\Omega})+\sigma_t(\vec{r})\psi(\vec{r},\vec{\Omega}) = \frac{1}{4\pi}\sigma_s(\vec{r})\int_{4\pi}\psi(\vec{r},\vec{\Omega}')d\vec{\Omega}'+\frac{1}{4\pi}q(\vec{r})\,, \quad \vec{r}\in\mathcal{D}\,, \tag{3.1}$$

$$\psi(\vec{r},\vec{\Omega})\Big|_{\vec{r}\in\partial\mathcal{D}} = \psi^{in}(\vec{r}_b,\vec{\Omega})\,, \quad \vec{\Omega}\cdot\vec{n}<0\,, \quad \vec{r}_b\in\partial\mathcal{D}\,, \tag{3.2}$$

where $\mathcal{D}=\{0\le x\le X,\ 0\le y\le Y\}$. The total probability of interaction per unit path length for a particle is given by $\sigma_t(\vec{r})$, and the probability of scattering per unit path length is $\sigma_s(\vec{r})$. An external source of particles is represented by $q(\vec{r})$

To derive the low-order equations of the NWF family of methods, we operate on the transport equation (3.1) by

$$\gamma_m\int_{\omega_m} w(\Omega_x,\Omega_y)(\bullet)d\vec{\Omega} \tag{3.3}$$

over spherical angular quadrants ω_m, $m=1,\ldots,4$, where $w(\Omega_x,\Omega_y)$ is a generally defined weight function of directional cosines,

$$\begin{aligned}
\omega_1 &= \{0\le\gamma\le\frac{\pi}{2}, 0\le\theta\le\pi\}\,,\\
\omega_2 &= \{\frac{\pi}{2}\le\gamma\le\pi, 0\le\theta\le\pi\}\,,\\
\omega_3 &= \{\pi\le\gamma\le\frac{3\pi}{2}, 0\le\theta\le\pi\}\,,\\
\omega_4 &= \{\frac{3\pi}{2}\le\gamma\le 2\pi, 0\le\theta\le\pi\}\,,
\end{aligned} \tag{3.4}$$

and

$$\gamma_m = \frac{\int_{\omega_m} d\vec{\Omega}}{\int_{\omega_m} w(\Omega_x, \Omega_y) d\vec{\Omega}} \ . \tag{3.5}$$

Partial scalar fluxes defined over angular quadrants are used to define the low-order system of equations and are written as

$$\phi_m = \int_{\omega_m} \psi d\vec{\Omega} \, . \tag{3.6}$$

The family of 2D NWF methods are then defined by the following high-order problem for the angular flux ψ and low-order problem for the partial scalar fluxes (3.6)

$$\Omega_x \frac{\partial}{\partial x}\psi + \Omega_y \frac{\partial}{\partial y}\psi + \sigma_t \psi = \frac{1}{4\pi}\sigma_s \phi + \frac{1}{4\pi} q \, , \tag{3.7}$$

$$G_m = \gamma_m \int\limits_{\omega_m} w(\Omega_x, \Omega_y)\psi d\vec{\Omega} \Big/ \int\limits_{\omega_m} \psi d\vec{\Omega} \, , \tag{3.8}$$

$$F_m^{\alpha} = \gamma_m \int\limits_{\omega_m} |\Omega_\alpha| w(\Omega_x, \Omega_y)\psi d\vec{\Omega} \Big/ \int\limits_{\omega_m} \psi d\vec{\Omega} \, , \tag{3.9}$$

$$\alpha = x, y \, , \quad m = 1, \ldots, 4 \, ,$$

$$\frac{\partial}{\partial x}(F_1^x \phi_1) + \frac{\partial}{\partial y}(F_1^y \phi_1) + \sigma_t G_1 \phi_1 = \frac{1}{4}(\sigma_s \phi + q) \, , \tag{3.10}$$

$$-\frac{\partial}{\partial x}(F_2^x \phi_2) + \frac{\partial}{\partial y}(F_2^y \phi_2) + \sigma_t G_2 \phi_2 = \frac{1}{4}(\sigma_s \phi + q) \, , \tag{3.11}$$

$$-\frac{\partial}{\partial x}(F_3^x \phi_3) - \frac{\partial}{\partial y}(F_3^y \phi_3) + \sigma_t G_3 \phi_3 = \frac{1}{4}(\sigma_s \phi + q) \, , \tag{3.12}$$

$$\frac{\partial}{\partial x}(F_4^x \phi_4) - \frac{\partial}{\partial y}(F_4^y \phi_4) + \sigma_t G_4 \phi_4 = \frac{1}{4}(\sigma_s \phi + q) \, , \tag{3.13}$$

$$0 \le x \le X, \ 0 \le y \le Y \ ,$$

$$\phi = \sum_{m=1}^{4} \phi_m \ , \tag{3.14}$$

with the following boundary conditions for the low-order equations (3.10)-(3.13):

$$\phi_m|_{x=0} = \int\limits_{\omega_m} \psi^{in}\big|_{x=0} \, d\vec{\Omega} \, , \ m = 1, 4 \, , \ 0 \le y \le Y \ , \tag{3.15}$$

$$\phi_m|_{x=X} = \int\limits_{\omega_m} \psi^{in}|_{x=X}\, d\vec{\Omega}\,,\ m = 2,3\,,\ 0 \le y \le Y\ , \tag{3.16}$$

$$\phi_m|_{y=0} = \int\limits_{\omega_m} \psi^{in}|_{y=0}\, d\vec{\Omega}\,,\ m = 1,2\,,\ 0 \le x \le X\ , \tag{3.17}$$

$$\phi_m|_{y=Y} = \int\limits_{\omega_m} \psi^{in}|_{y=Y}\, d\vec{\Omega}\,,\ m = 3,4\,,\ 0 \le x \le X\ . \tag{3.18}$$

Standard notations are used. Note that reflective and albedo boundary conditions can be defined by relating partial scalar fluxes. The low-order equations (3.10)-(3.13) have a similar form to the transport equation (3.7). There are streaming terms represented by the first-order derivatives, a removal term, and a coupling of partial scalar fluxes in the scattering source. The system of equations (3.7)-(3.18) is equivalent to the original linear transport problem (3.1) and (3.2).

The equations (3.7)-(3.18) are solved by means of the following iterative process:

$$\Omega_x \frac{\partial}{\partial x}\psi^{(k+1/2)} + \Omega_y \frac{\partial}{\partial y}\psi^{(k+1/2)} + \sigma_t \psi^{(k+1/2)} = \frac{1}{4\pi}\sigma_s \phi^{(k)} + \frac{1}{4\pi} q\,, \tag{3.19}$$

$$G_m^{(k+1/2)} = \gamma_m \int\limits_{\omega_m} w(\Omega_x, \Omega_y)\psi^{(k+1/2)} d\vec{\Omega} \Bigg/ \int\limits_{\omega_m} \psi^{(k+1/2)} d\vec{\Omega}\,, \tag{3.20}$$

$$F_m^{\alpha^{(k+1/2)}} = \gamma_m \int\limits_{\omega_m} |\Omega_\alpha| w(\Omega_x, \Omega_y)\psi^{(k+1/2)} d\vec{\Omega} \Bigg/ \int\limits_{\omega_m} \psi^{(k+1/2)} d\vec{\Omega}\,, \tag{3.21}$$

$$\alpha = x, y\,, \quad m = 1, \ldots, 4\,,$$

$$\frac{\partial}{\partial x}(F_1^{x^{(k+1/2)}}\phi_1^{(k+1)}) + \frac{\partial}{\partial y}(F_1^{y^{(k+1/2)}}\phi_1^{(k+1)}) + \sigma_t G_1^{(k+1/2)}\phi_1^{(k+1)} = \frac{1}{4}(\sigma_s\phi^{(k+1)} + q)\,, \tag{3.22}$$

$$-\frac{\partial}{\partial x}(F_2^{x^{(k+1/2)}}\phi_2^{(k+1)}) + \frac{\partial}{\partial y}(F_2^{y^{(k+1/2)}}\phi_2^{(k+1)}) + \sigma_t G_2^{(k+1/2)}\phi_2^{(k+1)} = \frac{1}{4}(\sigma_s\phi^{(k+1)} + q)\,, \tag{3.23}$$

$$-\frac{\partial}{\partial x}(F_3^{x^{(k+1/2)}}\phi_3^{(k+1)}) - \frac{\partial}{\partial y}(F_3^{y^{(k+1/2)}}\phi_3^{(k+1)}) + \sigma_t G_3^{(k+1/2)}\phi_3^{(k+1)} = \frac{1}{4}(\sigma_s\phi^{(k+1)} + q)\,, \tag{3.24}$$

$$\frac{\partial}{\partial x}(F_4^{x^{(k+1/2)}}\phi_4^{(k+1)}) - \frac{\partial}{\partial y}(F_4^{y^{(k+1/2)}}\phi_4^{(k+1)}) + \sigma_t G_4^{(k+1/2)}\phi_4^{(k+1)} = \frac{1}{4}(\sigma_s\phi^{(k+1)} + q)\,, \tag{3.25}$$

$$0 \le x \le X,\ 0 \le y \le Y\ ,$$

$$\phi^{(k+1)} = \sum_{m=1}^{4} \phi_m^{(k+1)} \ , \tag{3.26}$$

where

$$\phi_m^{(k+1)}\Big|_{x=0} = \int_{\omega_m} \psi^{in}\big|_{x=0} \, d\vec{\Omega} \, , \ m = 1,4 \, , \ 0 \le y \le Y \ , \tag{3.27}$$

$$\phi_m^{(k+1)}\Big|_{x=X} = \int_{\omega_m} \psi^{in}\big|_{x=X} \, d\vec{\Omega} \, , \ m = 2,3 \, , \ 0 \le y \le Y \ , \tag{3.28}$$

$$\phi_m^{(k+1)}\Big|_{y=0} = \int_{\omega_m} \psi^{in}\big|_{y=0} \, d\vec{\Omega} \, , \ m = 1,2 \, , \ 0 \le x \le X \ , \tag{3.29}$$

$$\phi_m^{(k+1)}\Big|_{y=Y} = \int_{\omega_m} \psi^{in}\big|_{y=Y} \, d\vec{\Omega} \, , \ m = 3,4 \, , \ 0 \le x \le X \ . \tag{3.30}$$

The iterative process is defined by the following three stages:

1. A transport sweep to calculate the angular flux $\psi^{(k+1/2)}$ (Eq. (3.19)).

2. The calculation of the factors $G_m^{(k+1/2)}$ and $F_m^{\alpha^{(k+1/2)}}$ from $\psi^{(k+1/2)}$ (Eqs. (3.20)-(3.21)).

3. Solving the low-order problem (Eqs. (3.22)-(3.30)) for $\phi_m^{(k+1)}$ using $G_m^{(k+1/2)}$ and $F_m^{\alpha^{(k+1/2)}}$.

On the initial iteration ($k = 0$) the transport sweep is not performed. Instead, the factors $G_m^{(1/2)}$ and $F_m^{\alpha^{(1/2)}}$ are calculated using an isotropic angular flux and used to complete a low-order solve.

3.2 Discretization Of The 2D NWF Methods

Many discretization schemes have been developed for use with the transport equation and for problems that are diffusive in nature. Selecting a transport discretization with good performance and applying it to the low-order problem gives a reasonable expectation of attaining similar properties.

The low-order equations are discretized by the lumped bilinear-discontinuous (BLD) method [48, 49]. The BLD discretization has been studied for diffusive problems and is known to limit to a stable and consistent form of the diffusion equation in the diffusion limit. We consider orthogonal spatial grids

$$x_{i+1/2} = x_{i-1/2} + \Delta x_i,\ i = 1, \ldots, N_x;\quad x_{1/2} = 0,\ x_{N_x+1/2} = X\,,$$

$$y_{j+1/2} = y_{j-1/2} + \Delta y_j,\ j = 1, \ldots, N_y;\quad y_{1/2} = 0,\ y_{N_y+1/2} = Y\,.$$

The BLD approximation of the partial scalar fluxes in the (i, j)-cell is

$$\phi_m(x,y) = \phi_{m,i,j} + \frac{2}{\Delta x_i}(x-x_i)\phi^x_{m,i,j} + \frac{2}{\Delta y_j}(y-y_j)\phi^y_{m,i,j} + \frac{4}{\Delta x_i \Delta y_j}(x-x_i)(y-y_j)\phi^{xy}_{m,i,j}\,, \quad (3.31)$$

where the partial scalar flux spatial moments are defined as

$$\phi^x_{m,i,j} = \frac{6}{\Delta x_i^2 \Delta y_j}\int_{x_i-1/2}^{x_i+1/2} dx \int_{y_j-1/2}^{y_j+1/2} (x-x_i)\phi_m(x,y)dy\,, \quad (3.32)$$

$$\phi^y_{m,i,j} = \frac{6}{\Delta x_i \Delta y_j^2}\int_{x_i-1/2}^{x_i+1/2} dx \int_{y_j-1/2}^{y_j+1/2} (y-y_j)\phi_m(x,y)dy\,, \quad (3.33)$$

$$\phi^{xy}_{m,i,j} = \frac{36}{\Delta x_i^2 \Delta y_j^2}\int_{x_i-1/2}^{x_i+1/2} dx \int_{y_j-1/2}^{y_j+1/2} (x-x_i)(y-y_j)\phi_m(x,y)dy\,, \quad (3.34)$$

and x_i and y_j are midpoints of the corresponding intervals. Thus, the partial scalar fluxes in each cell are defined in terms of the cell average partial scalar flux and the spatial moments.

The discretization of the low-order equations of the NWF method is discussed here. First, we integrate equations (3.22)-(3.25) over the (i, j)-cell which gives four balance equations. This is repeated with the equations weighted by $\frac{2}{\Delta x_i}(x-x_i)$, $\frac{2}{\Delta y_j}(y-y_j)$, and $\frac{4}{\Delta x_i \Delta y_j}(x-x_i)(y-y_j)$ to give twelve moment equations (three for each direction). These equations relate unknowns within each cell for the m^{th} direction as

$$\nu^x_m \Delta y_j (F^x_{m,i+1/2,j}\phi_{m,i+1/2,j} - F^x_{m,i-1/2,j}\phi_{m,i-1/2,j}) + \nu^y_m \Delta x_i (F^y_{m,i,j+1/2}\phi_{m,i,j+1/2} - F^y_{m,i,j-1/2}\phi_{m,i,j-1/2})$$

$$+ \sigma_{t,i,j} G_{m,i,j} \phi_{m,i,j} \Delta x_i \Delta y_j = \frac{1}{4} \Delta x_i \Delta y_j (\sigma_{s,i,j} \phi_{i,j} + q_{i,j}) \,, \tag{3.35}$$

$$\theta_x \nu_m^x \Delta y_j (F^x_{m,i+1/2,j} \phi_{m,i+1/2,j} + F^x_{m,i-1/2,j} \phi_{m,i-1/2,j} - 2F^x_{m,i,j} \phi_{m,i,j}) + \gamma_y \nu_m^y \Delta x_i (F^y_{m,i,j+1/2} \phi^x_{m,i,j+1/2}$$

$$- F^y_{m,i,j-1/2} \phi^x_{m,i,j-1/2}) + \sigma_{t,i,j} G_{m,i,j} \phi^x_{m,i,j} \Delta x_i \Delta y_j = \frac{1}{4} \Delta x_i \Delta y_j (\sigma_{s,i,j} \phi^x_{i,j} + q^x_{i,j}) \,, \tag{3.36}$$

$$\gamma_x \nu_m^x \Delta y_j (F^x_{m,i+1/2,j} \phi^y_{m,i+1/2,j} - F^x_{m,i-1/2,j} \phi^y_{m,i-1/2,j}) + \theta_y \nu_m^y \Delta x_i (F^y_{m,i,j+1/2} \phi_{m,i,j+1/2}$$

$$+ F^y_{m,i,j-1/2} \phi_{m,i,j-1/2} - 2F^y_{m,i,j} \phi_{m,i,j}) + \sigma_{t,i,j} G_{m,i,j} \phi^y_{m,i,j} \Delta x_i \Delta y_j = \frac{1}{4} \Delta x_i \Delta y_j (\sigma_{s,i,j} \phi^y_{i,j} + q^y_{i,j}) \,, \tag{3.37}$$

$$\delta_x \nu_m^x \Delta y_j (F^x_{m,i+1/2,j} \phi^y_{m,i+1/2,j} + F^x_{m,i-1/2,j} \phi^y_{m,i-1/2,j} - 2F^x_{m,i,j} \phi^y_{m,i,j}) + \delta_y \nu_m^y \Delta x_i (F^y_{m,i,j+1/2} \phi^x_{m,i,j+1/2}$$

$$+ F^y_{m,i,j-1/2} \phi^x_{m,i,j-1/2} - 2F^y_{m,i,j} \phi^x_{m,i,j}) + \sigma_{t,i,j} G_{m,i,j} \phi^{xy}_{m,i,j} \Delta x_i \Delta y_j = \frac{1}{4} \Delta x_i \Delta y_j (\sigma_{s,i,j} \phi^{xy}_{i,j} + q^{xy}_{i,j}) \,, \tag{3.38}$$

$$i = 1, \ldots, N_x \,, \quad j = 1, \ldots, N_y \quad m = 1, \ldots, 4 \,,$$

where

$$\nu_1^x = \nu_4^x = 1 \,, \quad \nu_2^x = \nu_3^x = -1 \,, \tag{3.39}$$

$$\nu_1^y = \nu_2^y = 1 \,, \quad \nu_3^y = \nu_4^y = -1 \,, \tag{3.40}$$

and $\sigma_{t,i,j}$, $\sigma_{s,i,j}$, and $q_{i,j}$ are now cell average quantities. Auxiliary equations must be defined to fully constrain the system of equations. These auxiliary conditions are defined by evaluating (3.31) at the midpoints of downstream direction faces of the (i,j)-cell. This gives the BLD discretization its desirable property of discontinuity by relating the cell-average unknowns to the downstream-direction unknowns of a cell. The partial scalar fluxes are then discontinuous at upstream cell faces which allows the finite element discretization to better represent discontinuous and high-gradient solution behavior that can't be accurately modeled with solely a

bilinear expansion of the unknowns in each cell. The BLD auxiliary equations are given by

$$\begin{aligned}
\phi_{1,i+1/2,j} &= \phi_{1,i,j} + \phi^x_{1,i,j}\,, & \phi_{3,i-1/2,j} &= \phi_{3,i,j} - \phi^x_{3,i,j}\,,\\
\phi^y_{1,i+1/2,j} &= \phi^y_{1,i,j} + \phi^{xy}_{1,i,j}\,, & \phi^y_{3,i-1/2,j} &= \phi^y_{3,i,j} - \phi^{xy}_{3,i,j}\,,\\
\phi_{1,i,j+1/2} &= \phi_{1,i,j} + \phi^y_{1,i,j}\,, & \phi_{3,i,j-1/2} &= \phi_{3,i,j} - \phi^y_{3,i,j}\,,\\
\phi^x_{1,i,j+1/2} &= \phi^x_{1,i,j} + \phi^{xy}_{1,i,j}\,, & \phi^x_{3,i,j-1/2} &= \phi^x_{3,i,j} - \phi^{xy}_{3,i,j}\,,\\
\\
\phi_{2,i-1/2,j} &= \phi_{2,i,j} - \phi^x_{2,i,j}\,, & \phi_{4,i+1/2,j} &= \phi_{4,i,j} + \phi^x_{4,i,j}\,,\\
\phi^y_{2,i-1/2,j} &= \phi^y_{2,i,j} - \phi^{xy}_{2,i,j}\,, & \phi^y_{4,i+1/2,j} &= \phi^y_{4,i,j} + \phi^{xy}_{4,i,j}\,,\\
\phi_{2,i,j+1/2} &= \phi_{2,i,j} + \phi^y_{2,i,j}\,, & \phi_{4,i,j-1/2} &= \phi_{4,i,j} - \phi^y_{4,i,j}\,,\\
\phi^x_{2,i,j+1/2} &= \phi^x_{2,i,j} + \phi^{xy}_{2,i,j}\,, & \phi^x_{4,i,j-1/2} &= \phi^x_{4,i,j} - \phi^{xy}_{4,i,j}\,.
\end{aligned} \tag{3.41}$$

Lumping parameters are denoted by θ_α, γ_α, and δ_α ($\alpha = x, y$). The standard BLD equations are obtained by the lumping parameters 3, 1, and 3, respectively. For mass-lumped BLD, the parameters are 1, 1/3, and 1/3. For fully lumped BLD, the parameters all have values of 1. Lumping adds robustness to a method, usually at the price of lost accuracy. Physically, lumping makes an equation more local. For example, mass lumping causes an equation to depend only on cell average scalar fluxes for the removal and source terms. The equations no longer depend on the moments which give a bilinear shape. Another way to think about this is in terms of mass-matrix lumping when equations are written in matrix form. Then, the coefficients are summed over each row of the matrix and the total is placed in the diagonal element with all other elements set to zero.

The number of low-order equations per cell is

- 4 balance equations
- 12 moment equations
- 16 auxiliary equations.

The cell average moment unknowns can be eliminated by combining equations to get a smaller system of equations with a total number of unknowns in a problem N_x by N_y cells given by

$$20N_xN_y + 8(N_x + N_y)\,. \tag{3.42}$$

Then, the cell average moment terms can easily be restored from the solution and equation (3.41).

The transport equation is approximated by the method of short characteristics [50, 51, 52, 53]. The method of short characteristics results in an angular flux distribution that is monotonic and nonnegative. The high-order equations are solved by sweeping through the angular and spatial mesh, where unknown downstream angular fluxes on vertices are solved for by

$$\psi_n(\gamma_l, \theta_m) = \psi^* e^{-\tau_{ijlm}} + \frac{1}{sin\theta_m} \int_0^{\Delta S_{ijl}} \frac{1}{4\pi} \left(\sigma_{s,ij}\phi_{ij} + q_{ij}\right) e^{\frac{-\sigma_{t,ij}s'}{sin\theta_m}} ds'\,, \tag{3.43}$$

where,

$$\tau_{ijlm} = \frac{\sigma_{t,ij}\Delta S_{ijl}}{sin\theta_m}\,, \tag{3.44}$$

and ψ^* is the incoming flux at the cell face which must be obtained through interpolation. Spherical geometry ordinates are specified by γ_l and θ_m. ΔS_{ijl} is the chord length of travel across the i, j cell for the l^{th} direction. There are many different approaches to interpolating and solving equation (3.43). The geometry used in this research is outlined by Figure 3.1 for one ordinate's direction of travel across a cell. First, the source contribution is calculated along

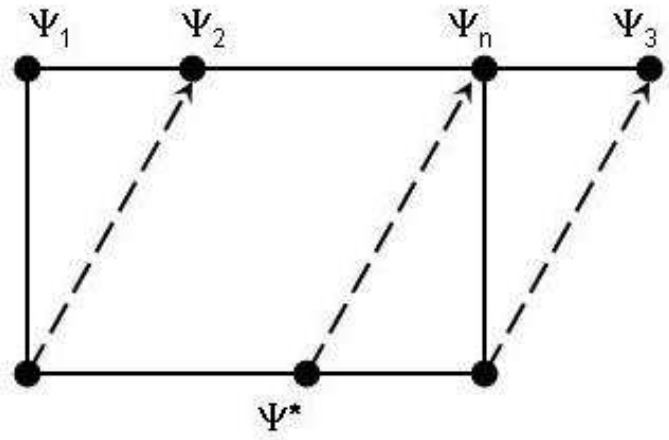

Figure 3.1: Method of Short Characteristics Interpolation Stencil.

the path of travel from ψ^* to ψ_n. Since ϕ_{ij} and q_{ij} are constant over the cell, this gives the value of the second half of equation (3.43) for ψ_2 and ψ_3. The first half of equation (3.43) is calculated for ψ_2 and ψ_3 using known data. ψ_1 is known. Then, ψ_n is calculated by either linear or parabolic interpolation along the outgoing face. If parabolic interpolation yields a value greater than (less than) each ψ_1, ψ_2, and ψ_3, then the method is monotonized. This is necessary to prevent introducing artificial oscillations from higher-order interpolation schemes. Monotonization is accomplished by setting the interpolant to the greatest (smallest) value of ψ_2 and ψ_3 [50]. This diagram similarly holds for ordinates that strike the other incoming face of the cell, where the other outgoing face is then used to interpolate along. Linear interpolation does not need monotonization, but it results in a first order spatially convergent transport discretization method while parabolic is a second order one.

The factors are calculated on vertices from the resulting angular flux distribution. Cell-average factors, $F^{\alpha}_{m,i,j}$ and $G_{m,i,j}$, are calculated as averages of factors evaluated on the four cell vertices. Face-average factors, $F^{\alpha}_{m,i+1/2,j}$ and $F^{\alpha}_{m,i,j+1/2}$, are averages of the two nearest

vertex values.

In the remainder of the chapter, the properties of the NWF family of methods are analyzed and specific methods defined by selection of the weight $w(\Omega_x, \Omega_y)$.

3.3 Continuous Form Analysis Of Asymptotic Diffusion Limit

To meet the diffusion limit, the leading-order solution of the low-order equations (3.10)-(3.13) must give rise to the diffusion equation [37, 40]. In order to develop a NWF method that satisfies this condition, an asymptotic diffusion limit analysis of the low-order equations of the NWF methods for general weight $w(\Omega_x, \Omega_y)$ under the assumption that the angular flux is isotropic is performed.

Evaluating the factors (3.8)-(3.9) with an isotropic angular flux, ψ = constant, the factors are

$$\begin{aligned} G_m &= 1\,, \\ F_m^\alpha &= \tilde{F}_m^\alpha\,, \quad \alpha = x, y\,, m = 1, \ldots, 4\,, \end{aligned} \tag{3.45}$$

where

$$\tilde{F}_m^\alpha = \frac{\gamma_m \int\limits_{\omega_m} |\Omega_\alpha| w(\Omega_x, \Omega_y) d\vec{\Omega}}{\int\limits_{\omega_m} d\vec{\Omega}}\,. \tag{3.46}$$

To perform the analysis, the following scaling of the cross sections and ansatz are introduced into equations (3.10)-(3.13):

$$\sigma_t = \frac{\hat{\sigma}_t}{\varepsilon}\,, \quad \sigma_a = \varepsilon \hat{\sigma}_a\,, \quad q = \varepsilon \hat{q}\,, \tag{3.47}$$

$$\phi_m = \sum_{n=0}^{\infty} \varepsilon^n \phi_m^{[n]}\,, \quad m = 1, \ldots, 4\,, \tag{3.48}$$

where $\varepsilon \ll 1$ is a scaling parameter. Then, coefficients of ε^{-1}, ε^0, and ε^1 terms are equated to give a system of equations. The resulting $O(\varepsilon^{-1})$ equation is

$$\phi_m^{[0]} = \frac{1}{4}\phi^{[0]}\,. \tag{3.49}$$

This shows that the leading order partial scalar fluxes are equal in each direction. The resulting $O(\varepsilon^0)$ equations are

$$\tilde{F}_1^x \frac{\partial}{\partial x}\phi_1^{[0]} + \tilde{F}_1^y \frac{\partial}{\partial y}\phi_1^{[0]} + \hat{\sigma}_t \phi_1^{[1]} = \frac{1}{4}\hat{\sigma}_t \phi^{[1]}\,, \tag{3.50}$$

$$-\tilde{F}_2^x \frac{\partial}{\partial x}\phi_2^{[0]} + \tilde{F}_2^y \frac{\partial}{\partial y}\phi_2^{[0]} + \hat{\sigma}_t \phi_2^{[1]} = \frac{1}{4}\hat{\sigma}_t \phi^{[1]}\,, \tag{3.51}$$

$$-\tilde{F}_3^x \frac{\partial}{\partial x}\phi_3^{[0]} - \tilde{F}_3^y \frac{\partial}{\partial y}\phi_3^{[0]} + \hat{\sigma}_t \phi_3^{[1]} = \frac{1}{4}\hat{\sigma}_t \phi^{[1]}\,, \tag{3.52}$$

$$\tilde{F}_4^x \frac{\partial}{\partial x}\phi_4^{[0]} - \tilde{F}_4^y \frac{\partial}{\partial y}\phi_4^{[0]} + \hat{\sigma}_t \phi_4^{[1]} = \frac{1}{4}\hat{\sigma}_t \phi^{[1]}\,. \tag{3.53}$$

These equations relate the $\phi_m^{[0]}$ and $\phi_m^{[1]}$ terms. The resulting $O(\varepsilon^1)$ equations are

$$\tilde{F}_1^x \frac{\partial}{\partial x}\phi_1^{[1]} + \tilde{F}_1^y \frac{\partial}{\partial y}\phi_1^{[1]} = \frac{1}{4}\left(-\hat{\sigma}_a \phi^{[0]} + \hat{q}\right)\,, \tag{3.54}$$

$$-\tilde{F}_2^x \frac{\partial}{\partial x}\phi_2^{[1]} + \tilde{F}_2^y \frac{\partial}{\partial y}\phi_2^{[1]} = \frac{1}{4}\left(-\hat{\sigma}_a \phi^{[0]} + \hat{q}\right)\,, \tag{3.55}$$

$$-\tilde{F}_3^x \frac{\partial}{\partial x}\phi_3^{[1]} - \tilde{F}_3^y \frac{\partial}{\partial y}\phi_3^{[1]} = \frac{1}{4}\left(-\hat{\sigma}_a \phi^{[0]} + \hat{q}\right)\,, \tag{3.56}$$

$$\tilde{F}_4^x \frac{\partial}{\partial x}\phi_4^{[1]} - \tilde{F}_4^y \frac{\partial}{\partial y}\phi_4^{[1]} = \frac{1}{4}\left(-\hat{\sigma}_a \phi^{[0]} + \hat{q}\right)\,. \tag{3.57}$$

The system of equations (3.49)-(3.57) can be reduced to an equation relating the leading order terms. This is then the equation that the method limits to in diffusive regions to leading order. The analysis shows that the leading-order solution of the low-order equations (3.10)-(3.13) satisfies the following second-order PDE in the interior of the optically thick diffusive region:

$$-\frac{1}{4}\left(\sum_{m=1}^{4}(\tilde{F}_m^x)^2\right)\frac{\partial}{\partial x}\frac{1}{\sigma_t}\frac{\partial \phi^{[0]}}{\partial x} - \frac{1}{4}\left(\sum_{m=1}^{4}(\tilde{F}_m^y)^2\right)\frac{\partial}{\partial y}\frac{1}{\sigma_t}\frac{\partial \phi^{[0]}}{\partial y}$$

$$-\frac{1}{4}\left(\tilde{F}_1^x\tilde{F}_1^y-\tilde{F}_2^x\tilde{F}_2^y+\tilde{F}_3^x\tilde{F}_3^y-\tilde{F}_4^x\tilde{F}_4^y\right)\left(\frac{\partial}{\partial x}\frac{1}{\sigma_t}\frac{\partial\phi^{[0]}}{\partial y}+\frac{\partial}{\partial y}\frac{1}{\sigma_t}\frac{\partial\phi^{[0]}}{\partial x}\right)$$

$$+\frac{1}{4}\left(\tilde{F}_1^x+\tilde{F}_4^x-\sum_{m=2}^{3}\tilde{F}_m^x\right)\frac{\partial\phi^{[1]}}{\partial x}+\frac{1}{4}\left(\sum_{m=1}^{2}\tilde{F}_m^y-\sum_{m=3}^{4}\tilde{F}_m^y\right)\frac{\partial\phi^{[1]}}{\partial y}+\sigma_a\phi^{[0]}=q\,. \tag{3.58}$$

The diffusion equation for the scalar flux, ϕ, is given by

$$-\frac{\partial}{\partial x}D\frac{\partial\phi}{\partial x}-\frac{\partial}{\partial y}D\frac{\partial\phi}{\partial y}+\sigma_a\phi=q\,, \tag{3.59}$$

with the diffusion coefficient

$$D=\frac{1}{3\sigma_t}\,. \tag{3.60}$$

The equation (3.58) then results in the diffusion equation (3.59) and hence the leading-order solution satisfies the diffusion equation, if the following five conditions are met:

$$\frac{1}{4}\sum_{m=1}^{4}(\tilde{F}_m^x)^2=\frac{1}{3}\,, \tag{3.61}$$

$$\frac{1}{4}\sum_{m=1}^{4}(\tilde{F}_m^y)^2=\frac{1}{3}\,, \tag{3.62}$$

$$\tilde{F}_1^x\tilde{F}_1^y-\tilde{F}_2^x\tilde{F}_2^y+\tilde{F}_3^x\tilde{F}_3^y-\tilde{F}_4^x\tilde{F}_4^y=0\,, \tag{3.63}$$

$$\tilde{F}_1^x+\tilde{F}_4^x-\sum_{m=2}^{3}\tilde{F}_m^x=0\,, \tag{3.64}$$

$$\sum_{m=1}^{2}\tilde{F}_m^y-\sum_{m=3}^{4}\tilde{F}_m^y=0\,. \tag{3.65}$$

The results of this analysis allow an evaluation of NWF methods with various weights. Note that if a weight satisfies only Eqs. (3.63)-(3.65), then Eq. (3.58) leads to a diffusion-like equation with a wrong diffusion coefficient, D. It is easy to conceive of and define many different forms of the weight $w(\Omega_x,\Omega_y)$, but not all are capable of meeting Eqs. (3.61)-(3.65). The continuous form asymptotic analysis acts as a filter that a weight must pass through in order for further effort to be expended in its analysis.

3.4 Discretized Form Analysis Of Asymptotic Diffusion Limit

An asymptotic diffusion limit analysis of the NWF methods approximated by means of the BLD discretization described before (see Sec. 3.2) on a uniform rectangular spatial grid is performed. The purpose of this analysis is to determine if the NWF methods limit to a stable and consistent discretized form of the diffusion equation with an accurate asymptotic boundary condition for unresolved boundary layers. This analysis is very lengthy and will be reproduced here in a summarized form by highlighting significant steps. The analysis is presented for the case of mass lumping. The same analysis can be performed without lumping, but it is not shown here. Note that the only terms affected by mass lumping are the removal terms, scattering source, and external source. The derivative terms remain the same.

This analysis is performed in two locations, inside a diffusive region and on the boundary of a diffusive region. On the boundary, the analysis is performed for a cell sufficiently far from a corner of the diffusive region to avoid 2D effects. First, scaled cross sections and external source terms

$$\begin{aligned} \sigma_t &= \frac{\hat{\sigma}_t}{\varepsilon}\,, \quad \sigma_a = \varepsilon\hat{\sigma}_a\,, \\ q &= \varepsilon\hat{q}\,, \quad q^x = \varepsilon\hat{q}^x\,, \quad q^y = \varepsilon\hat{q}^y\,, \quad q^{xy} = \varepsilon\hat{q}^{xy}\,, \end{aligned} \tag{3.66}$$

are substituted into equations (3.8)-(3.9) , (3.35)-(3.41), and (3.43)-(3.44). Second, the ansatz is introduced into the same equations. The ansatz consists of a power series expansion of all unknowns in the parameter ε,

$$f = \sum_{n=0}^{\infty} \varepsilon^n f^{[n]}\,, \tag{3.67}$$

where f generally represents unknowns. Every discretized angular flux, scalar flux, and partial

scalar flux-moment is expanded in this manner.

The first equations to be expanded are that of the high-order problem (3.43)-(3.44). Upon expanding both the angular flux and scalar flux and then collecting like terms of ε, it is found that

$$\begin{aligned} \psi_n^{[0]} &= \frac{1}{4\pi}\phi_{ij}^{[0]}\,, \\ \psi_n^{[1]} &= 0\,, \\ \psi_n^{[2]} &= \frac{1}{4\pi}\left(\phi_{ij}^{[2]} - \frac{\sigma_{a,ij}}{\sigma_{t,ij}}\phi_{ij}^{[0]}\right)\,. \end{aligned} \tag{3.68}$$

This means that to leading order the angular flux resulting from the method of short characteristics is isotropic. And, the $\psi^{[1]}$ terms are zero, which means that the angular flux varies from an isotropic distribution only by ε^2 terms and higher which are much smaller in magnitude.

The factors (3.8)-(3.9) are analyzed next. The weight is left in general form and the angular flux is expanded. After some algebra and using the results of (3.68), it is found that

$$G_{m,i-1/2,j-1/2}^{[0]} = \begin{cases} \dfrac{\gamma_m \int\limits_{\omega_m} w(\Omega_x,\Omega_y)\psi_{i-1/2,j-1/2}^{in} d\vec{\Omega}}{\int\limits_{\omega_m} \psi_{i-1/2,j-1/2}^{in} d\vec{\Omega}}\,, & \text{for } i-1/2, j-1/2 \in \partial\mathcal{D} \text{ and m is incoming,} \\ 1\,, & \text{for all other vertices and m,} \end{cases} \tag{3.69}$$

$$F_{m,i-1/2,j-1/2}^{\alpha,[0]} = \begin{cases} \dfrac{\gamma_m \int\limits_{\omega_m} w(\Omega_x,\Omega_y)\psi_{i-1/2,j-1/2}^{in} |\Omega_\alpha| d\vec{\Omega}}{\int\limits_{\omega_m} \psi_{i-1/2,j-1/2}^{in} d\vec{\Omega}}\,, & \text{for } i-1/2, j-1/2 \in \partial\mathcal{D} \text{ and m is incoming,} \\ \tilde{F}\,, & \text{for all other vertices and m,} \end{cases} \tag{3.70}$$

where α = x,y and $\tilde{F}$ is the factor evaluated with an isotropic angular flux. Note that ψ^{in} is leading order. $G^{[n]}$ and $F^{\alpha,[n]}$ are zero for n = 1 and 2.

The factors used by the low-order equations are face-average and cell-average factors. These are generally calculated as an average of the vertices bounding a face or the four vertices

bounding a cell. The analysis showed that in the cells at the interior of the interfaces of the thick diffusive regions, cell-average factors and downstream face-average factors need to be defined by the corresponding downstream vertex value, namely, given by:

$$\begin{aligned} G_{1,i,j} &= G_{1,i+1/2,j+1/2} \ , \\ G_{2,i,j} &= G_{2,i-1/2,j+1/2} \ , \\ G_{3,i,j} &= G_{3,i-1/2,j-1/2} \ , \\ G_{4,i,j} &= G_{4,i+1/2,j-1/2} \ , \end{aligned} \tag{3.71}$$

$$\begin{aligned} F^{\alpha}_{1,i,j} &= F^{\alpha}_{1,i+1/2,j} = F^{\alpha}_{1,i,j+1/2} = F^{\alpha}_{1,i+1/2,j+1/2} \ , \\ F^{\alpha}_{2,i,j} &= F^{\alpha}_{2,i-1/2,j} = F^{\alpha}_{2,i,j+1/2} = F^{\alpha}_{2,i-1/2,j+1/2} \ , \\ F^{\alpha}_{3,i,j} &= F^{\alpha}_{3,i-1/2,j} = F^{\alpha}_{3,i,j-1/2} = F^{\alpha}_{3,i-1/2,j-1/2} \ , \\ F^{\alpha}_{4,i,j} &= F^{\alpha}_{4,i+1/2,j} = F^{\alpha}_{4,i,j-1/2} = F^{\alpha}_{4,i+1/2,j-1/2} \ . \end{aligned} \tag{3.72}$$

This reassignment of factors is physically meaningful. Any angular flux distribution that enters into an optically thick highly diffusive cell becomes isotropic in it. Only in the boundary layer where the angular flux transitions to isotropic is it not necessarily so, and this is a very small area of such a cell. In the context of this finite element discretization, a face-average and cell-average factor can be interpreted as the value at the midpoint of the face and center of the cell, respectively. Thus, a cell average and face average factor located downstream of an incoming angular flux should correspond to the shape of the angular flux at that very location. A simple averaging over the whole cell or cell face does not lead to correct asymptotic values of the factors.

This completes what can be termed as mostly preliminary work in that nothing has

been done with the actual low-order equations and the weight is still in general form. Next, the analysis is completed for the interior of a diffusive region and a boundary cell far from corners.

3.4.1 Asymptotic Diffusion Limit Analysis in the Interior of a Diffusive Region

The low-order BLD discretized equations for an interior cell of a thick diffusive region were scaled and expanded in terms of ε in the previous section using (3.66) and (3.67). Next, the expansion of the factors, (3.69) and (3.70), are introduced into the scaled and expanded BLD discretized equations taking into account the downstream reassignment of factors given by (3.71) and (3.72). Then, coefficients of corresponding powers of ε are equated to give a system of linear equations. Reducing the system for the equation describing the behavior of the leading-order scalar flux in the interior of the optically-thick diffusive region is shown next.

After some straightforward manipulations, we get the following equations:

$\underline{O(\varepsilon^{-1})}$:

$$\phi^{[0]}_{m,ij} = \frac{1}{4}\phi^{[0]}_{ij}\,, \tag{3.73}$$

$$\phi^{x[0]}_{m,ij} = \frac{1}{4}\phi^{x[0]}_{ij}\,, \tag{3.74}$$

$$\phi^{y[0]}_{m,ij} = \frac{1}{4}\phi^{y[0]}_{ij}\,, \tag{3.75}$$

$$\phi^{xy[0]}_{m,ij} = \frac{1}{4}\phi^{xy[0]}_{ij}\,, \tag{3.76}$$

$\underline{O(1)}$:

$$\nu^x_k \Delta y_j \tilde{F}\left[\phi^{[0]}_{m,i+1/2,j} - \phi^{[0]}_{m,i-1/2,j}\right] + \nu^y_k \Delta x_i \tilde{F}\left[\phi^{[0]}_{m,i,j+1/2} - \phi^{[0]}_{m,i,j-1/2}\right]$$

$$+\sigma_{t,ij}\Delta x_i \Delta y_j \phi^{[1]}_{m,i,j} = \frac{1}{4}\Delta x_i \Delta y_j \sigma_{t,ij}\phi^{[1]}_{i,j}\,, \tag{3.77}$$

$$3\nu_k^x \Delta y_j \tilde{F}\left[\phi^{[0]}_{m,i+1/2,j} + \phi^{[0]}_{m,i-1/2,j} - 2\phi^{[0]}_{m,i,j}\right] + \nu_k^y \Delta x_i \tilde{F}\left[\phi^{x[0]}_{m,i,j+1/2} - \phi^{x[0]}_{m,i,j-1/2}\right]$$
$$+3\sigma_{t,ij}\Delta x_i \Delta y_j \phi^{x[1]}_{m,i,j} = \frac{3}{4}\Delta x_i \Delta y_j \sigma_{t,ij}\phi^{x[1]}_{i,j}\,, \tag{3.78}$$

$$\nu_k^x \Delta y_j \tilde{F}\left[\phi^{y[0]}_{m,i+1/2,j} - \phi^{y[0]}_{m,i-1/2,j}\right] + 3\nu_k^y \Delta x_i \tilde{F}\left[\phi^{[0]}_{m,i,j+1/2} + \phi^{[0]}_{m,i,j-1/2} - 2\phi^{[0]}_{m,i,j}\right]$$
$$+3\sigma_{t,ij}\Delta x_i \Delta y_j \phi^{y[1]}_{m,i,j} = \frac{3}{4}\Delta x_i \Delta y_j \sigma_{t,ij}\phi^{y[1]}_{i,j}\,, \tag{3.79}$$

$$3\nu_k^x \Delta y_j \tilde{F}\left[\phi^{y[0]}_{m,i+1/2,j} + \phi^{y[0]}_{m,i-1/2,j} - 2\phi^{y[0]}_{m,i,j}\right] + 3\nu_k^y \Delta x_i \tilde{F}\left[\phi^{x[0]}_{m,i,j+1/2} + \phi^{x[0]}_{m,i,j-1/2} - 2\phi^{x[0]}_{m,i,j}\right]$$
$$+9\sigma_{t,ij}\Delta x_i \Delta y_j \phi^{xy[1]}_{m,i,j} = \frac{9}{4}\Delta x_i \Delta y_j \sigma_{t,ij}\phi^{xy[1]}_{i,j}\,, \tag{3.80}$$

$$\begin{aligned}
\phi^{[0]}_{1,i+1/2,j} &= \phi^{[0]}_{1,i,j} + \phi^{x[0]}_{1,i,j}\,, & \phi^{[0]}_{3,i-1/2,j} &= \phi^{[0]}_{3,i,j} - \phi^{x[0]}_{3,i,j}\,,\\
\phi^{y[0]}_{1,i+1/2,j} &= \phi^{y[0]}_{1,i,j} + \phi^{xy[0]}_{1,i,j}\,, & \phi^{y[0]}_{3,i-1/2,j} &= \phi^{y[0]}_{3,i,j} - \phi^{xy[0]}_{3,i,j}\,,\\
\phi^{[0]}_{1,i,j+1/2} &= \phi^{[0]}_{1,i,j} + \phi^{y[0]}_{1,i,j}\,, & \phi^{[0]}_{3,i,j-1/2} &= \phi^{[0]}_{3,i,j} + \phi^{y[0]}_{3,i,j}\,,\\
\phi^{x[0]}_{1,i,j+1/2} &= \phi^{x[0]}_{1,i,j} + \phi^{xy[0]}_{1,i,j}\,, & \phi^{x[0]}_{3,i,j-1/2} &= \phi^{x[0]}_{3,i,j} - \phi^{xy[0]}_{3,i,j}\,,
\end{aligned} \tag{3.81}$$

$$\begin{aligned}
\phi^{[0]}_{2,i-1/2,j} &= \phi^{[0]}_{2,i,j} - \phi^{x[0]}_{2,i,j}\,, & \phi^{[0]}_{4,i+1/2,j} &= \phi^{[0]}_{4,i,j} + \phi^{x[0]}_{4,i,j}\,,\\
\phi^{y[0]}_{2,i-1/2,j} &= \phi^{y[0]}_{2,i,j} - \phi^{xy[0]}_{2,i,j}\,, & \phi^{y[0]}_{4,i+1/2,j} &= \phi^{y[0]}_{4,i,j} + \phi^{xy[0]}_{4,i,j}\,,\\
\phi^{[0]}_{2,i,j+1/2} &= \phi^{[0]}_{2,i,j} + \phi^{y[0]}_{2,i,j}\,, & \phi^{[0]}_{4,i,j-1/2} &= \phi^{[0]}_{4,i,j} - \phi^{y[0]}_{4,i,j}\,,\\
\phi^{x[0]}_{2,i,j+1/2} &= \phi^{x[0]}_{2,i,j} + \phi^{xy[0]}_{2,i,j}\,, & \phi^{x[0]}_{4,i,j-1/2} &= \phi^{x[0]}_{4,i,j} - \phi^{xy[0]}_{4,i,j}\,,
\end{aligned} \tag{3.82}$$

$\underline{O(\varepsilon^1)}$:

$$\nu_k^x \Delta y_j \tilde{F}\left[\phi^{[1]}_{m,i+1/2,j} - \phi^{[1]}_{m,i-1/2,j}\right] + \nu_k^y \Delta x_i \tilde{F}\left[\phi^{[1]}_{m,i,j+1/2} - \phi^{[1]}_{m,i,j-1/2}\right]$$
$$+\sigma_{t,ij}\Delta x_i \Delta y_j \phi^{[2]}_{m,i,j} = \frac{1}{4}\Delta x_i \Delta y_j \left[\sigma_{t,ij}\phi^{[2]}_{i,j} - \sigma_{a,ij}\phi^{[0]}_{i,j} + q^{[0]}_{i,j}\right]\,, \tag{3.83}$$

$$3\nu_k^x \Delta y_j \tilde{F}\left[\phi^{[1]}_{m,i+1/2,j} + \phi^{[1]}_{m,i-1/2,j} - 2\phi^{[1]}_{m,i,j}\right] + \nu_k^y \Delta x_i \tilde{F}\left[\phi^{x[1]}_{m,i,j+1/2} - \phi^{x[1]}_{m,i,j-1/2}\right]$$
$$+3\sigma_{t,ij}\Delta x_i \Delta y_j \phi^{x[2]}_{m,i,j} = \frac{3}{4}\Delta x_i \Delta y_j \left[\sigma_{t,ij}\phi^{x[2]}_{i,j} - \sigma_{a,ij}\phi^{x[0]}_{i,j} + q^{x[0]}_{i,j}\right]\,, \tag{3.84}$$

$$\nu_k^x \Delta y_j \tilde{F} \left[\phi^{y[1]}_{m,i+1/2,j} - \phi^{y[1]}_{m,i-1/2,j} \right] + 3\nu_k^y \Delta x_i \tilde{F} \left[\phi^{[1]}_{m,i,j+1/2} + \phi^{[1]}_{m,i,j-1/2} - 2\phi^{[1]}_{m,i,j} \right]$$
$$+3\sigma_{t,ij} \Delta x_i \Delta y_j \phi^{y[2]}_{m,i,j} = \frac{3}{4} \Delta x_i \Delta y_j \left[\sigma_{t,ij} \phi^{y[2]}_{i,j} - \sigma_{a,ij} \phi^{y[0]}_{i,j} + q^{y[0]}_{i,j} \right] , \tag{3.85}$$

$$3\nu_k^x \Delta y_j \tilde{F} \left[\phi^{y[1]}_{m,i+1/2,j} + \phi^{y[1]}_{m,i-1/2,j} - 2\phi^{y[1]}_{m,i,j} \right] + 3\nu_k^y \Delta x_i \tilde{F} \left[\phi^{x[1]}_{m,i,j+1/2} + \phi^{x[1]}_{m,i,j-1/2} - 2\phi^{x[1]}_{m,i,j} \right]$$
$$+9\sigma_{t,ij} \Delta x_i \Delta y_j \phi^{xy[2]}_{m,i,j} = \frac{9}{4} \Delta x_i \Delta y_j \left[\sigma_{t,ij} \phi^{xy[2]}_{i,j} - \sigma_{a,ij} \phi^{xy[0]}_{i,j} + q^{xy[0]}_{i,j} \right] , \tag{3.86}$$

$$\begin{aligned}
\phi^{[1]}_{1,i+1/2,j} &= \phi^{[1]}_{1,i,j} + \phi^{x[1]}_{1,i,j} , & \phi^{[1]}_{3,i-1/2,j} &= \phi^{[1]}_{3,i,j} - \phi^{x[1]}_{3,i,j} , \\
\phi^{y[1]}_{1,i+1/2,j} &= \phi^{y[1]}_{1,i,j} + \phi^{xy[1]}_{1,i,j} , & \phi^{y[1]}_{3,i-1/2,j} &= \phi^{y[1]}_{3,i,j} - \phi^{xy[1]}_{3,i,j} , \\
\phi^{[1]}_{1,i,j+1/2} &= \phi^{[1]}_{1,i,j} + \phi^{y[1]}_{1,i,j} , & \phi^{[1]}_{3,i,j-1/2} &= \phi^{[1]}_{3,i,j} + \phi^{y[1]}_{3,i,j} , \\
\phi^{x[1]}_{1,i,j+1/2} &= \phi^{x[1]}_{1,i,j} + \phi^{xy[1]}_{1,i,j} , & \phi^{x[1]}_{3,i,j-1/2} &= \phi^{x[1]}_{3,i,j} - \phi^{xy[1]}_{3,i,j} ,
\end{aligned} \tag{3.87}$$

$$\begin{aligned}
\phi^{[1]}_{2,i-1/2,j} &= \phi^{[1]}_{2,i,j} - \phi^{x[1]}_{2,i,j} , & \phi^{[1]}_{4,i+1/2,j} &= \phi^{[1]}_{4,i,j} + \phi^{x[1]}_{4,i,j} , \\
\phi^{y[1]}_{2,i-1/2,j} &= \phi^{y[1]}_{2,i,j} - \phi^{xy[1]}_{2,i,j} , & \phi^{y[1]}_{4,i+1/2,j} &= \phi^{y[1]}_{4,i,j} + \phi^{xy[1]}_{4,i,j} , \\
\phi^{[1]}_{2,i,j+1/2} &= \phi^{[1]}_{2,i,j} + \phi^{y[1]}_{2,i,j} , & \phi^{[1]}_{4,i,j-1/2} &= \phi^{[1]}_{4,i,j} - \phi^{y[1]}_{4,i,j} , \\
\phi^{x[1]}_{2,i,j+1/2} &= \phi^{x[1]}_{2,i,j} + \phi^{xy[1]}_{2,i,j} , & \phi^{x[1]}_{4,i,j-1/2} &= \phi^{x[1]}_{4,i,j} - \phi^{xy[1]}_{4,i,j} ,
\end{aligned} \tag{3.88}$$

$$m = 1, \ldots, 4 ,$$

$$i, j \neq 1,\ N_x,\ \text{or}\ N_y .$$

The $O(\varepsilon^{-1})$ equations show that the leading order cell-average scalar flux and flux-moments are isotropic. The $O(1)$ equations give a relationship between $\phi^{[0]}$ and $\phi^{[1]}$.

This set of equations, (3.73)-(3.88), are linearly combined in order to get a relationship solely in terms of the leading order scalar flux over four mesh cells. The first step in this process

is to combine the $O(\varepsilon^1)$ equations by the following relationship

$$\frac{1}{4}\left[\sum_{m=1}^{4} Eq.(3.83)\Big|_{i,j} + \sum_{m=1}^{4} Eq.(3.83)\Big|_{i+1,j} + \sum_{m=1}^{4} Eq.(3.83)\Big|_{i+1,j+1} + \sum_{m=1}^{4} Eq.(3.83)\Big|_{i,j+1}\right] +$$
$$\frac{1}{2}\left[\sum_{m=1}^{4} Eq.(3.84)\Big|_{i,j} - \sum_{m=1}^{4} Eq.(3.84)\Big|_{i+1,j} - \sum_{m=1}^{4} Eq.(3.84)\Big|_{i+1,j+1} + \sum_{m=1}^{4} Eq.(3.84)\Big|_{i,j+1}\right] +$$
$$\frac{1}{12}\left[\sum_{m=1}^{4} Eq.(3.85)\Big|_{i,j} + \sum_{m=1}^{4} Eq.(3.85)\Big|_{i+1,j} - \sum_{m=1}^{4} Eq.(3.85)\Big|_{i+1,j+1} - \sum_{m=1}^{4} Eq.(3.85)\Big|_{i,j+1}\right] +$$
$$\frac{1}{36}\left[\sum_{m=1}^{4} Eq.(3.86)\Big|_{i,j} - \sum_{m=1}^{4} Eq.(3.86)\Big|_{i+1,j} + \sum_{m=1}^{4} Eq.(3.86)\Big|_{i+1,j+1} - \sum_{m=1}^{4} Eq.(3.86)\Big|_{i,j+1}\right]. \tag{3.89}$$

The purpose of these operations are to remove all $\phi_m^{[2]}$ terms and obtain the correct leading-order discretized form of $\sigma_a\phi$ and q.

The next step is to operate on the terms representing $\nabla\cdot\vec{J}$. The following definitions are made:

$$\tilde{J}_{i,j}^{[1]} = \sum_{m=1}^{4} \tilde{F}\nu_m^{\alpha}\phi_{m,i,j}^{[1]}\,, \tag{3.90}$$
$$\tilde{J}_{i,j}^{\alpha,[1]} = \sum_{m=1}^{4} \tilde{F}\nu_m^{\alpha}\phi_{m,i,j}^{\alpha,[1]}\,, \tag{3.91}$$
$$\tilde{J}_{\alpha,i,j}^{[1]} = \hat{n}_{\alpha}\cdot\tilde{J}_{i,j}^{[1]}\,, \tag{3.92}$$
$$\alpha = x, y\,. \tag{3.93}$$

Equation (3.90) defines a total current-like quantity, equation (3.91) defines the x and y spatial moments of this quantity, and equation (3.92) defines the current-like quantity in the x and y directions. At this point, the total cross section and cell widths are left out of the definitions for ease of manipulation. A conversion is made to unknowns located on vertices. The BLD

discretization can be defined on faces or vertices equivalently. Consider the following conversion

$$\tilde{J}^{[1]}_{i,j} = \frac{1}{4}\left(\tilde{J}^{[1]}_1 + \tilde{J}^{[1]}_2 + \tilde{J}^{[1]}_3 + \tilde{J}^{[1]}_4\right), \tag{3.94}$$

$$\tilde{J}^{x,[1]}_{i,j} = \frac{1}{4}\left(-\tilde{J}^{[1]}_1 + \tilde{J}^{[1]}_2 + \tilde{J}^{[1]}_3 - \tilde{J}^{[1]}_4\right), \tag{3.95}$$

$$\tilde{J}^{y,[1]}_{i,j} = \frac{1}{4}\left(-\tilde{J}^{[1]}_1 - \tilde{J}^{[1]}_2 + \tilde{J}^{[1]}_3 + \tilde{J}^{[1]}_4\right), \tag{3.96}$$

$$\tilde{J}^{xy,[1]}_{i,j} = \frac{1}{4}\left(\tilde{J}^{[1]}_1 - \tilde{J}^{[1]}_2 + \tilde{J}^{[1]}_3 - \tilde{J}^{[1]}_4\right), \tag{3.97}$$

$$\tag{3.98}$$

where the vertices are numbered counter clockwise beginning from the southwest vertex $(i - 1/2, j - 1/2)$. Considerable manipulation of the equations are made to organize the terms into physically meaningful current relationships across the four cells.

A convenient way to write the result is in terms of currents defined on the faces of the cells using

$$J^{N,[1]}_{x,i,j} = \frac{-\tilde{F}^2(\phi^{[0]}_3 - \phi^{[0]}_4)}{\sigma_{t,i,j}\Delta x_{i,j}}, \tag{3.99}$$

$$J^{S,[1]}_{x,i,j} = \frac{-\tilde{F}^2(\phi^{[0]}_2 - \phi^{[0]}_1)}{\sigma_{t,i,j}\Delta x_{i,j}}, \tag{3.100}$$

$$J^{W,[1]}_{y,i,j} = \frac{-\tilde{F}^2(\phi^{[0]}_4 - \phi^{[0]}_1)}{\sigma_{t,i,j}\Delta y_{i,j}}, \tag{3.101}$$

$$J^{E,[1]}_{y,i,j} = \frac{-\tilde{F}^2(\phi^{[0]}_3 - \phi^{[0]}_2)}{\sigma_{t,i,j}\Delta y_{i,j}}, \tag{3.102}$$

where N, S, E, and W represent North, South, East, and West sides of a cell, respectively. Then, the leading order equation of scalar fluxes is written in terms of O(1) currents as

$$\frac{\Delta y_j}{2}\left[\left(\frac{2}{3}J^{N,[1]}_{x,i+1,j} + \frac{1}{3}J^{S,[1]}_{x,i+1,j}\right) - \left(\frac{2}{3}J^{N,[1]}_{x,i,j} + \frac{1}{3}J^{S,[1]}_{x,i,j}\right)\right]$$

$$+\frac{\Delta y_{j+1}}{2}\left[\left(\frac{2}{3}J^{S,[1]}_{x,i+1,j+1} + \frac{1}{3}J^{N,[1]}_{x,i+1,j+1}\right) - \left(\frac{2}{3}J^{S,[1]}_{x,i,j+1} + \frac{1}{3}J^{N,[1]}_{x,i,j+1}\right)\right]$$

$$+\frac{\Delta x_i}{2}\left[\left(\frac{2}{3}J^{E,[1]}_{y,i,j+1}+\frac{1}{3}J^{W,[1]}_{y,i,j+1}\right)-\left(\frac{2}{3}J^{E,[1]}_{y,i,j}+\frac{1}{3}J^{W,[1]}_{y,i,j}\right)\right]$$
$$+\frac{\Delta x_{i+1}}{2}\left[\left(\frac{2}{3}J^{W,[1]}_{y,i+1,j+1}+\frac{1}{3}J^{E,[1]}_{y,i+1,j+1}\right)-\left(\frac{2}{3}J^{W,[1]}_{y,i+1,j}+\frac{1}{3}J^{E,[1]}_{y,i+1,j}\right)\right]+A_{i,j}=Q_{i,j} \tag{3.103}$$

where,

$$A_{i,j}=\frac{1}{4}\left(\widehat{A}^{[0]}_{i,j}+\widehat{A}^{x,[0]}_{i,j}+\widehat{A}^{y,[0]}_{i,j}+\widehat{A}^{xy,[0]}_{i,j}\right), \tag{3.104}$$

$$Q_{i,j}=\frac{1}{4}\left(\widehat{Q}^{[0]}_{i,j}+\widehat{Q}^{x,[0]}_{i,j}+\widehat{Q}^{y,[0]}_{i,j}+\widehat{Q}^{xy,[0]}_{i,j}\right), \tag{3.105}$$

and,

$$\begin{aligned}
\widehat{A}^{[0]}_{i,j} &= \Delta x_i\Delta y_j\sigma_{a,i,j}\phi^{[0]}_{i,j}+\Delta x_{i+1}\Delta y_j\sigma_{a,i+1,j}\phi^{[0]}_{i+1,j}+\Delta x_{i+1}\Delta y_{j+1}\sigma_{a,i+1,j+1}\phi^{[0]}_{i+1,j+1}\\
&+ \Delta x_i\Delta y_{j+1}\sigma_{a,i,j+1}\phi^{[0]}_{i,j+1},\\
\widehat{A}^{x,[0]}_{i,j} &= \Delta x_i\Delta y_j\sigma_{a,i,j}\phi^{[0]}_{x,i,j}+\Delta x_{i+1}\Delta y_j\sigma_{a,i+1,j}\phi^{[0]}_{x,i+1,j}+\Delta x_{i+1}\Delta y_{j+1}\sigma_{a,i+1,j+1}\phi^{[0]}_{x,i+1,j+1}\\
&+ \Delta x_i\Delta y_{j+1}\sigma_{a,i,j+1}\phi^{[0]}_{x,i,j+1},\\
\widehat{A}^{y,[0]}_{i,j} &= \Delta x_i\Delta y_j\sigma_{a,i,j}\phi^{[0]}_{y,i,j}+\Delta x_{i+1}\Delta y_j\sigma_{a,i+1,j}\phi^{[0]}_{y,i+1,j}+\Delta x_{i+1}\Delta y_{j+1}\sigma_{a,i+1,j+1}\phi^{[0]}_{y,i+1,j+1}\\
&+ \Delta x_i\Delta y_{j+1}\sigma_{a,i,j+1}\phi^{[0]}_{y,i,j+1},\\
\widehat{A}^{xy,[0]}_{i,j} &= \Delta x_i\Delta y_j\sigma_{a,i,j}\phi^{[0]}_{xy,i,j}+\Delta x_{i+1}\Delta y_j\sigma_{a,i+1,j}\phi^{[0]}_{xy,i+1,j}+\Delta x_{i+1}\Delta y_{j+1}\sigma_{a,i+1,j+1}\phi^{[0]}_{xy,i+1,j+1}\\
&+ \Delta x_i\Delta y_{j+1}\sigma_{a,i,j+1}\phi^{[0]}_{xy,i,j+1},
\end{aligned} \tag{3.106}$$

$$\begin{aligned}
\widehat{Q}^{[0]}_{i,j} &= \Delta x_i\Delta y_j q^{[0]}_{i,j}+\Delta x_{i+1}\Delta y_j q^{[0]}_{i+1,j}+\Delta x_{i+1}\Delta y_{j+1}q^{[0]}_{i+1,j+1}\\
&+ \Delta x_i\Delta y_{j+1}q^{[0]}_{i,j+1},\\
\widehat{Q}^{x,[0]}_{i,j} &= \Delta x_i\Delta y_j q^{[0]}_{x,i,j}+\Delta x_{i+1}\Delta y_j q^{[0]}_{x,i+1,j}+\Delta x_{i+1}\Delta y_{j+1}q^{[0]}_{x,i+1,j+1}\\
&+ \Delta x_i\Delta y_{j+1}q^{[0]}_{x,i,j+1},\\
\widehat{Q}^{y,[0]}_{i,j} &= \Delta x_i\Delta y_j q^{[0]}_{y,i,j}+\Delta x_{i+1}\Delta y_j q^{[0]}_{y,i+1,j}+\Delta x_{i+1}\Delta y_{j+1}q^{[0]}_{y,i+1,j+1}
\end{aligned}$$

$$
\begin{aligned}
&+ \quad \Delta x_i \Delta y_{j+1} q^{[0]}_{y,i,j+1} \,, \\
\widehat{Q}^{xy,[0]}_{i,j} &= \Delta x_i \Delta y_j q^{[0]}_{xy,i,j} + \Delta x_{i+1} \Delta y_j q^{[0]}_{xy,i+1,j} + \Delta x_{i+1} \Delta y_{j+1} q^{[0]}_{xy,i+1,j+1} \\
&+ \quad \Delta x_i \Delta y_{j+1} q^{[0]}_{xy,i,j+1} \,. \qquad (3.107)
\end{aligned}
$$

Equation (3.103) can be written in terms of leading order scalar fluxes by substituting in the preceding current equations (3.99)-(3.102). For the sake of brevity and clarity, this is shown for the case of mass lumping, uniform rectangular mesh, and constant cross sections and source in each cell:

$$
\begin{aligned}
&-\frac{1}{6}\frac{\Delta y}{\Delta x}\frac{\tilde{F}^2}{\sigma_t}[\phi^{[0]}_{i-1/2,j+3/2} - 2\phi^{[0]}_{i+1/2,j+3/2} + \phi^{[0]}_{i+3/2,j+3/2} \\
&\quad +4\phi^{[0]}_{i-1/2,j+1/2} - 8\phi^{[0]}_{i+1/2,j+1/2} + 4\phi^{[0]}_{i+3/2,j+1/2} \\
&\quad +\phi^{[0]}_{i-1/2,j-1/2} - 2\phi^{[0]}_{i+1/2,j-1/2} + \phi^{[0]}_{i+3/2,j-1/2}] \\
&-\frac{1}{6}\frac{\Delta x}{\Delta y}\frac{\tilde{F}^2}{\sigma_t}[\phi^{[0]}_{i-1/2,j+3/2} + 4\phi^{[0]}_{i+1/2,j+3/2} + \phi^{[0]}_{i+3/2,j+3/2} \\
&\quad -2\phi^{[0]}_{i-1/2,j+1/2} - 8\phi^{[0]}_{i+1/2,j+1/2} - 2\phi^{[0]}_{i+3/2,j+1/2} \\
&\quad +\phi^{[0]}_{i-1/2,j-1/2} + 4\phi^{[0]}_{i+1/2,j-1/2} + \phi^{[0]}_{i+3/2,j-1/2}] \\
&+\Delta x \Delta y \sigma_a \phi^{[0]}_{i+1/2,j+1/2} = \frac{1}{4}\Delta x \Delta y \left[q_{i,j} + q_{i+1,j} + q_{i+1,j+1} + q_{i,j+1}\right] . \qquad (3.108)
\end{aligned}
$$

This is a stable and consistent nine-point discretization of the diffusion equation. However, the resulting discretized diffusion equation has the diffusion coefficient

$$
D = \frac{\tilde{F}^2}{\sigma_t} \,, \qquad (3.109)
$$

and hence in general it is not the correct diffusion coefficient (3.60). The choice of weight $w(\Omega_x, \Omega_y)$ will then determine the value of the resulting diffusion coefficient. If the conditions

(3.61)-(3.65) are met, then the low-order NWF equations discretized by the BLD method lead to the same discrete diffusion equation for the leading-order solution as the BLD discretization of the transport equation [40] with the correct diffusion coefficient.

3.4.2 Asymptotic Diffusion Limit Analysis in an Unresolved Boundary Cell of a Diffusive Region

We now analyze the behavior of the discretized NWF methods in the presence of a boundary layer that is not resolved by the spatial grid. Let us consider the boundary condition at $x = X$, where $\hat{n} = \hat{e}_x$. The NWF method low-order equations in one cell are considered. The analysis proceeds as before, considering the system of scaled equations with asymptotically expanded solution for the relationship governing the behavior of the leading-order scalar flux at the boundary. Recall that factors are evaluated at the boundary according to (3.69)–(3.70) and downstream face factors by the scheme (3.71)–(3.72). There are three assumptions made in the course of the analysis:

1. The cell is located a sufficient number of mean free paths away from any corner of the diffusive region boundary so as to avoid 2D effects.

2. The incoming angular flux is constant over the boundary and symmetric about the surface normal.

3. The outgoing angular flux is isotropic.

For the case of mass lumping, the downstream factor scheme prescribed in (3.71)–(3.72), and assumption 1, it is found that

$$J^{[1]}_{y,N_x,j} = \frac{-\tilde{F}^2}{\sigma_{t,N_x,j}\Delta x_{N_x}\Delta y_j}\left[\Delta x_{N_x}\left(\phi^{[0]}_{N_x,j+1/2} - \phi^{[0]}_{N_x,j-1/2}\right)\right.$$
$$\left. -\frac{\Delta y_j}{2\tilde{F}}\left(\phi_{2,X,j}\left(F^x_{2,X,j-1/2} + F^x_{2,X,j+1/2}\right) - \phi_{3,X,j}\left(F^x_{3,X,j-1/2} + F^x_{3,X,j+1/2}\right)\right)\right], \tag{3.110}$$

$$J^{[1]}_{x,N_x,j} = \frac{-\tilde{F}^2}{\sigma_{t,N_x,j}\Delta x_{N_x}}\left[\frac{1}{\tilde{F}}\left(\phi_{2,X,j}\left(F^x_{2,X,j-1/2} + F^x_{2,X,j+1/2}\right)\right.\right.$$
$$\left.\left. +\phi_{3,X,j}\left(F^x_{3,X,j-1/2} + F^x_{3,X,j+1/2}\right)\right) - \phi^{[0]}_{N_x-1/2,j}\right], \tag{3.111}$$

which represent the x and y-currents across the boundary cell in the form of Fick's Law. The current in the y-direction (3.110) has a parasitic source in the second line of the equation which is not desired. Further analysis shows that this parasitic source will cancel in the context of the diffusion equation (3.103) and thus not affect the solution. The current in the direction normal to the boundary fits the desired form of Fick's Law, where the scalar flux at the boundary is easily extracted from the $d\phi/dx$ terms of equation (3.111). The total scalar flux on the boundary is then given by

$$\phi^{[0]}_{X,j} = \frac{1}{\tilde{F}}\left[\phi_{2,X,j}\left(F^x_{2,X,j-1/2} + F^x_{2,X,j+1/2}\right) + \phi_{3,X,j}\left(F^x_{3,X,j-1/2} + F^x_{3,X,j+1/2}\right)\right]. \tag{3.112}$$

Applying the second assumption simplifies this relationship to

$$\phi^{[0]}_{X,j} = \frac{2}{\tilde{F}}\sum_{m=2}^{3} F^x_{m,X,j}\phi_{m,X,j}\,. \tag{3.113}$$

Note that (3.112) is a general description subject only to the first and third assumptions. Expanding the factors in terms of quadrature sums gives

$$\phi^{[0]}_{X,j} = \frac{2\pi\sum_{\vec{n}_x\cdot\vec{\Omega}_m<0}\left[w(|\Omega_{x,m}|,|\Omega_{y,m}|)|\Omega_{x,m}|\right]\psi_{in}(\vec{\Omega}_m)\zeta_m}{\sum_{m\in\omega_1} w(|\Omega_{x,m}|,|\Omega_{y,m}|)|\Omega_{x,m}|\zeta_m}, \tag{3.114}$$

where ζ_m are quadrature weights. The equation (3.114) approximates the following boundary relationship in a continuous form:

$$\phi^{[0]}(X,y) = 2\int_{\vec{n}\cdot\vec{\Omega}<0} \widetilde{W}(|\Omega_x|,|\Omega_y|)\psi_{in}(X,y,\vec{\Omega})d\vec{\Omega}\,, \tag{3.115}$$

where

$$\widetilde{W}(|\Omega_x|,|\Omega_y|) = \frac{\pi w(|\Omega_x|,|\Omega_y|)|\Omega_x|}{\int_{\omega_1} w(|\Omega_x|,|\Omega_y|)|\Omega_x|d\vec{\Omega}}\,. \tag{3.116}$$

The asymptotic analysis of other boundaries, for instance at $y = 0$, results in a similar expression. The transport equation's boundary weight function (1.51) depends only on $\mu = |\vec{n}\cdot\vec{\Omega}|$, which for the boundary considered is $|\Omega_x|$. Note that the resulting boundary weight function for the NWF method (3.116) is generally a function of both directional cosines, $|\Omega_x|$ and $|\Omega_y|$.

3.5 NWF Weight Selection

We now consider what form the general weight $w(\Omega_x,\Omega_y)$ shall take in order to result in a specific method of the NWF family of methods with the characteristics we desire. Specifically, these characteristics are an accurate approximation of the diffusion equation and boundary condition by the leading-order scalar flux within optically thick diffusive regions in the asymptotic diffusion limit. Let us consider methods with a general bilinear weight function of directional cosines

$$w(\Omega_x,\Omega_y) = 1 + \beta_x|\Omega_x| + \beta_y|\Omega_y| + \beta_{xy}|\Omega_x\Omega_y|\,. \tag{3.117}$$

For the weight (3.117) and specified above ranges for the partial fluxes (i.e. ω_m), we get

$$\tilde{F}_m^{\alpha} = \frac{\frac{1}{2} + \frac{1}{3}(\beta_x + \frac{2}{\pi}\beta_y) + \frac{1}{8}\beta_{xy}}{1 + \frac{1}{2}(\beta_x + \beta_y) + \frac{2}{3\pi}\beta_{xy}}\,. \tag{3.118}$$

Note that the use of a general constant term in (3.117) will not result in a different NWF method.

The continuous form asymptotic diffusion limit analysis developed in Section (3.3) provides a pathway to analyze various NWF methods defined by the choice of differing weights, $w(\Omega_x, \Omega_y)$. In order for a specific NWF method to limit to the correct differential-form diffusion equation, the five requirements (3.61)-(3.65) must be satisfied by the selected weight. It is not necessary to have a bilinear polynomial weight, only a linear weight, in order to satisfy these conditions. Considering this and that the polynomial approximation (1.52) of the asymptotic boundary condition of the transport equation contains no bilinear directional cosine terms, we first consider methods derived from a linear polynomial weight ($\beta_{xy} = 0$). Then, the five requirements (3.61)-(3.65) are met if the following two conditions on the weight (3.117) are true:

$$\beta_x = \beta_y = \beta\,, \tag{3.119}$$

where

$$\beta = \frac{\pi\sqrt{3}(\sqrt{3}-2)}{2(\pi(\sqrt{3}-1)-2)} \approx -2.43\,. \tag{3.120}$$

The linear form of the weight (3.117) and parameter β determine a specific method within the family of NWF methods for which the low-order equations lead to the correct diffusion equation in the diffusion limit provided that the factors are calculated with an isotropic angular flux. In case of the weight $w(\Omega_x, \Omega_y) = 1 + \beta(|\Omega_x| + |\Omega_y|)$, we have $\tilde{F}_m^{\alpha^2} = \frac{1}{3}$ and obtain the right diffusion coefficient. The low-order equations of methods with $w = 1$, $w = |\Omega_x| + |\Omega_y|$, and $w = 1 + |\Omega_x| + |\Omega_y|$ give rise to a diffusion-like equation, but with a wrong diffusion coefficient. The values of the diffusion coefficients for these methods are shown in Table 3.1.

Table 3.1: Values of the Diffusion Coefficients (D) for Specific NWF Methods

Weight	$w=1$	$w=\|\Omega_x\|+\|\Omega_y\|$	$w=1+\|\Omega_x\|+\|\Omega_y\|$	$w=1+\beta(\|\Omega_x\|+\|\Omega_y\|)$
D	$\frac{1}{4\sigma_t}$	$(\frac{\pi+2}{3\pi})^2\frac{1}{\sigma_t}\approx\frac{1}{3.36\sigma_t}$	$(\frac{4+5\pi}{12\pi})^2\frac{1}{\sigma_t}\approx\frac{1}{3.66\sigma_t}$	$\frac{1}{3\sigma_t}$

We now examine the resulting weight function in the boundary condition, $\widetilde{W}(|\Omega_x|,|\Omega_y|)$, for various NWF methods considered thus far. Note that $\mu=|\hat{n}\cdot\vec{\Omega}|$, which for the boundary considered is $|\Omega_x|$. For the NWF method with $w(\Omega_x,\Omega_y)=1$, we get

$$\begin{aligned}\widetilde{W}(|\Omega_x|) &= 2|\Omega_x| \\ &\approx 2\mu\ . \end{aligned} \tag{3.121}$$

For the case $w(\Omega_x,\Omega_y)=|\Omega_x|+|\Omega_y|$, the boundary weight function is

$$\begin{aligned}\widetilde{W}(|\Omega_x|,|\Omega_y|) &= \frac{3\pi}{2+\pi}[|\Omega_x|^2+|\Omega_y||\Omega_x|] \\ &\approx 1.833[|\Omega_y|\mu+\mu^2]\ . \end{aligned} \tag{3.122}$$

The weight $w(\Omega_x,\Omega_y)=1+|\Omega_x|+|\Omega_y|$ results in the boundary weight function

$$\begin{aligned}\widetilde{W}(|\Omega_x|,|\Omega_y|) &= \frac{6\pi}{5\pi+4}[|\Omega_x|+|\Omega_x|^2+|\Omega_y||\Omega_x|] \\ &\approx 0.956[(1+|\Omega_y|)\mu+\mu^2]\ . \end{aligned} \tag{3.123}$$

If $w(\Omega_x,\Omega_y)=1+\beta\left(|\Omega_x|+|\Omega_y|\right)$, we have

$$\begin{aligned}\widetilde{W}(|\Omega_x|,|\Omega_y|) &= \left[\frac{1}{2}+\beta(\frac{2+\pi}{3\pi})\right]^{-1}\left(|\Omega_x|+\beta|\Omega_x|^2+\beta|\Omega_y||\Omega_x|\right) \\ &\approx (2.942|\Omega_y|-1.209)\mu+2.942\mu^2\ . \end{aligned} \tag{3.124}$$

The transport equation's boundary weight function (1.51) does not depend on the azimuthal variation of the incoming angular flux, but only upon $\mu=|\hat{n}\cdot\vec{\Omega}|$, which for the

boundary considered is $|\Omega_x|$. Note that the resulting boundary weight functions for the considered weights, $w(\Omega_x, \Omega_y)$, each differ from the polynomial approximation of $W(\mu)$. Each weight considered, except for $w(\Omega_x, \Omega_y) = 1$, results in a boundary condition weight function with azimuthal dependence, namely directionally dependent coefficients in polynomials of μ.

We now consider what can be gained by using a bilinear polynomial weight of the form given in (3.117), rather than a linear weight. Two conditions are placed on β_x, β_y, and β_{xy} by the five requirements (3.61)-(3.65) which result in a method that limits to the diffusion equation with the correct diffusion coefficient. Having the bilinear coefficient, β_{xy}, gives an extra degree of freedom which can be used to improve the accuracy of a method's boundary condition weight function.

We consider the following ways of manipulating a method's resulting boundary condition weight function through the choice of how to fully constrain the bilinear polynomial weight coefficients:

A. Exactly match the linear coefficients of the NWF boundary condition weighting function $\widetilde{W}$ (Eq. (3.116)) and the polynomial approximation of analytic asymptotic function $\widehat{W}$ (Eq. (1.52)).

B. Exactly match the quadratic coefficients of the NWF boundary condition weighting function $\widetilde{W}$ (Eq. (3.116)) and the polynomial approximation of analytic asymptotic function $\widehat{W}$ (Eq. (1.52)).

C. Obtain both positive linear and quadratic coefficients of the NWF boundary condition weighting function $\widetilde{W}$ (Eq. (3.116)).

D. Match the value of the polynomial approximation of the analytic asymptotic function

$\widehat{W}$ (Eq. (1.52)) exactly at the one ordinate in the quadrature set closest to the surface normal.

$D_{l,m}$. The same as Case D, except any one ordinate in the quadrature set specified by (θ_l, γ_m), other than that closest to the surface normal, is used.

To understand the subtle differences amongst the resulting boundary condition weight functions, it is useful to examine their shapes. The boundary condition weight functions of the differential form transport equation (exact form), the BLD discretized transport equation (no low-order scheme), the linear polynomial weight NWF method with $\beta \approx -2.43$, cases A-D, $D_{1,2}$, and $D_{1,3}$ are plotted for one spherical octant in Figures (3.2)-(3.18). The cases D and $D_{l,m}$ are formulated using the compatible quadruple-range quadrature with 9 ordinates per octant [54] where $l = 1$ denotes the polar cone nearest to the x-y plane and the azimuthal angle with respect to the surface normal ranges over $m = 1, \ldots, 3$. Note that case D is equivalent to case $D_{1,1}$. The relative errors of each versus the analytic result for the transport equation is also shown. Note that the resulting values of β_x, β_y, and β_{xy} are shown in the following table for these bilinear polynomial weight methods.

Table 3.2: Resulting values of β_x, β_y, and β_{xy} for the bilinear polynomial weights.

Case	β_x	β_y	β_{xy}
A	-1.718	-1.718	9.141
B	-54.32	-54.32	-664.9
C	0.0657	0.0657	32
D	-2.282	-2.282	1.918
$D_{1,2}$	-2.216	-2.216	2.768
$D_{1,3}$	-1.169	-1.169	16.18

It is important to consider the shape and magnitude of the boundary condition weight

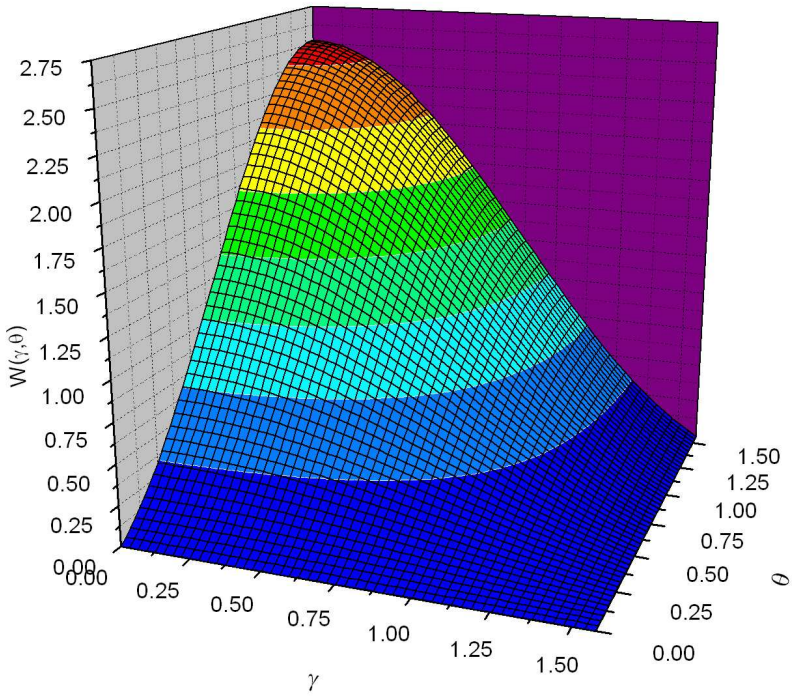

Figure 3.2: Analytic BC Weight Function.

functions over a whole octant due to its effect on the resulting boundary condition scalar flux. Note that only one octant need be examined due to symmetry. The BLD discretized transport equation's results in Figures 3.3 and 3.4 show a peak of reasonable magnitude but shifted away from the surface normal ($\gamma = 0, \theta = \pi/2$) where it is located in the analytic weight function in Figure 3.2. This results in small relative errors near $\gamma = 0$ and $\theta = 0$, but increasing errors over the octant to a maximum at $\gamma = \theta = \pi/2$. The NWF method's results with linear polynomial weight and $\beta \approx -2.43$ are in Figures 3.5 and 3.6. The behavior is very similar to that of the BLD transport equation in shape, but the peak magnitude is more accurate and there is a negative region for small θ. This gives large errors over the majority of the octant. Despite differing

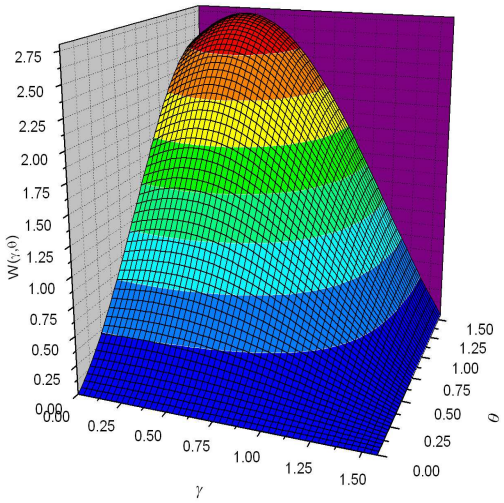

Figure 3.3: BLD Discretized Transport Equation BC Weight Function.

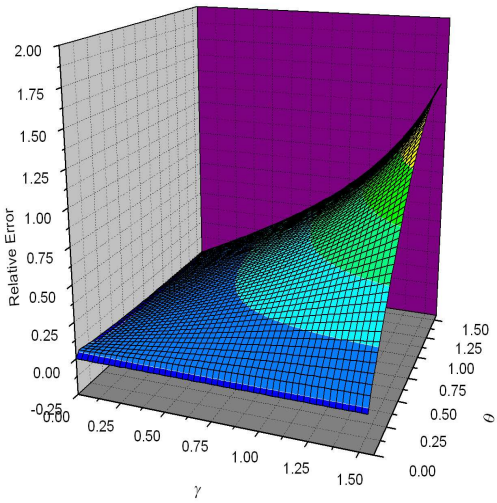

Figure 3.4: BLD Discretized Transport Equation BC Weight Function Relative Error vs. Analytic.

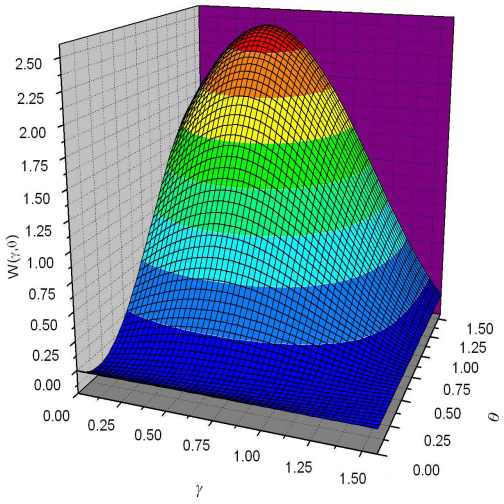

Figure 3.5: $\beta \approx -2.43$ BC Weight Function.

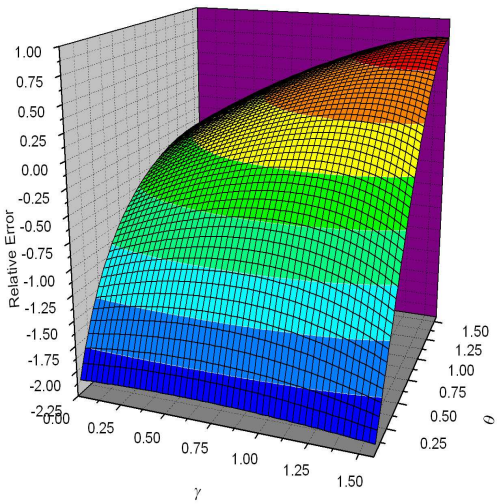

Figure 3.6: $\beta \approx -2.43$ BC Weight Function Relative Error vs. Analytic.

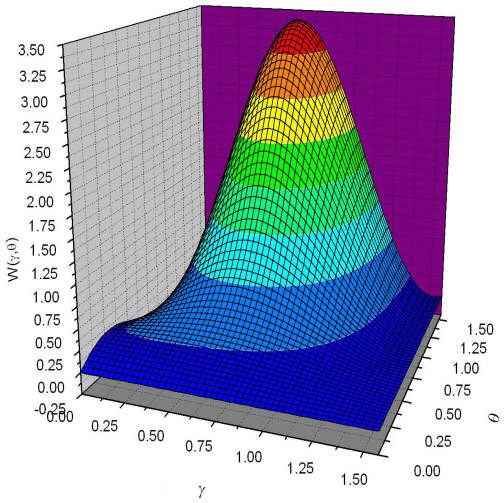

Figure 3.7: Case A BC Weight Function.

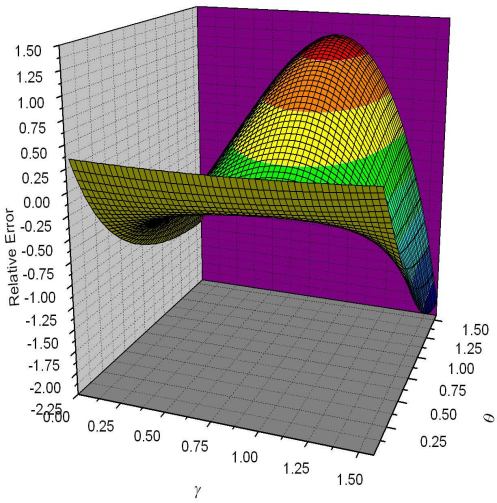

Figure 3.8: Case A BC Weight Function Relative Error vs. Analytic.

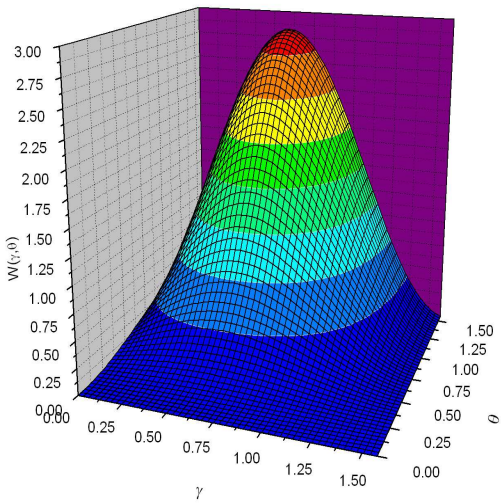

Figure 3.9: Case B BC Weight Function.

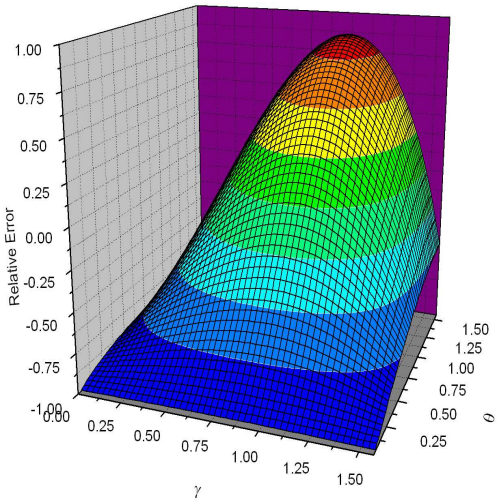

Figure 3.10: Case B BC Weight Function Relative Error vs. Analytic.

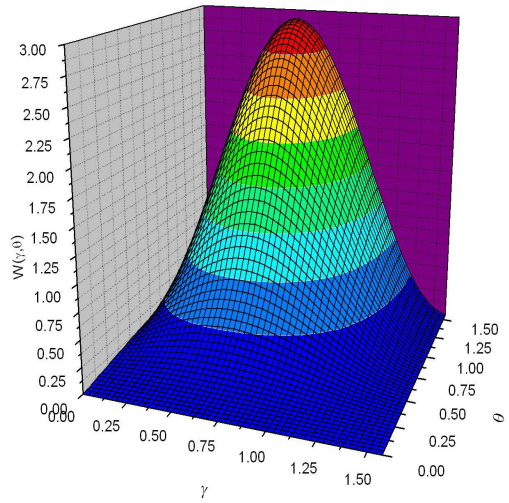

Figure 3.11: Case C BC Weight Function.

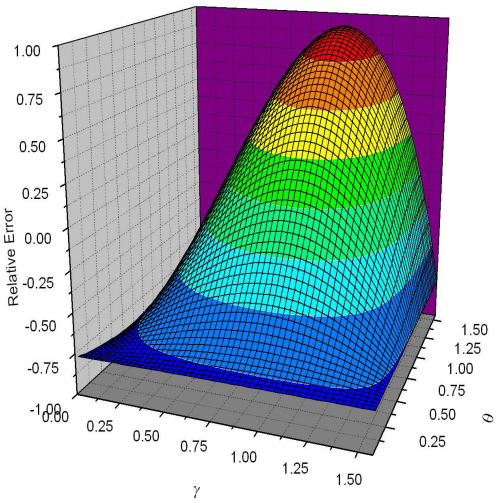

Figure 3.12: Case C BC Weight Function Relative Error vs. Analytic.

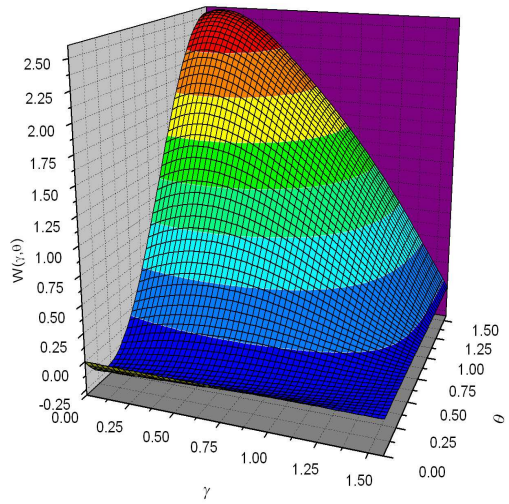

Figure 3.13: Case D BC Weight Function.

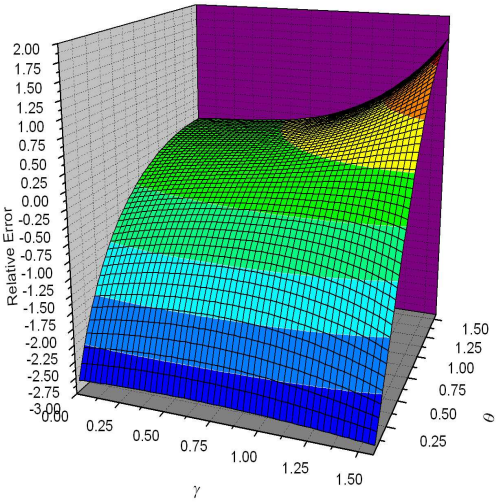

Figure 3.14: Case D BC Weight Function Relative Error vs. Analytic.

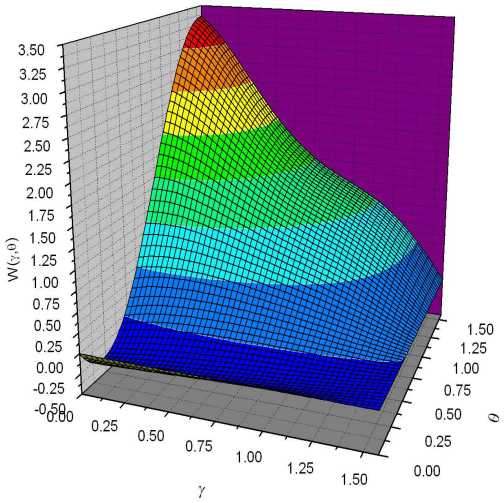

Figure 3.15: Case $D_{1,2}$ BC Weight Function.

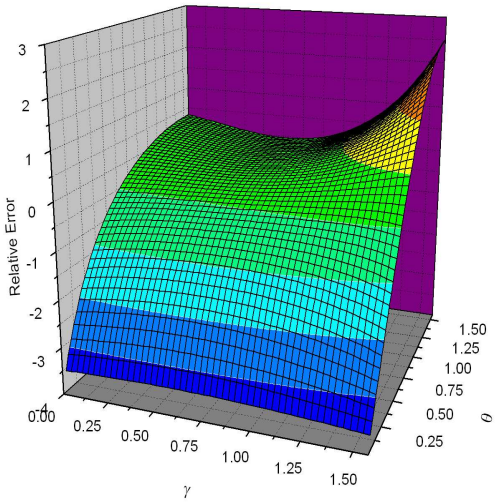

Figure 3.16: Case $D_{1,2}$ BC Weight Function Relative Error vs. Analytic.

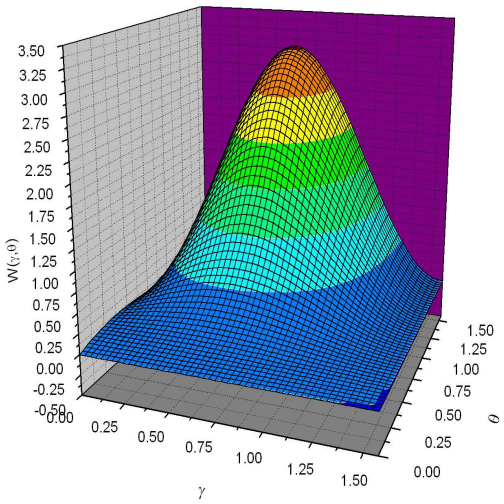

Figure 3.17: Case $D_{1,3}$ BC Weight Function.

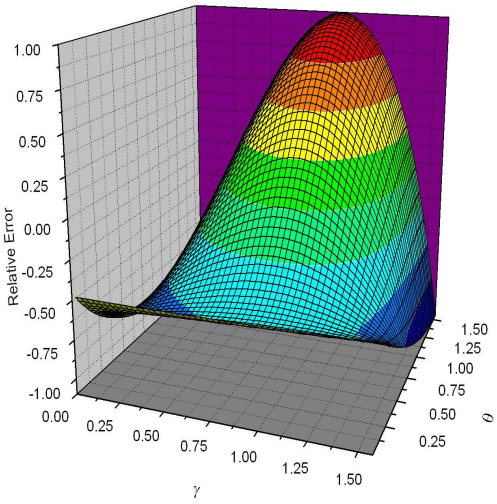

Figure 3.18: Case $D_{1,3}$ BC Weight Function Relative Error vs. Analytic.

strategies, cases A, B, and C in Figures 3.7–3.12 have distributions very close to each other in shape with B and C having nearly equal, although inaccurate, peak magnitudes. These three methods also result in large errors over the whole octant. Since case D, Figures 3.13 and 3.14, is required to match the analytic boundary condition weight function at (γ_1, θ_1), its distribution is peaked very close to the surface normal and has an accurate magnitude in this region. The deficiencies are that there is a negative region for small θ and the overall shape varies from the analytic result. This method produces small relative errors over a large part of the octant with larger errors occurring near $\gamma = \theta = \pi/2$ and for small θ. Case $D_{1,2}$, Figures 3.15 and 3.16, gives a peaked distribution that is reasonable in shape but only correct in magnitude where it is constrained to be so. This causes the error to be high in all other locations of the octant. Case $D_{1,3}$, Figures 3.17 and 3.18, gives poor results and errors very close to that of cases A, B, and C. All methods considered perform well for an isotropic incoming flux due to equation (3.115) becoming an integral only of the boundary condition weight function. The shape and magnitude of the boundary condition weight function, and therefore the specific NWF method employed, is important for all angular flux distributions encountered other than isotropic.

Next, we define a metric in order to compare the accuracy of the resulting boundary condition weight function. First, consider that what ultimately matters is the magnitude of the resulting scalar flux at the boundary, which is a weighted integral of the incoming angular flux (see (3.115)). We desire the NWF scalar flux at the boundary (3.115) to be close to the one defined by the asymptotic boundary condition (1.50) for a range of angular flux distributions. We numerically calculate the analytic asymptotic and NWF methods' boundary condition using a range of angular flux distributions generated by passing an isotropic angular flux through an

absorber of variable optical thickness. The compatible quadruple-range quadrature with an equal number of azimuthal angles on each polar cone is used with 9 ordinates/octant [54]. As the optical thickness of the absorbing slab is increased, the distribution becomes more anisotropic in the direction of the boundary surface normal. To model a highly anisotropic angular flux distribution we consider an incoming cone beam of particles at the boundary. This beam is defined by setting the angular flux equal to one only for the two ordinates closest to the surface normal of the boundary. All other angular fluxes of the boundary condition are set to zero. All of the resulting incoming flux boundary conditions are symmetric about the surface normal which corresponds to the second assumption made in the diffusion limit analysis (see Section 3.4.2). The resulting boundary condition scalar fluxes and relative errors are shown in Tables 3.3–3.6. The asymptotic boundary condition for the BLD discretized transport equation is also shown.

Table 3.3: Values of the Asymptotic Diffusion Limit Boundary Conditions.

$\sigma_a h$	Analytic	BLD Trans.	$1+\beta(\lvert\Omega_x\rvert+\lvert\Omega_y\rvert)$	A	B	C
0.0	1.99E+0	2.00E+0	2.00E+0	2.01E+0	2.00E+0	2.00E+0
0.2	1.45E+0	1.45E+0	1.45E+0	1.45E+0	1.45E+0	1.45E+0
1.0	4.81E-1	4.80E-1	4.73E-1	4.35E-1	4.56E-1	4.53E-1
2.0	1.35E-1	1.34E-1	1.30E-1	1.05E-1	1.18E-1	1.16E-1
4.0	1.26E-2	1.26E-2	1.15E-2	7.21E-3	9.55E-3	9.18E-3
6.0	1.34E-3	1.33E-3	1.18E-3	5.99E-4	9.12E-4	8.65E-4
Cone Beam	9.11E+0	9.05E+0	7.73E+0	3.00E+0	5.57E+0	5.16E+0

It is now clear that the choice of weights is hardly trivial with regards to the resulting asymptotic diffusion limit boundary condition. The method with a linear polynomial weight that possesses the diffusion limit ($\beta \approx -2.43$) performs well over the range of anisotropic fluxes. Consider especially that its boundary condition has not been manipulated and results purely

Table 3.4: Values of the Asymptotic Diffusion Limit Boundary Conditions (Continued).

$\sigma_a h$	D	$D_{1,2}$	$D_{1,3}$
0.0	2.00E+0	2.00E+0	2.00E+0
0.2	1.45E+0	1.45E+0	1.45E+0
1.0	4.84E-1	4.96E-1	4.48E-1
2.0	1.37E-1	1.44E-1	1.13E-1
4.0	1.28E-2	1.41E-2	8.67E-3
6.0	1.35E-3	1.53E-3	7.96E-4
Cone Beam	9.11E+0	1.05E+1	4.60E+0

Table 3.5: Relative Errors of the Asymptotic Diffusion Limit Boundary Conditions.

$\sigma_a h$	BLD Trans.	$1+\beta(\lvert\Omega_x\rvert+\lvert\Omega_y\rvert)$	A	B	C
0.0	0.033%	0.033%	0.348%	0.177%	0.205%
0.2	-0.112%	-0.249%	-0.419%	-0.326%	-0.341%
1.0	-0.304%	-1.607%	-9.471%	-5.201%	-5.888%
2.0	-0.423%	-3.948%	-22.08%	-12.24%	-13.82%
4.0	-0.568%	-8.739%	-42.85%	-24.33%	-27.31%
6.0	-0.641%	-11.97%	-55.38%	-31.81%	-35.60%
Cone Beam	-0.702%	-15.19%	-67.02%	-38.88%	-43.40%

Table 3.6: Relative Errors of the Asymptotic Diffusion Limit Boundary Conditions (Continued).

$\sigma_a h$	D	$D_{1,2}$	$D_{1,3}$
0.0	-0.059%	-0.152%	-0.242%
0.2	-0.199%	-0.149%	-0.361%
1.0	0.697%	3.02%	-6.81%
2.0	1.36%	6.73%	-15.9%
4.0	1.25%	11.3%	-31.3%
6.0	0.755%	13.6%	-40.7%
Cone Beam	-3.74E-12%	15.3%	-49.5%

from the discretizations used and the five requirements (3.61)-(3.65). Moving on from this good result, we notice that the addition of a bilinear term in the weight specified in various reasonable ways can cause such disastrous results as seen for methods A, B, and C. Method D results in a marked improvement over the linear polynomial method with $\beta \approx -2.43$. The magnitude of

the error for case D is very similar to the BLD discretized transport equation. Since Case D was derived specifically for the location of the ordinate closest to the boundary surface normal, the error is numerically zero for the highly forward peaked incoming angular flux of the cone beam. Cases $D_{1,2}$ and $D_{1,3}$ perform poorly because of their inaccurate boundary condition weight function distributions. Their performance will improve only if an anisotropic angular flux streams in the directions they are derived for, while case D produces accurate boundary conditions for the whole range of angular fluxes considered.

The formulation of case $D_{l,m}$ can be performed for any ordinate in the quadrature set. This presents an opportunity for an adaptive use of the NWF methods to accurately handle situations of anisotropic angular fluxes in any direction. Grazing angle incoming fluxes are common in practical problems containing heterogeneities and present a challenge to the accuracy of numerical methods. The performance of the BLD discretized transport equation and case $D_{l,m}$ for $l = 1$ and $m = 1, \ldots, M$ are examined for the case of grazing angles at each individual direction of the quadrature set on the polar cone nearest the x-y plane. The compatible quadruple-range quadrature is used with 9 and 12 ordinates per octant. Tables 3.7–3.10 show the resulting boundary condition scalar flux and relative errors versus the analytic values.

Table 3.7: Values of the Asymptotic Diffusion Limit Boundary Conditions for Grazing Angle Inputs (9 ordinates per octant).

Incoming Grazing Angle	Analytic	BLD Trans.	$D_{1,1}$ (D)	$D_{1,2}$	$D_{1,3}$
(θ_1, γ_1)	4.56E+0	5.01E+0	4.56E+0	5.25E+0	2.30E+0
(θ_1, γ_2)	2.72E+0	4.08E+0	3.22E+0	2.72E+0	4.87E+0
(θ_1, γ_3)	4.20E-1	9.15E-1	8.32E-1	9.60E-1	4.20E-1

Table 3.8: Relative Errors of the Asymptotic Diffusion Limit Boundary Conditions for Grazing Angle Inputs (9 ordinates per octant).

Incoming Grazing Angle	BLD Trans.	$D_{1,1}$ (D)	$D_{1,2}$	$D_{1,3}$
(θ_1, γ_1)	9.91%	-3.70E-10%	15.3%	-49.5%
(θ_1, γ_2)	50.3%	18.7%	1.37E-10%	79.1%
(θ_1, γ_3)	118%	98.1%	128%	4.14E-9%

Table 3.9: Values of the Asymptotic Diffusion Limit Boundary Conditions for Grazing Angle Inputs (12 ordinates per octant).

Incoming Grazing Angle	Analytic	BLD Trans.	$D_{1,1}$ (D)	$D_{1,2}$	$D_{1,3}$	$D_{1,4}$
(θ_1, γ_1)	4.63E+0	4.90E+0	4.63E+0	5.30E+0	7.79E+0	2.13E+0
(θ_1, γ_2)	3.72E+0	4.90E+0	3.97E+0	3.72E+0	2.82E+0	4.88E+0
(θ_1, γ_3)	1.62E+0	2.82E+0	2.28E+0	2.14E+0	1.62E+0	2.81E+0
(θ_1, γ_4)	2.40E-1	5.52E-1	5.21E-1	5.97E-1	8.78E-1	2.40E-1

Table 3.10: Relative Errors of the Asymptotic Diffusion Limit Boundary Conditions for Grazing Angle Inputs (12 ordinates per octant).

Incoming Grazing Angle	BLD Trans.	$D_{1,1}$ (D)	$D_{1,2}$	$D_{1,3}$	$D_{1,4}$
(θ_1, γ_1)	5.84%	-2.20E-6%	14.4%	68.3%	-54.0%
(θ_1, γ_2)	31.3%	6.52%	-6.65E-7%	-24.4%	30.9%
(θ_1, γ_3)	73.7%	40.9%	32.3%	-9.24E-6%	73.2%
(θ_1, γ_4)	130%	117%	149%	266%	-4.22E-6%

First, notice that each $D_{l,m}$ method has numerically zero error for incoming grazing angular fluxes at the ordinates that each are derived for. The case D ($D_{1,1}$) method results in the lowest overall errors for all grazing angles and is more accurate than the BLD discretized transport equation. This suggests that case D is the best choice for general use of the NWF methods. It may be possible to analyze the angular flux distribution shape through the values of the factors F_k^α and G_k and adaptively choose an appropriate $D_{l,m}$ method which will result in the highest accuracy possible of the asymptotic diffusion limit boundary condition at that location.

Higher order polynomial weights may be considered in deriving the NWF methods,

but they are not necessary to produce the asymptotic diffusion equation and will introduce third-order and higher terms into the asymptotic boundary condition. These higher order terms of course do not exist in the quadratic polynomial that approximates the exact analytic result of the transport equation but may exist in the exact form itself. The following section presents numerical results that enable one to compare and analyze the properties of different NWF methods.

3.6 Numerical Results

We present numerical results of two test problems to demonstrate the performance of the proposed 2D NWF family of methods with respect to the diffusion limit. The first problem is designed to test the diffusion limit performance of the method in the interior of a diffusive region. The second problem investigates both the diffusion limit and the boundary condition properties of the method. We show the results for the NWF methods with weights $w(\Omega_x, \Omega_y) = 1$, $w(\Omega_x, \Omega_y) = |\Omega_x| + |\Omega_y|$, $w(\Omega_x, \Omega_y) = 1 + |\Omega_x| + |\Omega_y|$, $w(\Omega_x, \Omega_y) = 1 + \beta\,(|\Omega_x| + |\Omega_y|)$, and $w(\Omega_x, \Omega_y) = 1 + \beta_x|\Omega_x| + \beta_y|\Omega_y| + \beta_{xy}|\Omega_x\Omega_y|$ with method D.

Note that the factors in the NWF methods involve integration over individual quadrants of the angular flux multiplied by polynomials of directional cosines. Taking into account this fact, we use Gauss-type quadratures [54], namely, the compatible quadruple-range quadrature with an equal number of azimuthal angles on each polar cone.

3.6.1 Problem 1

We consider a unit square having $\sigma_t = 1/\varepsilon$, $\sigma_a = \varepsilon$, and $q = \varepsilon$ for $\varepsilon = 10^{-2}, 10^{-3}$, 10^{-4}, and 10^{-5} [40]. Note, that as $\varepsilon \to 0$ the domain becomes more and more diffusive. A uniform spatial mesh of 19x19 equal cells is used with vacuum boundary conditions. The angular discretization is 9 ordinates per octant, 3 per polar level, unless otherwise stated. Two cases of method D are presented, D(9) and D(12), which use 9 and 12 ordinates per octant, respectively. This means that each D(N) method is formulated for the ordinate closest to the surface normal in the angular quadrature set specified by N ordinates per octant. This results in distinct methods. The convergence criterion is

$$\max_j \left| \vec{\phi}_j^{(k)} - \vec{\phi}_j^{(k-1)} \right| < \tilde{\epsilon}(1 - \rho^{(k)}) \,, \tag{3.125}$$

where

$$\rho^{(k)} = \frac{\max_j |\vec{\phi}_j^{(k)} - \vec{\phi}_j^{(k-1)}|}{\max_j |\vec{\phi}_j^{(k-1)} - \vec{\phi}_j^{(k-2)}|} \,, \tag{3.126}$$

with $\tilde{\epsilon} = 10^{-8}$, and $\vec{\phi}$ represents all low-order unknowns.

Tables 3.11 and 3.12 show measures of the error of the NWF methods' solutions in Problem 1 as compared to the fine-mesh numerical solution obtained by the QD method. Note that the low-order equations of the QD method give rise to the diffusion equation in diffusive regions. The low-order QD equations are discretized by means of a finite-volume method of second-order accuracy. The QD solution accurately reproduces the solution of this problem on a fine mesh. Relative errors of the cell-average scalar flux in the cell located at the center of the domain are listed in Table 3.11. The relative errors of the solution in the L_2-norm are shown in Table 3.12.

Table 3.11: Problem 1: Relative Errors of the Cell-Average Scalar Flux in the Cell Located at the Center of the Domain.

Weight	$w=1$	w=$\|\Omega_x\|$+$\|\Omega_y\|$	w=1+$\|\Omega_x\|$+$\|\Omega_y\|$	w=1+β($\|\Omega_x\|$+$\|\Omega_y\|$)	D(9)	D(12)
$\varepsilon = 10^{-2}$	2.56E-1	1.01E-1	1.75E-1	7.13E-3	1.92E-2	2.20E-2
$\varepsilon = 10^{-3}$	2.68E-1	9.82E-2	1.79E-1	-2.18E-3	-6.13E-4	-2.18E-3
$\varepsilon = 10^{-4}$	2.69E-1	9.86E-2	1.80E-1	-1.99E-3	-4.17E-4	-1.99E-3
$\varepsilon = 10^{-5}$	2.69E-1	9.86E-2	1.80E-1	-1.97E-3	-3.97E-4	-1.97E-3

Table 3.12: Problem 1: Relative Errors of the Scalar Flux in L_2 Norm.

Weight	$w=1$	w=$\|\Omega_x\|$+$\|\Omega_y\|$	w=1+$\|\Omega_x\|$+$\|\Omega_y\|$	w=1+β($\|\Omega_x\|$+$\|\Omega_y\|$)	D(9)	D(12)
$\varepsilon = 10^{-2}$	2.32E-1	8.56E-2	1.55E-1	1.81E-2	1.95E-2	2.09E-2
$\varepsilon = 10^{-3}$	2.54E-1	8.82E-2	1.67E-1	1.96E-2	1.88E-2	1.96E-2
$\varepsilon = 10^{-4}$	2.56E-1	8.90E-2	1.68E-1	1.99E-2	1.91E-2	1.99E-2
$\varepsilon = 10^{-5}$	2.56E-1	8.91E-2	1.68E-1	1.99E-2	1.92E-2	1.99E-2

These results demonstrate that the NWF methods with the weights $w(\Omega_x, \Omega_y) = 1 + \beta(|\Omega_x| + |\Omega_y|)$ and $w(\Omega_x, \Omega_y) = 1 + \beta_x|\Omega_x| + \beta_y|\Omega_y| + \beta_{xy}|\Omega_x\Omega_y|$ with case D reproduce the maximum of the solution with small errors, especially in case of extremely diffusive regions. These methods also have the smallest relative errors in the L_2 norm. Larger errors of the NWF method with other weights $w(\Omega_x, \Omega_y)$ are explained by the fact that the equations of these methods lead to the diffusion equation with a wrong diffusion coefficient (Eq.(3.109) and Table 3.1) in the interior of diffusive regions.

This problem also exemplifies the ability of angular quadrature sets to accurately integrate polynomials of directional cosines over quadrants. Note that the method with weight $w(\Omega_x, \Omega_y) = 1 + \beta(|\Omega_x| + |\Omega_y|)$ and D(12) give the same results in all but the least diffusive media, but D(9) differs. All three methods limit to the same diffusion equation in the asymptotic diffusion limit with the same analytic diffusion coefficient given by (3.109). The difference is that the angular quadrature order is not high enough to accurately integrate the bilinear polynomial

of directional cosines with 9 ordinates/octant. With 12 ordinates/octant the quadruple-range quadrature is capable of accurately integrating $\tilde{F}_m^{\alpha}$ for the case of a bilinear weight and isotropic angular flux. The resulting diffusion coefficients for the D(9) and D(12) methods in the most diffusive media ($\varepsilon = 10^{-5}$) are $(3.006\sigma_t)^{-1}$ and $(3.000\sigma_t)^{-1}$, respectively. But, now notice that the D(9) method results in lower errors. Since there are no boundary condition effects in this problem, this is not because of shape differences of the boundary condition weighting function. The only difference between the three methods in the diffusion limit for this specific problem is the value of the diffusion coefficient (3.109). The case D(9) diffusion coefficient, although not accurate, produces a solution with lesser errors for this problem.

3.6.2 Problem 2

We consider a two-region boundary layer problem $0 \leq x, y \leq 11$ having $\sigma_t = \sigma_a = 2$, $\Delta x = 0.1$, and $q = 0$ from $0 \leq x \leq 1$ and $\sigma_t = \sigma_s = 100$, $\Delta x = 1$, and $q = 0$ from $1 \leq x \leq 11$ ($\Delta y = 1$ everywhere). There is an isotropic incoming angular flux with magnitude $\frac{1}{2\pi}$ on the left boundary and vacuum on the rest. The angular quadrature set and convergence criterion are the same as in Problem 1, except here only case D(9) is considered. This problem tests a method's ability to reproduce an accurate diffusion solution in the interior of a diffusive region with a spatially unresolved boundary layer.

Figure 3.19 shows the scalar flux from the low-order problem along the middle of the spatial domain at $y = 5.5$. Cell-average values are displayed in solid and face-average values are in outline form. The red curve represents the fine-mesh solution with resolved boundary layer obtained by the QD method. Figure 3.20 demonstrates the absolute value of the relative errors of the low-order scalar flux with respect to the fine mesh solution.

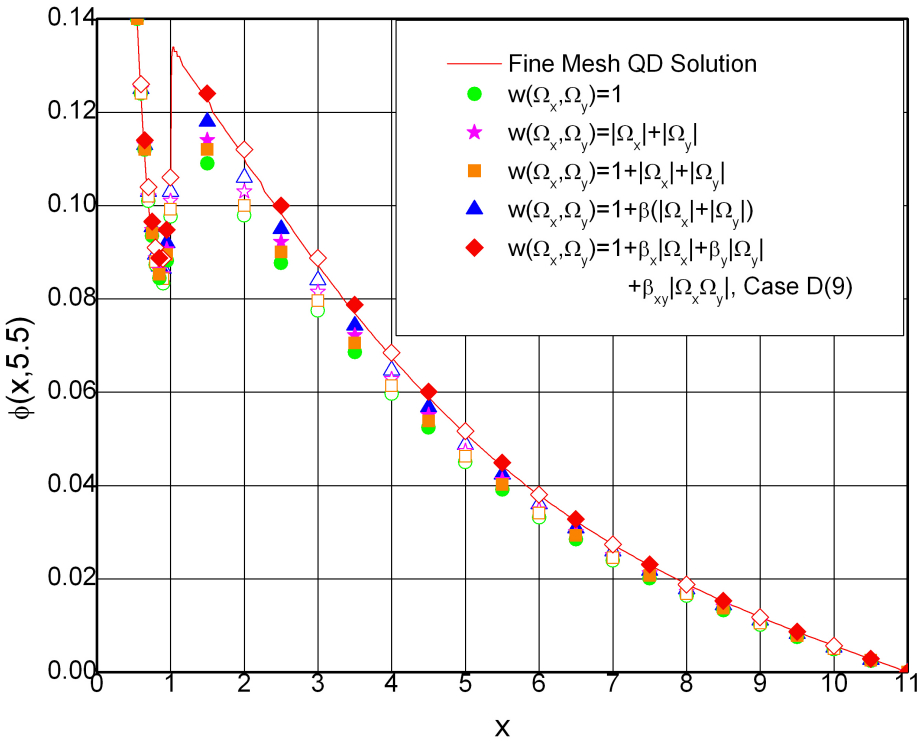

Figure 3.19: Problem 2: Cell Average and Cell Face Total Low-Order Scalar Flux.

The physics of the problem were previously described in Section (2.6.3). The only difference is that this problem is 2D. This causes the shape of the scalar flux to be curved rather than a straight line in the diffusive region.

The presented results show that the NWF method with the smallest errors in the diffusive region with highly anisotropic angular flux coming from the purely absorbing region is the method with the weight $w(\Omega_x, \Omega_y) = 1 + \beta_x|\Omega_x| + \beta_y|\Omega_y| + \beta_{xy}|\Omega_x\Omega_y|$ constrained by requirements (3.61)-(3.65) and method D. Note that at the right boundary (x=11) the solution is very small ($\phi = 3.724 \times 10^{-5}$), which results in an increase of the relative error.

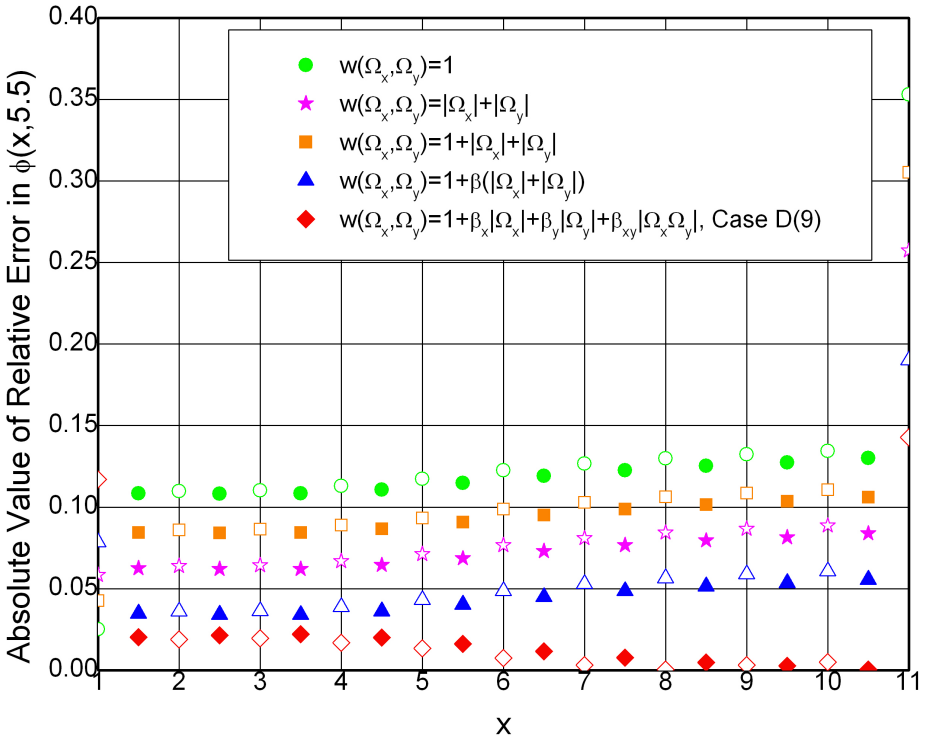

Figure 3.20: Problem 2: Absolute Value of Relative Errors of the Scalar Flux versus QD Fine Mesh Solution of Figure 3.19.

Chapter 4

ANALYSIS OF THE 2D NWF METHOD CONVERGENCE PROPERTIES

In this chapter, the stability analysis of the 2D Nonlinear Weighted Flux methods is shown. It is an objective of the 2D method development work that the resulting NWF methods have fast convergence properties. These properties are estimated theoretically and numerically for a range of problem specifications in this chapter.

4.1 Fourier Analysis

We now perform a Fourier analysis of the 2D NWF iterative method in differential form. This analysis progresses in the same fashion as described in Sections 1.2.6 and 2.5. The

2D NWF methods are considered in general form with a weight given by

$$w(\Omega_x, \Omega_y) = a + b\left(|\Omega_x| + |\Omega_y|\right) + c|\Omega_x\Omega_y|\,, \tag{4.1}$$

where a, b, and c define a specific method within the NWF family.

First, the iterative method equations are linearized around a special class of infinite-medium problems with a flat source and constant cross sections whose solution is

$$\psi(x, y, \vec{\Omega}) = \frac{q}{4\pi\sigma_a}\,, \tag{4.2}$$

$$\phi(x, y) = \frac{q}{\sigma_a}\,, \tag{4.3}$$

$$\phi_m(x, y) = \frac{q}{4\sigma_a}\,. \tag{4.4}$$

The solution at iteration k is assumed to be near to (4.2)–(4.4) according to the following

$$\psi^{(k+1/2)}(x, y, \vec{\Omega}) = \frac{q}{\sigma_a}\left(\frac{1}{4\pi} + \epsilon\eta^{(k+1/2)}(x, y, \vec{\Omega})\right)\,, \tag{4.5}$$

$$\phi^{(k)}(x, y) = \frac{q}{\sigma_a}\left(1 + \epsilon\xi^{(k)}(x, y)\right)\,, \tag{4.6}$$

$$\phi_m^{(k)}(x, y) = \frac{q}{\sigma_a}\left(\frac{1}{4} + \epsilon\xi_m^{(k)}(x, y)\right)\,, \tag{4.7}$$

where $m = 1, \ldots, 4$ and $\epsilon \ll 1$. The convergence rate for this problem class is then given by the rate at which η, ξ, and ξ_m go to zero. Then, equations (4.5)–(4.7) are substituted into all equations of the iterative method: the high-order problem (3.7), the factors (3.8)–(3.9) and (3.5), and the low-order problem (3.10)–(3.14). The resulting linearized equations are:

$$\Omega_x\frac{\partial}{\partial x}\eta^{(k+1/2)} + \Omega_y\frac{\partial}{\partial y}\eta^{(k+1/2)} + \sigma_t\eta^{(k+1/2)} = \frac{1}{4\pi}\sigma_s\xi^{(k)}\,, \tag{4.8}$$

$$\nu_m^x\gamma_m C_1\frac{\partial}{\partial x}\xi_m^{(k+1)} + \nu_m^y\gamma_m C_1\frac{\partial}{\partial y}\xi_m^{(k+1)} + \sigma_t\xi_m^{(k+1)} = \frac{1}{4}\sigma_s\xi^{(k+1)}$$

$$-\nu_m^x\gamma_m\frac{\partial}{\partial x}\int_{\omega_m}\left[-C_1 + a|\Omega_x| + b|\Omega_x|\left(|\Omega_x| + |\Omega_y|\right) + c|\Omega_x|^2|\Omega_y|\right]\eta^{(k+1/2)}d\vec{\Omega}$$

$$-\nu_m^y \gamma_m \frac{\partial}{\partial y} \int_{\omega_m} \left[-C_1 + a|\Omega_y| + b|\Omega_y| \left(|\Omega_x| + |\Omega_y| \right) + c|\Omega_x||\Omega_y|^2 \right] \eta^{(k+1/2)} d\vec{\Omega}$$

$$-\sigma_t \int_{\omega_m} \left[(a\gamma_m - 1) + a|\Omega_x| + \gamma_m b \left(|\Omega_x| + |\Omega_y| \right) + \gamma_m c|\Omega_x||\Omega_y| \right] \eta^{(k+1/2)} d\vec{\Omega} \,, \tag{4.9}$$

$$\xi^{(k+1)} = \sum_{m=1}^{4} \xi_m^{(k+1)} \,, \tag{4.10}$$

where,

$$C_1 = \left(\frac{1}{2} a + \frac{2+\pi}{3\pi} b + \frac{1}{8} c \right) \,, \tag{4.11}$$

$$\gamma_m = \left(a + b + \frac{2}{3\pi} c \right)^{-1} \,, \tag{4.12}$$

$$m = 1, \ldots, 4 \,,$$

and spatial and angular dependence notation has been dropped.

Next, a Fourier analysis is performed on the linearized method by introducing the Fourier ansatz,

$$\eta^{(k+1/2)}(x, y, \vec{\Omega}) = a(\vec{\Omega}) \omega^k(\lambda_x, \lambda_y) e^{i\sigma_t(\lambda_x x + \lambda_y y)} \,, \tag{4.13}$$

$$\xi_m^{(k)}(x, y) = A_m \omega^k(\lambda_x, \lambda_y) e^{i\sigma_t(\lambda_x x + \lambda_y y)} \,, \tag{4.14}$$

$$\xi^{(k)}(x, y) = \omega^k(\lambda_x, \lambda_y) e^{i\sigma_t(\lambda_x x + \lambda_y y)} \,, \tag{4.15}$$

$$m = 1, \ldots, 4 \,,$$

into Eqs. (4.8)-(4.10). Then, a system of equations in terms of the eigenvalue spectrum and the magnitudes of the error modes, namely $\omega(\lambda_x, \lambda_y)$, $a(\vec{\Omega})$, and A_m is obtained. The following equations result:

$$\sum_{m=1}^{4} A_m = 1 \,, \tag{4.16}$$

$$\omega(\lambda_x, \lambda_y) \left[i A_m \gamma_m C_1 \left(\nu_m^x \lambda_x + \nu_m^y \lambda_y \right) + A_m - \frac{c}{4} \right] = -i\gamma_m \frac{c}{4\pi} \left[\nu_m^x \lambda_x \Gamma_1^m + \nu_m^y \lambda_y \Gamma_2^m \right] - \frac{c}{4\pi} \Gamma_3^m \,, \tag{4.17}$$

$$\Gamma_1^m = \int_{\omega_m} \frac{-C_1 + a|\Omega_x| + b|\Omega_x|\left(|\Omega_x| + |\Omega_y|\right) + c|\Omega_x|^2|\Omega_y|}{1 + i\left(\Omega_x\lambda_x + \Omega_y\lambda_y\right)} d\vec{\Omega}\,, \tag{4.18}$$

$$\Gamma_2^m = \int_{\omega_m} \frac{-C_1 + a|\Omega_y| + b|\Omega_y|\left(|\Omega_x| + |\Omega_y|\right) + c|\Omega_x||\Omega_y|^2}{1 + i\left(\Omega_x\lambda_x + \Omega_y\lambda_y\right)} d\vec{\Omega}\,, \tag{4.19}$$

$$\Gamma_3^m = \int_{\omega_m} \frac{(a\gamma_m - 1) + \gamma_m b\left(|\Omega_x| + |\Omega_y|\right) + \gamma_m c|\Omega_x||\Omega_y|}{1 + i\left(\Omega_x\lambda_x + \Omega_y\lambda_y\right)} d\vec{\Omega}\,, \tag{4.20}$$

$$m = 1, \ldots, 4\,,$$

where $a(\vec{\Omega})$ has been eliminated already by the relation

$$a(\vec{\Omega}) = \frac{c}{4\pi\left[1 + i(\Omega_x\lambda_x + \Omega_y\lambda_y)\right]}\,. \tag{4.21}$$

Obtaining the spectrum of eigenvalues as a function of λ_x and λ_y from this system begins with solving equation (4.17) for A_m and then summing over $m = 1, \ldots, 4$ to obtain an equation solely in terms of $\omega(\lambda_x, \lambda_y)$. After considerable manipulation and multiplying by the complex conjugates of terms, it is found that

$$\begin{aligned}
\omega(\lambda_x,\lambda_y)\pi\left(C_2 - \frac{4}{c}\right) &= \frac{1}{Q_1 Q_1^*}\Big\{ i\gamma_m\left[\lambda_x\left(\Gamma_1^1 - \Gamma_1^3\right) + \lambda_y\left(\Gamma_2^1 - \Gamma_2^3\right)\right] \\
&+ \left(\Gamma_3^1 + \Gamma_3^3\right) + \gamma_m^2 C_1\left(\lambda_x + \lambda_y\right)\left[\lambda_x\left(\Gamma_1^1 + \Gamma_1^3\right) + \lambda_y\left(\Gamma_2^1 + \Gamma_2^3\right)\right] \\
&+ i\gamma_m C_1\left(\lambda_x + \lambda_y\right)\left(\Gamma_3^3 - \Gamma_3^1\right)\Big\} \\
&+ \frac{1}{Q_2 Q_2^*}\Big\{ i\gamma_m\left[\lambda_x\left(\Gamma_1^4 - \Gamma_1^2\right) + \lambda_y\left(\Gamma_2^2 - \Gamma_2^4\right)\right] \\
&+ \left(\Gamma_3^2 + \Gamma_3^4\right) + \gamma_m^2 C_1\left(-\lambda_x + \lambda_y\right)\left[-\lambda_x\left(\Gamma_1^2 + \Gamma_1^4\right) + \lambda_y\left(\Gamma_2^2 + \Gamma_2^4\right)\right] \\
&+ i\gamma_m C_1\left(-\lambda_x + \lambda_y\right)\left(\Gamma_3^4 - \Gamma_3^2\right)\Big\}\,,
\end{aligned} \tag{4.22}$$

where,

$$Q_1 = \left[1 + i\gamma_m C_1\left(\lambda_x + \lambda_y\right)\right]\,, \tag{4.23}$$

$$Q_2 = \left[1 + i\gamma_m C_1\left(-\lambda_x + \lambda_y\right)\right]\,, \tag{4.24}$$

$$C_2 = 2\left[\frac{1}{1+\gamma_m^2 C_1^2\left(\lambda_x+\lambda_y\right)^2}+\frac{1}{1+\gamma_m^2 C_1^2\left(-\lambda_x+\lambda_y\right)^2}\right], \tag{4.25}$$

and * denotes the complex conjugate of a term.

Assuming that the angular quadrature to be used for numerical integration has rotational symmetry over each quadrant, the following simplifications to the Γ terms in the preceding equations can be made in order to remove all complex quantities:

$$\begin{aligned}
R_1 &= i\left(\Gamma_1^1-\Gamma_1^3\right) && (4.26)\\
&= 2\sum_{m\in\omega_1}\frac{\left[-C_1+a|\Omega_x|+b|\Omega_x|\left(|\Omega_x|+|\Omega_y|\right)+c|\Omega_x|^2|\Omega_y|\right]_m\left(\Omega_{x,m}\lambda_x+\Omega_{y,m}\lambda_y\right)}{1+\left(\Omega_{x,m}\lambda_x+\Omega_{y,m}\lambda_y\right)^2}\zeta_m\,,\\
R_2 &= \left(\Gamma_1^1+\Gamma_1^3\right) && (4.27)\\
&= 2\sum_{m\in\omega_1}\frac{\left[-C_1+a|\Omega_x|+b|\Omega_x|\left(|\Omega_x|+|\Omega_y|\right)+c|\Omega_x|^2|\Omega_y|\right]_m}{1+\left(\Omega_{x,m}\lambda_x+\Omega_{y,m}\lambda_y\right)^2}\zeta_m\,,\\
R_3 &= i\left(\Gamma_1^4-\Gamma_1^2\right) && (4.28)\\
&= -2\sum_{m\in\omega_1}\frac{\left[-C_1+a|\Omega_x|+b|\Omega_x|\left(|\Omega_x|+|\Omega_y|\right)+c|\Omega_x|^2|\Omega_y|\right]_m\left(\Omega_{x,m}\lambda_x+\Omega_{y,m}\lambda_y\right)}{1+\left(-\Omega_{x,m}\lambda_x+\Omega_{y,m}\lambda_y\right)^2}\zeta_m\,,\\
R_4 &= i\left(\Gamma_1^2+\Gamma_1^4\right) && (4.29)\\
&= 2\sum_{m\in\omega_1}\frac{\left[-C_1+a|\Omega_x|+b|\Omega_x|\left(|\Omega_x|+|\Omega_y|\right)+c|\Omega_x|^2|\Omega_y|\right]_m}{1+\left(-\Omega_{x,m}\lambda_x+\Omega_{y,m}\lambda_y\right)^2}\zeta_m\,,\\
S_1 &= i\left(\Gamma_2^1-\Gamma_2^3\right) && (4.30)\\
&= 2\sum_{m\in\omega_1}\frac{\left[-C_1+a|\Omega_y|+b|\Omega_y|\left(|\Omega_x|+|\Omega_y|\right)+c|\Omega_x||\Omega_y|^2\right]_m\left(\Omega_{x,m}\lambda_x+\Omega_{y,m}\lambda_y\right)}{1+\left(\Omega_{x,m}\lambda_x+\Omega_{y,m}\lambda_y\right)^2}\zeta_m\,,\\
S_2 &= \left(\Gamma_2^1+\Gamma_2^3\right) && (4.31)\\
&= 2\sum_{m\in\omega_1}\frac{\left[-C_1+a|\Omega_y|+b|\Omega_y|\left(|\Omega_x|+|\Omega_y|\right)+c|\Omega_x||\Omega_y|^2\right]_m}{1+\left(\Omega_{x,m}\lambda_x+\Omega_{y,m}\lambda_y\right)^2}\zeta_m\,,\\
S_3 &= i\left(\Gamma_2^2-\Gamma_2^4\right) && (4.32)\\
&= 2\sum_{m\in\omega_1}\frac{\left[-C_1+a|\Omega_y|+b|\Omega_y|\left(|\Omega_x|+|\Omega_y|\right)+c|\Omega_x||\Omega_y|^2\right]_m\left(-\Omega_{x,m}\lambda_x+\Omega_{y,m}\lambda_y\right)}{1+\left(-\Omega_{x,m}\lambda_x+\Omega_{y,m}\lambda_y\right)^2}\zeta_m\,,\\
S_4 &= \left(\Gamma_2^2+\Gamma_2^4\right) && (4.33)
\end{aligned}$$

$$= 2\sum_{m\in\omega_1}\frac{\left[-C_1+a|\Omega_y|+b|\Omega_y|\left(|\Omega_x|+|\Omega_y|\right)+c|\Omega_x||\Omega_y|^2\right]_m}{1+\left(-\Omega_{x,m}\lambda_x+\Omega_{y,m}\lambda_y\right)^2}\zeta_m\,,$$

$$T_1 = \left(\Gamma_3^1+\Gamma_3^3\right) \tag{4.34}$$

$$= 2\sum_{m\in\omega_1}\frac{\left[(a\gamma_m-1)+\gamma_m b\left(|\Omega_x|+|\Omega_y|\right)+\gamma_m c|\Omega_x||\Omega_y|\right]_m}{1+\left(\Omega_{x,m}\lambda_x+\Omega_{y,m}\lambda_y\right)^2}\zeta_m\,,$$

$$T_2 = \left(\Gamma_3^3-\Gamma_3^1\right) \tag{4.35}$$

$$= -2\sum_{m\in\omega_1}\frac{\left[(a\gamma_m-1)+\gamma_m b\left(|\Omega_x|+|\Omega_y|\right)+\gamma_m c|\Omega_x||\Omega_y|\right]_m\left(\Omega_{x,m}\lambda_x+\Omega_{y,m}\lambda_y\right)}{1+\left(\Omega_{x,m}\lambda_x+\Omega_{y,m}\lambda_y\right)^2}\zeta_m\,,$$

$$T_3 = \left(\Gamma_3^2+\Gamma_3^4\right) \tag{4.36}$$

$$= 2\sum_{m\in\omega_1}\frac{\left[(a\gamma_m-1)+\gamma_m b\left(|\Omega_x|+|\Omega_y|\right)+\gamma_m c|\Omega_x||\Omega_y|\right]_m}{1+\left(-\Omega_{x,m}\lambda_x+\Omega_{y,m}\lambda_y\right)^2}\zeta_m\,,$$

$$T_4 = i\left(\Gamma_3^4-\Gamma_3^2\right) \tag{4.37}$$

$$= -2\sum_{m\in\omega_1}\frac{\left[(a\gamma_m-1)+\gamma_m b\left(|\Omega_x|+|\Omega_y|\right)+\gamma_m c|\Omega_x||\Omega_y|\right]_m\left(-\Omega_{x,m}\lambda_x+\Omega_{y,m}\lambda_y\right)}{1+\left(-\Omega_{x,m}\lambda_x+\Omega_{y,m}\lambda_y\right)^2}\zeta_m\,.$$

Quadrature weights are given by ζ_m.

Then, the eigenvalues as a function of the wave numbers λ_x, λ_y, and the scattering ratio, c, are

$$\begin{aligned}\omega(\lambda_x,\lambda_y) = &\left[\frac{c}{\pi C_2\left(c-\frac{4}{C_2}\right)}\right]\Big\{\left[1+\gamma_m^2C_1^2(\lambda_x+\lambda_y)^2\right]^{-1}\left[\gamma_m\lambda_xR_1+\gamma_m\lambda_yS_1+T_1\right.\\ &\left.+\gamma_m^2C_1\left(\lambda_x+\lambda_y\right)\left(\lambda_xR_2+\lambda_yS_2\right)+\gamma_mC_1\left(\lambda_x+\lambda_y\right)T_2\right]\\ &+\left[1+\gamma_m^2C_1^2(-\lambda_x+\lambda_y)^2\right]^{-1}\left[\gamma_m\lambda_xR_3+\gamma_m\lambda_yS_3+T_3\right.\\ &\left.+\gamma_m^2C_1\left(-\lambda_x+\lambda_y\right)\left(-\lambda_xR_4+\lambda_yS_4\right)+\gamma_mC_1\left(-\lambda_x+\lambda_y\right)T_4\right]\Big\}.\end{aligned} \tag{4.38}$$

The spectral radius of the NWF family of methods for this special class of problems is then given by

$$\rho=\sup_{\lambda_x,\lambda_y}\left|\omega(\lambda_x,\lambda_y)\right|. \tag{4.39}$$

4.2 Theoretical Results

The theoretical spectral radius is evaluated for this class of infinite-medium problems by equations (4.38) and (4.39). Table (4.1) contains the spectral radii as a function of scattering ratio for the NWF methods with weights $w(\Omega_x, \Omega_y) = 1$, $w(\Omega_x, \Omega_y) = |\Omega_x| + |\Omega_y|$, $w(\Omega_x, \Omega_y) = 1 + \beta(|\Omega_x| + |\Omega_y|)$, and $w(\Omega_x, \Omega_y) = 1 + \beta_x|\Omega_x| + \beta_y|\Omega_y| + \beta_{xy}|\Omega_x\Omega_y|$ with method D. The scattering ratios considered are $c = 0.1$, 0.9, 0.99, and 0.999. The quadrature sums of Eqs. (4.26)-(4.37) are evaluated using 220 ordinates per octant, the finest angular quadrature set available for the compatible quadruple-range quadrature. Note that the formulation of method D is performed for 12 ordinates per octant and denoted as $D(12)$.

Table 4.1: Theoretically Estimated Spectral Radii for NWF Methods versus Scattering Ratio.

Method	$w = 1$	w=$\|\Omega_x\|$+$\|\Omega_y\|$	w=1+β($\|\Omega_x\|$+$\|\Omega_y\|$)	D(12)
$c = 0.1$	3.35E-2	3.46E-2	3.53E-2	4.12E-2
$c = 0.9$	5.21E-1	5.37E-1	5.49E-1	6.41E-1
$c = 0.99$	6.24E-1	6.44E-1	6.58E-1	7.68E-1
$c = 0.9999$	6.36E-1	6.57E-1	6.71E-1	7.83E-1

4.3 Numerical Results

Numerical tests are considered in this section as a way of estimating the convergence properties of the NWF methods. These convergence properties are measured by the total number of transport sweeps required for convergence and numerical estimates of the spectral radius. Numerically estimated spectral radii are determined by means of

$$\rho_2^{(k)} = \frac{\|\vec{\phi}^{(k)} - \vec{\phi}^{(k-1)}\|_2}{\|\vec{\phi}^{(k-1)} - \vec{\phi}^{(k-2)}\|_2} \tag{4.40}$$

for the last iteration of each NWF method where $\vec{\phi}$ includes all low-order unknowns. Comparison to methods such as DSA, QD, Symmetrized QD (SQD), and linear multiple balance AADR(d) (AADR(d)-LMB) are made using published results [55, 56] and an existing code for the case of QD [57, 58].

4.3.1 Problem 1

We consider a homogenous square problem ($0 \leq x, y \leq 8$) with cross sections of $\sigma_t = 1$ and $\sigma_s = 0.95$ as shown in Figure 4.1 [55]. There is an external source of magnitude $q = 1$ from $6 \leq x, y \leq 8$. The top and right hand side boundary conditions are reflective and the rest are vacuum. A uniform mesh varies in size as $h = 2$, 1, 0.5, 0.25, and 0.125. An angular quadrature of 12 ordinates per octant is used (4 ordinates on each of 3 polar cones). The cited data was calculated with an S_8 Gauss-Legendre quadrature (10 ordinates per octant). The convergence criterion of (3.125) is used with with $\tilde{\epsilon} = 10^{-5}$. Published results use a relative pointwise convergence criterion with the same value of $\tilde{\epsilon}$.

Table 4.2 has the number of transport iterations required to converge for the NWF methods, diamond-differenced DSA, SQD, and QD versus mesh size (equally, optical thickness). Table 4.3 contains the spectral radii numerically estimated from equation (4.40).

Table 4.2: Problem 1: Number of Transport Iterations versus Mesh Size.

Method	DD-DSA	SQD	QD	$w = 1$	w=$\lvert\Omega_x\rvert$+$\lvert\Omega_y\rvert$	w=1+β($\lvert\Omega_x\rvert$+$\lvert\Omega_y\rvert$)	D(12)
$h = 0.125$	8	7	10	12	11	11	11
$h = 0.25$	8	8	10	8	8	8	8
$h = 0.5$	8	8	10	6	6	6	6
$h = 1$	9	8	10	5	5	5	5
$h = 2$	12	8	8	4	4	4	4

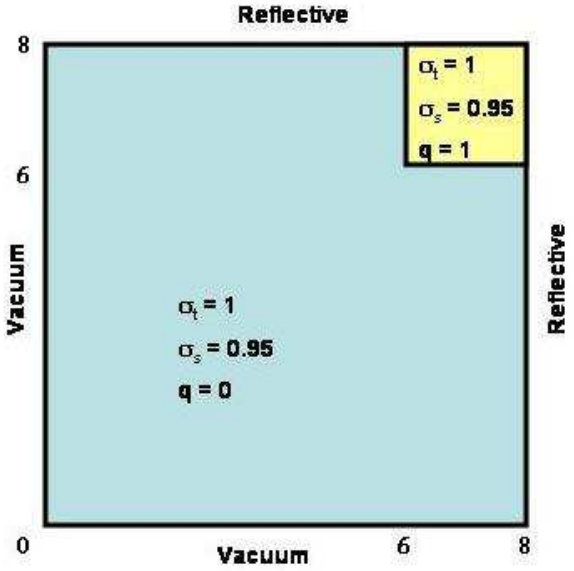

Figure 4.1: Problem 1: Geometry and Material Specifications.

Table 4.3: Problem 1: Numerically Estimated Spectral Radii for NWF Methods versus Mesh Size.

Method	$w = 1$	w=$\|\Omega_x\|$+$\|\Omega_y\|$	w=1+β($\|\Omega_x\|$+$\|\Omega_y\|$)	D(12)
$h = 0.125$	0.47	0.47	0.47	0.46
$h = 0.25$	0.32	0.33	0.33	0.31
$h = 0.5$	0.16	0.18	0.18	0.17
$h = 1$	0.06	0.08	0.10	0.11
$h = 2$	0.04	0.04	0.05	0.05

4.3.2 Problem 2

We consider a heterogeneous square problem ($0 \leq x, y \leq 12$) with $\sigma_t = 1$ everywhere as shown in Figure 4.2 [55]. From $8 \leq x, y \leq 12$, $\sigma_s = 0.9$ and $q = 1$. From $4 \leq x, y \leq 12$ excluding the previous region, $\sigma_s = 0.97$ and $q = 0$. From $0 \leq x, y \leq 12$ excluding the previous regions, $\sigma_s = 0.5$ and $q = 0$. The top and right hand side boundary conditions are reflective and the rest are vacuum. The mesh is uniform and varies in size as $h = 2$, 1, 0.5, 0.25, and 0.125.

The angular quadrature and convergence criterion are the same as the previous problem.

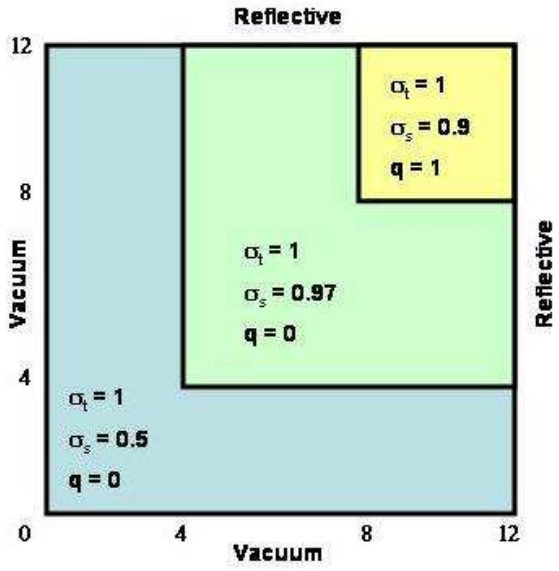

Figure 4.2: Problem 2: Geometry and Material Specifications.

Table 4.4 has the number of transport iterations required to converge for the NWF methods, diamond-differenced DSA, SQD, and QD versus mesh size. Table 4.5 contains the numerically estimated spectral radii.

Table 4.4: Problem 2: Number of Transport Iterations versus Mesh Size.

Method	DD-DSA	SQD	QD	$w = 1$	w=$\|\Omega_x\|$+$\|\Omega_y\|$	w=1+β($\|\Omega_x\|$+$\|\Omega_y\|$)	D(12)
$h = 0.125$	8	8	10	11	11	11	11
$h = 0.25$	8	9	10	8	8	7	7
$h = 0.5$	8	8	10	6	6	6	6
$h = 1$	9	8	10	5	5	5	5
$h = 2$	13	9	9	4	4	3	4

Table 4.5: Problem 2: Numerically Estimated Spectral Radii for NWF Methods versus Mesh Size.

Method	$w=1$	$w=\|\Omega_x\|+\|\Omega_y\|$	$w=1+\beta(\|\Omega_x\|+\|\Omega_y\|)$	D(12)
$h=0.125$	0.48	0.48	0.49	0.48
$h=0.25$	0.32	0.32	0.32	0.30
$h=0.5$	0.17	0.15	0.16	0.16
$h=1$	0.06	0.10	0.10	0.11
$h=2$	0.02	0.04	0.05	0.07

4.3.3 Problem 3

We consider a square problem ($0 \leq x, y \leq 8$) similar to Problem 1 with homogenous cross sections as shown in Figure 4.3, and the total cross section is varied as $\sigma_t =$ 0.01, 0.1, 1, 2, 4, and 6 [56]. The scattering ratio, $c = \frac{\sigma_s}{\sigma_t}$, is spatially constant throughout with $c = 1$, thus $\sigma_s = \sigma_t$. There is an external source of magnitude $q = 1$ from $4 \leq x, y \leq 8$. The top and right hand side boundary conditions are reflective and the rest are vacuum. The mesh size is $\Delta x = \Delta y = 1$. The convergence criterion is $\tilde{\epsilon} = 10^{-4}$. The angular quadrature is the same as Problem 1 with respect to the NWF methods and the published results.

Table 4.6 has the number of transport iterations required to converge for the NWF methods, diamond-differenced DSA, and AADR(d)-LMB versus σ_t.

Table 4.6: Problem 3: Number of Transport Iterations versus σ_t.

Method	DD-DSA	AADR(d)-LMB	$w=1$	$w=\|\Omega_x\|+\|\Omega_y\|$	$w=1+\beta(\|\Omega_x\|+\|\Omega_y\|)$	D(12)
$\sigma_t=0.01$	4	4	4	4	4	4
$\sigma_t=0.1$	6	5	6	6	6	6
$\sigma_t=1$	5	6	6	6	6	7
$\sigma_t=2$	5	5	5	5	6	6
$\sigma_t=4$	8	6	4	4	5	5
$\sigma_t=6$	8	6	3	4	4	4

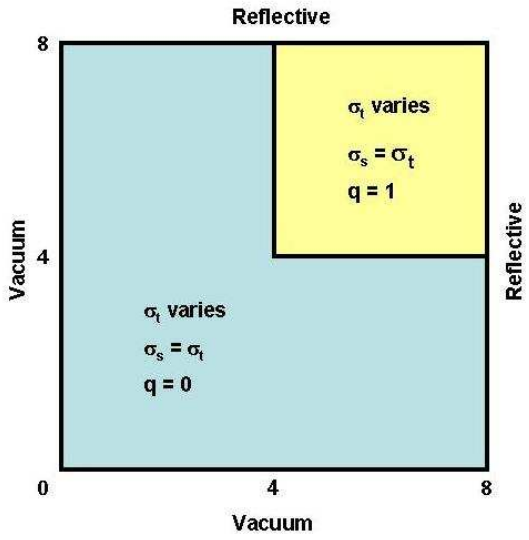

Figure 4.3: Problem 3: Geometry and Material Specifications.

4.3.4 Problem 4

We consider a square ($0 \leq x, y \leq 30$) optically-thick coarse-mesh iron-water problem as shown in Figure 4.4 [56]. The cross sections are defined in Table 4.7. The external source is of magnitude $q = 1$ and from $18 \leq x, y \leq 30$. The top and right hand side boundary conditions are reflective and the rest are vacuum. The mesh is a uniform 10x10 cells. The convergence criterion is $\tilde{\epsilon} = 10^{-4}$. The angular quadrature is 12 ordinates per octant (4 ordinates on each of 3 polar cones), whereas the cited data was calculated with an S_8 Gauss-Legendre quadrature (10 ordinates per octant).

Table 4.8 has the number of transport iterations required to converge for the NWF methods and AADR(d)-LMB [56].

Table 4.7: Problem 4: Material Properties.

Material	σ_t	c	q
1 (Water)	3.33	0.994	1
2 (Water)	3.33	0.994	0
3 (Iron)	1.33	0.831	0

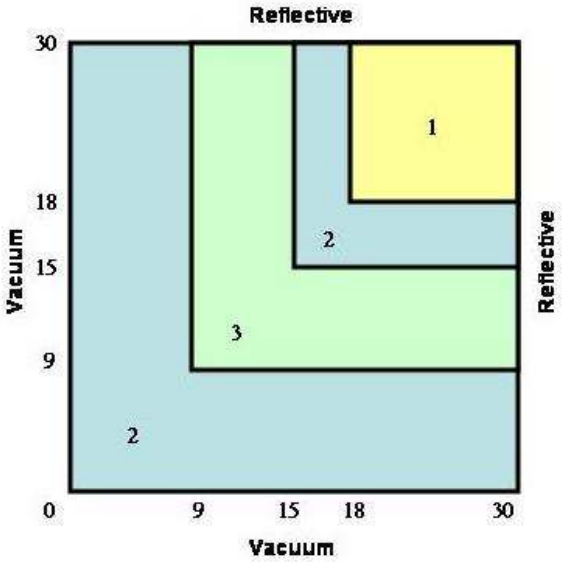

Figure 4.4: Problem 4: Geometry and Material Region Specifications.

Table 4.8: Problem 4: Number of Transport Iterations for Convergence.

Method	AADR(d)-LMB	$w = 1$	w=$\|\Omega_x\|$+$\|\Omega_y\|$	w=1+β($\|\Omega_x\|$+$\|\Omega_y\|$)	D(12)
Number of iterations	6	3	4	4	4

4.3.5 Problem 5

We consider a square ($0 \leq x, y \leq 64$) homogenous problem with uniform 64x64 mesh. The cross sections and external source vary in magnitude as $\sigma_t = \kappa$, $c = 0.9999$, and $q = \kappa$ for $\kappa =$ 1E+3, ..., 1E-10. Therefore, $\sigma_s = 0.9999\kappa$. All boundary conditions are vacuum.

The convergence criterion is $\tilde{\epsilon} = 10^{-8}$. The angular quadrature is 12 ordinates per octant (4 ordinates on each of 3 polar cones). The number of transport iterations to converge and the spectral radii estimates at the last iteration are shown in Table 4.9 for the NWF case D(12) method. Note that there is no spectral radii data for the two thickest cases because their error reached a minimum after only two iterations.

Table 4.9: Problem 5: Number of Transport Iterations for Convergence and Spectral Radii Estimates.

κ	Number of Iterations	Spectral Radius
1E+3	2	N\A
1E+2	2	N\A
1E+1	3	1.43E-4
1E+0	10	1.18E-1
1E-1	23	4.66E-1
1E-2	9	1.36E-1
1E-3	5	1.80E-2
1E-4	3	1.73E-3
1E-5	3	1.74E-4
1E-6	3	1.74E-5
1E-7	3	8.72E-7
1E-8	3	8.72E-8
1E-9	3	8.72E-9
1E-10	3	8.72E-10

4.4 Discussion

Numerical convergence results were presented for five problems which varied in scattering ratio, optical thickness, and heterogeneity. In Problem 1, the optical thickness is varied via the mesh size. Table 4.2 shows that each of the NWF methods considered converges very

fast for optically thick mesh as compared to DD-DSA, SQD, and QD. The NWF methods convergence rate slows for finer mesh. Table 4.3 shows that the corresponding spectral radii estimates of the NWF methods support the same two trends. Both tables of data reveal a minimal performance difference between the NWF methods considered. Problem 2 introduces heterogeneities and again varies the optical thickness of mesh cells. The transport iteration counts in Table 4.4 and spectral radii in Table 4.5 show that the NWF methods converge fast for optically thick heterogeneous problems and slow down for less optically thick mesh. Note the behavior of the other methods, where DSA performs best on fine mesh, SQD performance varies slightly, and QD performs best on coarse mesh. Although similar to Problem 1, Problem 3 offers a comparison to different methods and varies the optical thickness of mesh cells through changes in σ_t. The NWF methods converge faster than the DD-DSA and AADR(d)-LMB methods on optically thick mesh, and the same or one iteration slower on intermediate and fine mesh. The NWF methods for this problem converge as fast for the most optically thin mesh cells as for the optically thickest. Problem 4 is heterogeneous with optically thick mesh cells and the NWF methods continue the trend of fast convergence for such problems. The NWF methods all converge significantly faster than the AADR(d)-LMB method. The fifth problem demonstrates the performance of the NWF method case D(12) for the largest problem size considered, a wide range of optical thicknesses, and for a high scattering ratio. The convergence is very fast for optically thick cases. The convergence then slows significantly as the optical thickness is reduced, but speeds up again as the mesh becomes very optically thin. The reported spectral radii correspond directly to this trend. Stability is exhibited for all problems and optical thicknesses considered.

The results of the Fourier analysis show that the NWF methods are stable but will converge slowly for high scattering ratios. This analysis considers a special class of problems with constant solution. A homogenous problem sufficiently large in size, with optically thin enough spatial mesh, and small influence of leakage will approximate that considered by the Fourier analysis. The NWF methods convergence properties from Fourier analysis and numerical problems are both correct and can be reconciled with each other. Consider the Fourier analysis results for c=0.9999 in Table 4.1 and the numerical results of Problem 5 in Table 4.9. For large σ_t the problem has optically thick coarse mesh and is diffusive for which the NWF case D(12) performs well. The analysis predicts that the convergence rate will slow as the mesh becomes optically thin. This is exhibited in Problem 5 as $\sigma_t \rightarrow$ 1E-1 and the spectral radius increases to 0.466 requiring 23 iterations for convergence. As $\sigma_t \rightarrow 0$, the leakage of the system increases and dominates the convergence properties of the method. A Fourier analysis of the discretized equations would bridge this gap in the results. Leakage effects also explain why in Problem 3 the convergence slowed for intermediate thicknesses but was faster for optically thin mesh. The theoretical and numerical results for the 1D NWF methods exhibit the same trend of slowed convergence on thin mesh as evidenced by Tables 2.1, 2.2, and 2.3. In 1D the numerical results correspond much closer to theory because slabs of large physical dimension with reduced leakage effects were considered.

The numerical tests showed that the NWF methods are stable over the wide range of media properties considered and converge fast for optically thick meshes of practical size and high scattering ratio. Of the problems considered, the NWF methods performed as well or better than the AADR(d)-LMB method which is formulated for optimal convergence.

Chapter 5

CONCLUSION

5.1 Summary

The goal of this research is to develop new parameterized flux methods for the accurate and efficient solution of multidimensional transport problems in Cartesian geometry which contain diffusive subdomains. The primary type of transport problems considered are that of radiative transfer. Examples of application areas important to science and engineering are astrophysics, atmospheric sciences, reactor physics, radiation shielding, etc. The NWF methods possess certain advantages in that they are defined in terms of partial scalar fluxes, do not require consistent discretization with the transport equation, and are flexible in their ability to be coupled to multiphysics applications. For a transport method to produce the correct solution inside diffusive material regions, it must possess the asymptotic diffusion limit in that it limits to an accurate form of the diffusion equation with boundary conditions that closely approximate that known from analysis of the transport equation.

The second chapter presents the development and analysis of the new NWF family of

methods in 1D slab geometry. The low-order equations are derived by integrating the transport equation with a general weight of μ over positive and negative directions. Linear fractional factors that depend weakly on the angular flux are defined to close the system of equations. The low-order problems of these methods are based on the equations for the partial scalar fluxes, and hence they are similar to the flux and α-WN methods. We use a lumped LD discretization to discretize the low-order system of equations and the step characteristic method for the high-order. An asymptotic diffusion limit analysis is performed for the continuous and discretized form equations both in the interior of a diffusive region and on the boundary of the region. A NWF method whose leading order solution limits to the diffusion equation and has an accurate boundary condition in diffusive regions is defined by the choice of weights subject to constraints resulting from the asymptotic analysis. Numerical results of problems are presented which show that the new method produces accurate solutions for problems containing diffusive regions with unresolved boundary layers as the asymptotic analysis showed. A Fourier analysis shows that the NWF family of methods exhibit fast convergence, especially for optically thick cells. The convergence properties of this method are close to the properties of the QD, DSA and α-WN (with α=0.366) methods. As a result, we developed a flux method with the combination of features that are important for solving transport problems with optically thick regions and that none of the α-WN methods (including the FF and SF methods) possesses.

The third chapter extends the NWF methods to 2D Cartesian geometry. Integrating the transport equation with a general weight of Ω_x and Ω_y over spherical angular quadrants results in the low-order equations of the NWF family of methods defined in terms of partial scalar fluxes. These equations are closed by linear fractional factors similar to the 1D methods.

A lumped BLD finite element discretization and the method of short characteristics is applied independently to the low and high-order problems, respectively, on uniform grids. It is a goal that the 2D methods possess the same desirable combination of properties as was achieved in 1D. An asymptotic diffusion limit analysis is performed for the NWF methods in continuous and discretized form in the interior of a diffusive region. The discretized method is also analyzed on the boundary. The performed analysis revealed a method with a particular linear weight function the low-order equations of which lead to the diffusion equation in the asymptotic diffusion limit and possesses a conditionally accurate asymptotic boundary condition. The use of a bilinear weight function results in a method that both limits to the diffusion equation and an accurate boundary condition in the asymptotic diffusion limit. This method is similar in accuracy to the BLD discretized transport equation for unresolved boundary layer problems with incoming angular fluxes ranging from isotropic to very anisotropic, and outperforms it for grazing angle incoming angular fluxes. The bilinear weight can be formulated such that the asymptotic diffusion limit boundary condition is exact for specific directions. Numerical results show that the developed method performs as the analysis predicts.

The fourth chapter analyzes the convergence properties of the 2D NWF family of methods via Fourier analysis and numerical problems. The Fourier analysis of the continuous form equations shows that the NWF methods exhibit slowed convergence for a specific class of infinite-medium problems with constant cross sections and source with high scattering ratio. For a wide range of numerical problems, the NWF methods exhibited convergence properties very similar to DSA, QD, SQD, and ADR(d)-LMB. The NWF methods converge very fast for optically thick mesh of homogeneous and heterogeneous problems. Convergence slows only for

optically thin mesh with small leakage. The NWF methods exhibit stability in all numerical problems considered and for the analytic results of the continuous form Fourier analysis.

5.2 Recommendations for Future Work

5.2.1 Efficient Solution of the Low-Order NWF Equations

In order for the NWF methods to be useful for problems of practical size, the efficient solution of the low-order equations must be developed. The BiCGSTAB Krylov method is attractive since the low-order equations are not SPD. In order for BiCGSTAB to be efficient, an effective preconditioner must be supplied. Incomplete LU decompositions, such as ILUTP [59, 60], are simple to implement from existing code packages [61] but are inefficient for large matrices. A likely path of research is to formulate a sweep-based preconditioner [62]. This uses transport sweeps and diffusion solves to provide the action of the preconditioner. Another approach is to construct an approximate inverse which is highly parallelizable [59].

5.2.2 Fourier Analysis of the 2D Discretized NWF Equations

In order to further characterize and understand the convergence properties of the NWF methods in 2D Cartesian geometry, a Fourier analysis of the discretized equations can be performed. This analysis will provide exactly how the discretized method performs for a specific class of problems with mesh that varies in optical thickness and materials that vary in scattering ratio. Numerical problems must be formulated and results interpreted, but an analysis of a method shows once and for all the convergence behavior. Further, it would be very useful to perform a heterogenous medium Fourier analysis to study the NWF methods'

convergence properties for this type of problem.

5.2.3 Adaptive Selection and Use of NWF Methods

It is possible to constrain the bilinear weight of the 2D NWF methods developed in Chapter 3 in many different ways. For instance, it was shown that the asymptotic diffusion limit boundary condition can be accurately approximated for isotropic, anisotropic of varying degree, and grazing angle incoming angular fluxes at the material interface. It may be possible to analyze the shape of the angular flux using the factors G_m and F_m^α in order to select specific NWF methods which perform optimally in different regions of the problem. It is expected that problems will arise due to discontinuous behavior of the values of the factors in neighboring cells.

5.2.4 Variable Eddington Factor Approach to Solving the Low-Order Equations

The NWF methods that meet the diffusion limit can be used for developing approximate mathematical models for radiative transfer and particle transport that are similar to the Variable Eddington Factor (VEF) approach [63]. The VEF methods are based on a set of low-order equations for moments of the angular flux and some *apriori* closure relationships, for instance, Levermore-Pomraning or Minerbo closures [64, 65]. For some class of transport problems, these approximate models can be more accurate than the flux-limited diffusion model or P_1 theory. The low-order NWF equations can be used in combination with, for example, Minerbo closure to derive a model with new features.

5.2.5 Extension to 3D and Other Geometries

The next obvious extension of this work is to 3D. Many physics models require 3D modeling of radiation transport. It would be useful to extend the NWF methods to 3D Cartesian and rz geometries. For the former, it should be straightforward to augment the 2D bilinear weights with Ω_z terms to create an analog to what has been developed so far. For the latter, the form of the equations are not the same and this will require developing the NWF methods from scratch, but with the same spirit as has been done here. The analysis of the NWF methods in these geometries will need to be performed anew.

BIBLIOGRAPHY

[1] D.Y. ANISTRATOV and V.YA. GOL'DIN, "Nonlinear Methods for Solving Particle Transport Problems", *Transport Theory Statist. Phys.*, **22**, 125, (1993).

[2] M.L. ADAMS and E.W. LARSEN, "Fast Iterative Methods for Discrete-Ordinates Particle Transport Calculations," *Prog. Nucl. Energy*, **40**, 3 (2002).

[3] V.YA. GOL'DIN, "A Quasi-Diffusion Method for Solving the Kinetic Equation," *USSR Comp. Math. and Math. Phys.* **4**, 136 (1964).

[4] T.A. GERMOGENOVA, "Convergence of Some Approximate Methods of Solving the Transport Equation," *Soviet Mathematics - Doklady* **9**, 855 (1968).

[5] V.YA. GOL'DIN, G.V. DANILOVA and B.N. CHETVERUSHKIN, "Approximate Method of Solving the Time-Dependent Kinetic Equation," in *Computational Methods in Transport Theory* (Atomizdat, Moscow, 1969), 50 (in Russian).

[6] V.V. GORSKII and S.T. SURZHIKOV, "Use of the Semimoment Method to Solve the Shock Layer Radiative Heat-Transfer Problem," *J. of Eng. Physics*, **42**, No. 1, 108 (1982).

[7] D.Y. ANISTRATOV and E. W. LARSEN, "Nonlinear and Linear α-Weighted Methods for Particle Transport Problems," *J. of Computational Physics*, **173**, 664 (2001).

[8] M.L. ADAMS, "New Nonlinear Methods for Linear Transport Calculations," Proceedings of *Joint International Conference on Mathematical Methods and Supercomputing in Nuclear Applications*, Karlsruhe, Germany, April 19-23, 1993, 683, American Nuclear Society (1993).

[9] S.G. HONG and N.Z. CHO, "A Rebalance Approach to Nonlinear Iteration for Solving the Neutron Transport Equations", *Ann. Nuc. Energy*, **24**, 2, 147–160 (1997).

[10] H.J. KOPP, "Synthetic Method Solution of the Transport Equation", *Nucl. Sci. Eng.*, **17**, 65, (1963).

[11] V.I. LEBEDEV, "The Iterative KP MEthod for the Kinetic Equation", Proceedings of *Conference on Mathematical Methods for Solution of Nuclear Physics Problems*, Nov 17-20, 1964, Dubna, 93 (1964).

[12] E.M. GELBARD and H.M. HAGEMAN, "The Synthetic Method as Applied to the Kinetic Equations", *Nucl. Sci. Eng.*, **37**, 288, (1969).

[13] W.H. REED, "The Effectiveness of Acceleration Techniques for Iterative Methods in Transport Theory", *Nucl. Sci. Eng.*, **45**, 245, (1971).

[14] R.E. ALCOUFFE, "A Stable Diffusion Synthetic Acceleration Method for Neutron Transport Iterations", *Trans. Am. Nucl. Soc.*, **23**, 203, (1976).

[15] R.E. ALCOUFFE, "Diffusion Synthetic Acceleration Methods for for the Diamond-Differenced Discrete-Ordinates Equations", *Nucl. Sci. Eng.*, **64**, 344, (1977).

[16] E.W. LARSEN, "Unconditionally Stable Diffusion Synthetic Acceleration Methods for the Slab Geometry Discrete-Ordinates Equations. Part I: Theory", *Nucl. Sci. Eng.*, **82**, 47, (1982).

[17] D.R. MCCOY and E.W. LARSEN, "Unconditionally Stable Diffusion Synthetic Acceler-

ation Methods for the Slab Geometry Discrete-Ordinates Equations. Part II: Numerical Results", *Nucl. Sci. Eng.*, **82**, 64, (1982).

[18] L.J. LORENCE, E.W. LARSEN, and J.E. MOREL, "An S_2 Synthetic Acceleration Scheme for the One-Dimensional S_N Equations", *Trans. Am. Nucl. Soc.*, **52**, 417, (1986).

[19] V.N. MOROZEV, "On Solution of Kinetic Equations by the S_n Method," *Theory and Design of Nuclear Reactors*, (Gosatomizdat, Moscow, 1962), 91 (in Russian).

[20] G.L. RAMONE, M.L. ADAMS, and P.F. NOWAK, "A Transport Synthetic Acceleration Method for Transport Iterations", *Nucl. Sci. Eng.*, **125**, 257, (1997).

[21] T.A. GERMOGENOVA, and T.A. SUSHKEVICH, "Solution of the Transport Equation by Means of the Method of Averaged Fluxes," *Problems of Shielding Physics, Atomizdat*, **3**, 34 (1969) (In Russian).

[22] V.Ya. GOLDIN, V.A. KUZYUK, and A.K. RAKHMATULINA, "Nonlinear Method of Electron Transport Calculation," *USSR Comp. Math. and Math. Phys.*, **16**, No. 2, 131 (1976).

[23] S.T. SURZHIKOV, "Calculations of the Selective Radiative Transfer in Two-Dimensional Cylindrical Geometry Zeroth Approximation of Quadramoments Method", *Preprint, Institute of Mechanics Problems, USSR Academy of Sciences*, **352** (1988), (In Russian).

[24] E.L. WACHPRESS, *I*terative Solution of Elliptic Systems and Applications to the Neutron Diffusion Equations of Reactor Physics, Prentice-Hall, Englewood Cliffs, NJ (1966).

[25] R. FROELICH, "A Theoretical Foundation for Coarse Mesh Variation Techniques," GA-7870, General Atomic (1967).

[26] W.F. MILLER JR., "Generalized Rebalance: A Common Framework for Transport Acceleration Methods," *Nuclear Science and Engineering*, **65**, 226 (1978).

[27] M.L. ADAMS and W.R. MARTIN, *Trans. Am. Nucl. Soc.*, **53**, 282 (1986).

[28] M.L. ADMAS and W.R. MARTIN, "Boundary Projection Acceleration: A New Approach to Synthetic Acceleration of Transport Calculations ," *Nuclear Science and Engineering*, **100**, 177 (1988).

[29] R.D. LAWRENCE, *Trans. Am. Nucl. Soc.*, **53**, 280 (1986).

[30] C.J. PARK and N.Z. CHO, "A Linear Multiple Balance Method with High Order Accuracy for Discrete Ordinates Neutron Transport Equations," *Ann. Nucl. Energy*, **28**, 1499 (2001).

[31] C.J. PARK and N.Z. CHO, "Convergence Analysis of Additive Angular Dependent Rebalance Acceleration for the Discrete Ordinates Transport Calculations," *Nucl. Sci. Eng.*, **142**, 64–74 (2002).

[32] E.W. LARSEN and J.B. KELLER, "Asymptotic Solution of Neutron Transport Problems for Small Mean Free Paths", *J. Math. Phys.*, **15**, 75, (1974).

[33] G.J. HABETLER and B.J. MATKOWSKY, "Uniform Asymptotic Expansions in Transport Theory with Small MEan Free Paths, and the Diffusion Approximation", *J. Math. Phys.*, **16**, 846, (1975).

[34] K.M. CASE and P.E. ZWEIFEL, *L*inear Transport Theory, Addison-Wesley, Reading, MA (1967).

[35] E.W. LARSEN, J.E. MOREL, and W.F. MILLER JR., "Asymptotic Solutions of Numerical Transport Problems in optically Thick, Diffusive Regions", *JCP*, **69**, 283-324, (1987).

[36] E.W. LARSEN, and J.E. Morel "Asymptotic Solutions of Numerical Transport Problems in Optically Thick, Diffusive Regimes II," *J. of Computational Physics*, **83**, 212 (1989).

[37] E. W. LARSEN, "The Asymptotic Diffusion Limit of Discretized Transport Problems," *Nucl. Sci. Eng.*, **112**, 336 (1992).

[38] M.L. ADAMS, "Even-Parity Finite-Element Transport Methods in the Diffusion Limit," *Progress in Nuclear Energy*, **25**, 2-3, 159 (1991).

[39] M.L. ADAMS, "Subcell Balance Methods for Radiative Transfer on Arbitrary Grids," *Transport Theory Statist. Phys.*, **26**, 4&5, 385 (1997).

[40] M.L. ADAMS, "Discontinuous Finite Element Transport Solutions in Thick Diffusive Problems," *Nuclear Science and Engineering*, **137**, 298 (2001).

[41] G.R. CEFUS and E.W. LARSEN, "Stability Analysis of the Quasidiffusion and Second Moment Methods for Iteratively Solving Discrete-Ordinates Problems", *Transport Theory Statist. Phys.*, **18**, 493 (1989-90).

[42] L. ROBERTS and D.Y. ANISTRATOV, "Nonlinear Weighted Flux Methods for Particle Transport Problems," Proceedings of *M&C 2005, International Conference on Mathe-*

matics and Computations, Supercomputing, Reactor Physics and Nuclear Biological Applications, Avignon, France, September, 2005, American Nuclear Society Topical Meeting of M&C Division (2005).

[43] L. ROBERTS and D.Y. ANISTRATOV, "Nonlinear Weighted Flux Methods for Particle Transport Problems," *Transport Theory Statist. Phys.*, **36**, 7 (2007).

[44] L. ROBERTS and D.Y. ANISTRATOV, "Nonlinear Weighted Flux Methods for Particle Transport Problems In 2D Cartesian Geometry," Proceedings of *M&C 2007, Joint International Topical Meeting on Mathematics & Computation and Supercomputing in Nuclear Applications,* American Nuclear Society Topical Meeting of M&C Division, Monterey, CA, April, 2007, 13 pp.

[45] T.R. HILL, Technical Report No. LA-5990-MS, Los Alamos Scientific Laboratory, June 1975 (unpublished).

[46] R.E. ALCOUFFE, E.W. LARSEN, W.F. MILLER and B.R. WIENKE, "Computational Efficiency of Numerical Methods for the Multigroup," Discrete-Ordinates Neutron Transport Equations: The Slab Geometry Case,", *Nucl. Sci. Eng.* **71**, 111 (1979).

[47] M.M. MIFTEN and E.W. LARSEN, "The Quasi-Diffusion Method for Solving Transport Problems in Planar and Spherical Geometries," *Transport Theory Statist. Phys.*, **22**, 165 (1993).

[48] M.L. ADAMS and W.R. MARTIN, "Diffusion Synthetic Acceleration of Discontinuous Finite Element Transport Iterations," *Nuclear Science and Engineering*, **111**, 145 (1992).

[49] J.E. MOREL, J.E. DENDY, JR., and T.A. WARING, "Diffusion-Accelerated Solution of the Two-Dimensional S_n Equations with Bilinear-Discontinuous Differencing," *Nuclear Science and Engineering*, **115**, 304 (1993).

[50] V.Ya. GOL'DIN, A.V. KOLPAKOV, and A.V. MISYUREV, "Solution of the Nonstationary Transport Equation Without Explicit Determination of the Front," *Akad. Nauk SSSR Inst. Prikl. Mat. Preprint*, **68**, 21 pp (1983).

[51] V.Ya. GOL'DIN, "Characteristic Difference Scheme for Non-Stationary Kinetic Equation," *Soviet Mathematics - Doklady*, **1**, 902 (1960).

[52] V.Ya. GOL'DIN, N.N. KALITKIN, and T.V. SHISHOVA, "Nonlinear Difference Schemes for Hyperbolic Equations," *USSR Comp. Math. and Math. Phys.* **5**, 229 (1968).

[53] K. TAKEUCHI, "A Numerical Method for Solving the Neutron Transport Equation in Finite Cylindrical Geometry," *J. Nucl. Sci.*, **6**, 446 (1969).

[54] I.K. ABU-SHUMAYS, "Angular Quadratures for Improved Transport Computations," *Transport Theory Statist. Phys.*, **30**, 169 (2001).

[55] M.M. MIFTEN, and E.W. LARSEN, "A Symmetrized Quasidiffusion Method for Solving Transport Problems in Multidimensional Geometries," in *Proceedings of Joint International Conference on Mathematical Methods and Supercomputing in Nuclear Applications, April 19-23, 1993, Karlsruhe, Germany* pp. 707-717.

[56] C.J. PARK, and N.Z. CHO, "Convergence Analysis of Additive Angular Dependent Rebalance Acceleration for the Discrete Ordinates Transport Calculations," *Nuclear Science and Engineering*, **142**, 64 (2002).

[57] H. HIRUTA, *Advanced Computational Methodology for Full-Core Neutronics Calculations*, Ph.D. dissertation, North Carolina State University, Raleigh, NC, USA (2004).

[58] H. HIRUTA, computer code QDTRAN, North Carolina State University, Raleigh, NC, USA (2004).

[59] Y. SAAD, *I*terative Methods for Sparse Linear Systems, Second Edition, SIAM (2003).

[60] B.W. PATTON, J.P. HOLLOWAY, "Application of Preconditioned GMRES to the Numerical Solution of the Neutron Transport Equation," *Annals of Nuclear Energy*, **29**, 109 (2002).

[61] Y. SAAD, computer code library SPARSKIT, University of Minnesota, Minneapolis, MN, USA (2000).

[62] J.E. MOREL, "Basic Krylov Methods with Application to Transport," Proceedings of *M&C 2005, International Conference on Mathematics and Computations, Supercomputing, Reactor Physics and Nuclear Biological Applications*, Avignon, France, September, 2005, American Nuclear Society Topical Meeting of M&C Division (2005).

[63] C.D. LEVERMORE, "Relating Eddington Factors to Flux Limiters," *J. Quant. Spectrosc. Radiat. Transfer*, **31**, 149, (1984)

[64] C.D. LEVERMORE and G.C. POMRANING, "A Flux-Limited Diffusion Theory," *Astrophys. J.*, **248**, 321, (1981).

[65] G.N. MINERBO, "Maximum Entropy Eddington Factors," *J. Quant.Spectrosc. Radiat. Transfer*, **20**, 541 (1978).